NOVEL ALGORITHMS FOR DETCTION/CLASSIFICATION OF MEDIUM/LOW-VOLTAGE ARCING FAULTS IN SWITCHGEAR & MOTOR COILS: FROM CONCEPT TO REALIZATION

by

MANDHIR SINGH SAHNI

Presented to the Faculty of the Graduate School of

The University of Texas at Arlington in Partial Fulfillment

of the Requirements

for the Degree of

DOCTOR OF PHILOSOPHY

THE UNIVERSITY OF TEXAS AT ARLINGTON

August 2008

ACKNOWLEDGEMENTS

I would hereby like to acknowledge the strong motivational and guiding impact of my supervising Professor Dr. Wei-Jen Lee which has been instrumental in me overcoming various technical and research challenges encountered during the course of my doctoral work and dissertation. He, apart from being the guiding light in terms of the technical and research aspects of the dissertation, has been a great source of inspiration over the period of 5 years that I have had the honor of interacting with him. He has helped underline the virtues of perseverance, hard-work, patience and due-diligence in carrying out state-of-the-art research in the relevant field of interest.

Apart from that, I would like to mention the role and impact other professors such as Dr. Bei Gou, Dr. Rasool Kenarangui, Dr. Babak Fahimi and Dr. Mo-Shing Chen have had either through academic curriculum or through research/personal interaction over the course of the last 5 years at the Electrical Engineering department at University of Texas, Arlington.

I would especially like to dedicate this doctoral dissertation to my parents, my father Mr. Daljit Sahni and my mother Dr. Rajender Sahni, who have been unselfishly co-operative for the last 5 years and without the support of these 2 people, this would never have been possible. This document is testament to my small tribute to them for their never-ending support and love.

Lastly, but not the least, I would like to acknowledge the presence and support of close friends and associates here at University of Texas Arlington who have served to be family away from home during the course of this long and arduous journey.

November 11, 2007

ABSTRACT

NOVEL ALGORITHMS FOR MEDIUM/LOW-VOLTAGE ARCING FAULTS IN SWITCHGEAR & MOTOR COILS: FROM CONCEPT TO REALIZATION

Mandhir Singh Sahni, PhD.

The University of Texas at Arlington, 2007

Supervising Professor: Dr. Wei-Jen Lee

Switchgear arcing faults have been a primary cause for concern for the manufacturing industry and safety personnel alike. The deregulation of the power industry being in full swing and ever-growing competitiveness in the distribution sector calls for the transition from preventive to predictive maintenance. Switchgear forms an integral part of the distribution system in any power system set-up. Keeping in mind the switchgear arcing faults, the transition mentioned above applies most of all to the switchgear industry. Apart from the fact that it is the primary cause of serious injuries to electrical workers worldwide, switchgear arcing faults directly affect the quality and continuity of electric power to the consumers. A great amount of technological

advancement has taken place in the development of arc resistant/proof switchgear. However, most of these applications focus on minimizing the damage after the occurrence of the arcing fault. The problem associated with the compromise on the quality and continuity of electric power in such a scenario still awaits a technical as well as economically feasible solution.

This dissertation describes the development of a novel approach for the detection of arcing faults in medium/low-voltage switchgear. The basic concept involves the application of differential protection for the detection of any arcing within the switchgear. The new approach differs from the traditional differential concept in the fact that it employs higher order harmonic components of the line current as the input for the differential scheme. Actual arc generating test-benches have been set up in the Power System Simulation Laboratory at Energy Systems Research Center to represent both medium and low voltage levels. Hall-effect sensors in conjunction with Data Acquisition in LabVIEW are employed to record the line current data before, during and after the arcing phenomenon. The methodology is first put to test via simulation approach for medium voltage levels and then corroborated by actual hardware laboratory testing for low voltage levels. The plots provided from the data gathering and simulation process clearly underline the efficiency of this approach to detect switchgear arcing faults. Both magnitude and phase differential concepts seem to provide satisfactory results. Apart from the technical efficiency, the approach is financially feasible considering the fact that the differential protection is already being comprehensively employed worldwide.

Developments spanning a major portion of the previous decade have witnessed the emergence of high/medium/low-voltage arcing fault as one of the more prominent issues confronting the power industry and associated researchers alike. Research over the past decade has been dedicated to the modeling, detection and/or monitoring of arcing faults at various voltage levels and power system apparatuses. Furthermore, the research presented in this dissertation presents and compares the performance of statistical methodologies utilized to classify the severity of low-voltage arcing in a motor coil. The approaches revolve around the utilization of statistical techniques such as Spectral Angle Mapper (SAM), Spectral Information Divergence (SID) and Linear Discriminant Analysis (LDA) to classify the severity of the motor coil arcing fault.

Dedicated test-benches are utilized to simulate the arcing phenomenon of varying severity in a motor coil within laboratory environment. Hall-effect sensors in conjunction with the data acquisition module of LabVIEW provide an able means for data collection which is then subjected to off-line analysis. The conceptual approach preceding the classification process revolves around the extraction of pre-decided features associated with the current signal gathered during the arcing process. These features are associated with the higher order harmonic content of the current signal. Comparative analysis of the higher-order harmonic content in the arcing current as obtained from the test-bench and that from contemporary mathematical models for low-voltage arcing faults is presented to validate the choice of parameters for the spectral

signature. The extracted features are utilized for classifying the severity of the motor coil arcing fault using the approaches mentioned above.

That apart, Support Vector Machines have gained tremendous popularity in the last decade or so in the field of pattern recognition, classification and regression applications. The dissertation also presents the approach, implementation and results associated with the utilization of one-class and multi-class SVM techniques for the classification of motor coil arcing fault severity levels. The data pre-processing, filtering and feature extraction process do remain the same as that utilized for SAM, SID and LDA techniques. However, the Gaussian Kernel function has been utilized to map non-linear scatter spread on to a higher dimension Euclidean space H. The training data is utilized to construct the SVM classifier the parameters of which, such as Lagrangian multipliers, the bias, the penalty factor and the number of support vector machines are utilized to test the accuracy of the SVM classification algorithm on the test data. Detailed elaboration on the technique, the implementation methodology and the results has been provided in relevant sections.

The performance of the classification approaches has been evaluated based on the accuracy of classification, robustness and feasibility of implementation of the approach. The classification results seem very promising in terms of accuracy and feasibility of approach for real-time implementation.

TABLE OF CONTENTS

Appendix

LIST OF FIGURES

LIST OF TABLES

CHAPTER 1

INTRODUCTION

1.1 Background Information

Arcing faults have been a primary cause for concern for the manufacturing industry and safety personnel alike. Apart from the fact that it is the primary cause of serious injuries to electrical workers worldwide, arcing faults directly affect the quality and continuity of electric power to the consumers. A great amount of technological advancement has taken place in the development of arc resistant/proof switchgear and Personnel Protective Equipments (PPE) over the last couple of decades. However, a majority of these applications and/or developments focus on minimizing the damage after the occurrence of the arcing fault. The problem associated with the compromise on the quality and continuity of electric power in such a scenario still awaits a technical as well as economically feasible solution. Despite modern advances in power system protection and the adoption of the National Electrical Code (NEC) Section 230-95 working personnel continue to be injured and/or killed from arcing faults initiated by accidental physical contact or through glow-to-arc transition [1]. The deregulation of the power industry being in full swing and ever-growing competitiveness in the distribution sector calls for the transition from preventive to predictive maintenance.

A majority of research documented in this dissertation focuses on the design, development and implementation of novel algorithms that may facilitate this transition

preventive to predictive maintenance, albeit within a laboratory environment. While a majority of the test-benches utilized to mimic the generation of arcing faults at various power system locations have been developed within a controlled laboratory environment, the validity of the resulting arcing fault currents has been verified by means of mathematical model simulation and comparative analysis techniques.

The ensuing sub-sections comprising this section discuss the electrical and physics aspect associated with arcing faults thereby defining and conceptually elaborating on the basics of the arcing fault. Apart from that, the ensuing sub-sections also discuss the historical evolution of arcing faults and the associated research and development for the detection and/or mitigation of arcing faults at the low/medium-voltage levels. The sub-section finally concludes by encapsulating the realistic hazards associated with arcing faults usually encountered at the low/medium voltage level.

1.1.1 Arcing Fault – Definition & Concept

The issue of arcing faults and the widespread concern surrounding the consequences of arcing faults has gained significant ground over the last decade or so. By definition, an arc fault is an unintended, self-sustaining discharge of electricity in a highly conductive ionized gas, which allows current flow between the conductors, limited only by circuit parameters that are predominantly resistive [2]. In other words, an arc is an electrical discharge flowing between two electrodes through a gas or vapor [3]. Figure 1.1 shown below depicts the 3 distinct regions of an arc namely the anode, the cathode and the positive column [2]. The majority of the voltage is seen across the

cathode whereas the anode usually experiences a much smaller voltage drop and the voltage gradient across the positive column remains fairly constant.

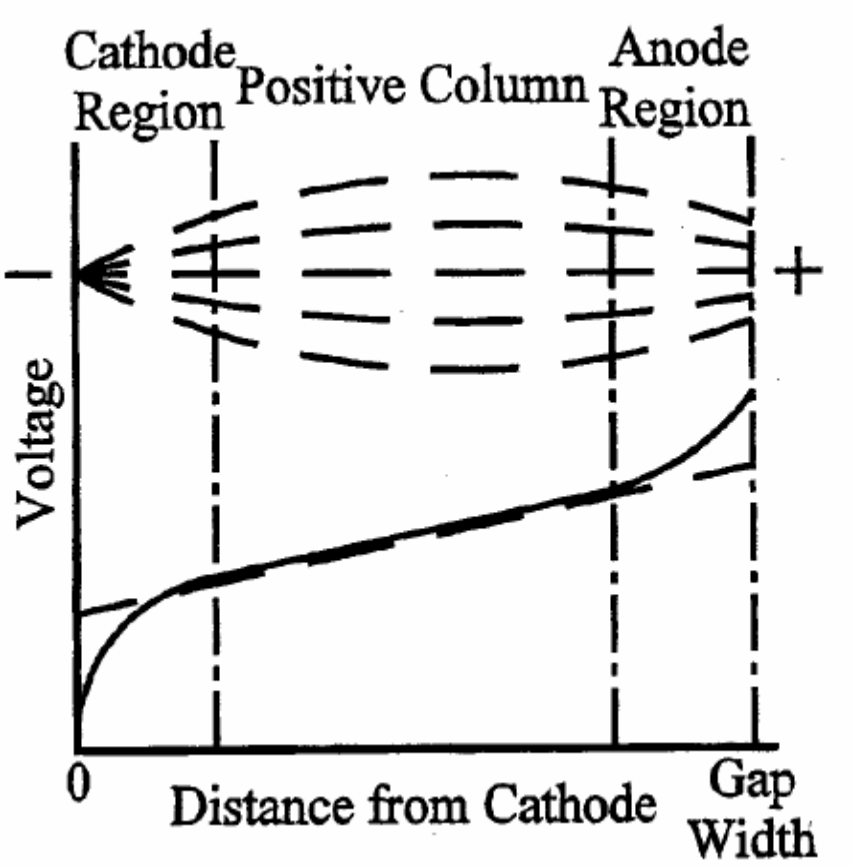

Figure 1.1: 3 Distinct Regions of an Arc [3]

Arc initiation can primarily occur due to the following 3 causes:

- Spark Discharge – A transient spark discharge does possess the capability of initiating an arc if the potential associated with the spark is large enough to ionize the air between the 2 conducting electrodes.
- Accidental Physical Contact – This method of arc initiation is probably the most common one when focusing on the low-voltage arcing faults.

- Glow-to-Arc Transition – The “glow” and the “arc” are basically 2 different stages with the former being characterized by relatively high voltage low current flow and the latter being characterized by low voltage and higher current flow. The transition of the glow to the arc stage occurs when a great number of electrons are released from the cathode normally occurring due to impurities, scratches or presence of local hot-spots on the electrode surface.

Gammon and Mathews discuss the arc initiation methods in more elaborate details in [3]. The arc, once extinguished, requires a certain potential termed as the “re-strike” potential in order to re-ignite. Once the re-strike potential has been achieved the arc re-ignites with the arc current flowing with opposite polarity. Although some mathematical models, such as Kauffman & Page, utilize a constant re-strike potential, research in this area over the years has pointed to various factors contributing to the determination of the re-strike potential. Some common factors influencing the re-strike potential are the level of ionization, environment of arc space and the conditions at the electrode. An elaborate discussion associated with the re-strike potential for arcing faults and influencing factors is presented in [4].

Some relevant and important industry standards concerning the prevention of arc and/or arc flash incidents are:

- OSHA 29 Code of Federal Regulations (CFR) Part 1910 Sub-part S.
- National Fire Protection Act (NFPA) 70-2002 NEC

- NFPA 70E-2000 Standard for Electrical Safety Requirements for Employee Workplaces
- IEEE Standard 1584-2002 Guide for performing Arc Flash Hazard Calculations

With a basic understanding of the electrical and physical concepts associated with arcing faults (with specific focus of low-voltage systems) and the definition of various key terms associated with arcing faults under the belt, the ensuing sub-section deals with the historical evolution of mathematical models utilized to represent the arcing faults in low-voltage systems.

1.1.2 Historical Evolution of Arcing Fault Models

This sub-section endeavors to summarize the rapid strides made in the modification of existing and/or development of new mathematical models to define the arcing faults thereby facilitating a better understanding of arcing faults. While arcing faults have been identified as a potential hazard at low-voltages since as early as the 1920s, the incidents relating to arcing faults began to rapidly increase starting in the 1960s. It was during this era that the electrical system underwent a metamorphosis in order to meet the ever-increasing system demands resulting in drastically increased number of arcing fault incidents at low-voltages [3]. It was during this time frame that the research and industry personnel started paying their attention on the development of mathematical models adequate enough to represent real world arcing faults in low-voltage systems.

Although the low-voltage arcing was mostly encountered at the 480Y-277 V level, numerous cases of devastating fires breaking out due to arcing faults at the 208Y-120 V level were encountered during this period. The late 1920s and the early 1930s saw a considerable increase of interest in the re-strike voltage, a crucial factor in the development and sustaining of the arcing faults. By early 1940s, certain trends were being associated with the arc-voltage with the first characterizing it as a flat-topped voltage with the arc current being a fixed percentage of the available short-circuit current [5]. While research further down the years has clearly proven otherwise identifying that the arc current magnitude is clearly variable with the gap width and impedance of ground path being key factors in determining the magnitude of arc current, it signaled the beginning of an era that would see many rapid strides made in the modeling of arcing faults for low voltage systems.

Over the period from 1960 through the early part of 2000 witnessed numerous models and/or modifications to models in a constant endeavor to accurately represent the arcing faults in low voltage systems spanning a period of over 3 decades. Some significant low-voltage arcing fault models published during this period include:

- Instantaneous model to predict the arc current in purely inductive systems by Kauffman & Page (1960);
- Differential equation-based model for arcing faults by Conrad & Dalasta (1967);
- Model to predict r.m.s arc current without any assumption on arc voltage by Fisher (1970);

- Curve-fit based damage indicator model by Stanback (1975);
- Research work presenting role of arcing in residential fires by Beland (1980s);
- Finally, generalized instantaneous arc fault model for resistive-inductive systems by Mathews (1993);

While details associated with each of these mathematical models is beyond the purview of this document, the same is presented in elaborate detail in [3]. However the relevant and contemporary generalized instantaneous arcing fault models utilized for comparative analysis have been discussed in detail in the ensuing chapters of the dissertation.

While witness the significant development in research associated with arcing fault models of low-voltage systems for the past several decades, it would important to place this research and its application in perspective. A majority of the aforementioned research and development was and to a certain extent still is focused on the estimation of arc fault current magnitudes for various commercial, industrial and residential facilities in order to develop suitable arc resistant protective systems to minimize the damage in the eventuality of the arcing fault.

As would be evident in the proceeding sub-section the 4 decades spanned in the discussion above witnessed tremendous instants of catastrophic damage initiated due to arcing faults a great percentage of which are still applicable to the current situation.

1.1.3 Low-voltage arcing faults: Associated Hazards

The hazards associated with arcing faults ranging from low to medium to high voltage levels, are widespread in terms of varied applications where extensive power system networks are utilized.

One such area that had until recently been plagued with frequent fires due to arcing faults in the switchgear or other aspects of the power system networks is the navy shipboard systems. The realization that electrical fires, originating from arcing faults, were occurring with alarming regularity dawned in the 1970s with a great percentage of these being located in the main electrical distribution switchboards of the submarine fleet. Main submarine electrical switchboards conduct thousands of amps over bare copper bus bar 1–12 inches wide and 0.25–1 inch thick. Large circuit breakers control the flow of current to remote loads and smaller switchboards. An arc of several hundred amps can exist and not cause a breaker to open since normal loads draw much higher current. The arc is not a short across the circuit, but a resistive load yielding heat; therefore, the breakers do not open. Faulty connections due to corrosion, faulty initial fastening, vibration, etc., cause 60–80% of arcs. Contamination and foreign objects can also be a possible reason for the initiation of the arcing faults [6]. Figure 1.2 depicts the extent of damage caused by an electrical fire in one of the main distribution switchboards of the naval power systems.

Figure 1.2: Damage from arc-initiated fire in navy shipboard systems [6]

Another such critical field in which arcing fault protection is considered of extremely high priority is the aeronautical systems or the aircraft power systems. With limited isolation and fire extinguishing capabilities while in flight, the presence of an arcing fault on-board a flight could pose a major threat to personnel, tremendous financial and physical damage. The gravity of the situation was summarized by the development of the Aging Aircraft Integrated Product Team which developed the Arc Fault Circuit Breaker (AFCB), a technology developed jointly by the navy, FAA, and the industry to protect aging aircraft from arc fault related problems [7]. [7] discusses in elaborate detail the design, development and the testing of the AFCB prototype in operational aircraft environment.

Arcing faults between conductors produces light and heat and is blamed for a residential and/or commercial electrical fire every five minutes in the United States. These are low power arcs of a few amps on a 115 VAC circuit [9]. Arc fault generates

large amounts of heat that can severely burn human skin and set clothing on fire when occurring in residential premises. Temperatures at the arc can reach four times the temperature of the sun's surface thereby posing greatly increased personnel safety threat. Any exposure to an arc flash frequently results in a variety of serious injuries such as severe burns, damaged eyesight, ruptured eardrums, collapsed lungs, psychological trauma and in some cases – death. Arc flash hazards pose another concern, that of liability and government regulations. On average, approximately 5 to 10 arc flash explosions occur on the job every day in the United States.

The discussion presented in the sub-section above, clearly underlines the hazards associated with arcing faults for low to medium to high voltage levels with specific focus on low voltage arcing faults. While this section focused more on providing an overview of arcing faults, the conceptual explanation and definitions, prevalent and relevant standards, historical evolution of arcing fault current models and the hazards associated with the arc faults, the following section focuses on the definition of the problem at hand along with a clearly outlined objective.

1.2 Definition\Significance of Problem

Apart from the varied nature of the fault itself, the diversity of the causes of the arcing faults compounds the problem associated with the mitigation of these faults. As is a well known fact, the current inside of an arc is not always high enough to trip a regular circuit breaker. In cases where the arcing current is large enough to do so, the time that has elapsed in the development of the arcing energy proves catastrophic. In the

former scenario where the arc current levels are lower than the regular breaker ratings, an arc fault adds to the existing load current causing a fast three-phase imbalance. In case it is large enough for the breakers, the breakers have not been found to be fast enough to prevent a catastrophe.

The basic objective motivating the research documented in this dissertation comprises of the transition of arc fault detection and classification methods from preventive to predictive in nature. In other words, while a majority of the research documented in this field currently focuses on minimizing damage after the occurrence of the fault by adequately designed mitigation/protection equipment based on mathematical models and simulations, the objective behind the research in this dissertation aims to develop novel algorithms to detect and/or classify/categorize these arcing faults. Arcing faults in two major low-voltage power system components have been focused on namely:

- *Switchgear*

As is evident from the discussion presented above, the issue of arcing fault presents itself as rather challenging engineering problem to the power and manufacturing industry alike. The research under this area focuses on the design, development and implementation of a novel methodology for the detection of arcing faults (to ground) within low/medium voltage switchgear. As mentioned above, the arcing fault differs from other short-circuit phenomenon in that the current levels need not necessarily be high enough for traditional protective equipment to be effective. The initial sections in this chapter focus on providing conceptual details associated with the

phenomenon of arcing and the relevant definitions thereof. This chapter also endeavors to provide the reader with the hazards associated with arcing faults in the normal day to day operation of residential, commercial and industrial power systems thereby underlining the industrial application and relevance of the research documented in this dissertation.

Hence the definition of the problem with respect to the switchgear arcing faults comprises of the following:

- Design an innovative test-bench capable of re-producing low/medium voltage switchgear arcing faults within a controlled laboratory environment.
- Develop and realize the test-bench in the Power System Simulation Laboratory, Energy Systems Research Center (ESRC).
- Identify unique characteristics associated with the arc fault current that can be utilized for the following:
    - Corroboration of the validity of the arc fault current characteristics by means of a comparative analysis of the identified characteristics between the laboratory model and mathematical model.
    - Design of novel algorithm(s) to detect the presence of arcing faults in low/medium voltage switchgear.
- Implementation of the aforementioned novel algorithms to the arc fault

current signature obtained from the laboratory test-bench in order to evaluate the performance of the algorithm(s)

- Corroborate the versatility of the proposed algorithms by testing them under simulation and actual field-like conditions

- *Motor Coil*

While the issue associated with low/medium voltage switchgear arcing faults revolves more around detection of the fault, the problem definition associated with motor coil arcing faults focuses more on classification of severity of arcing faults. The primary reason for that is that mere detection of the presence of arcing fault in a motor coil may not be sufficient to mitigate the arcing fault as would have been possible in the case of the switchgear and hence the a more complex problem of classifying the severity of the motor coil arcing fault in terms of the percentage of the coil shorted through the arc has been dealt with in this dissertation. Hence the definition of the problem with respect to the motor coil arcing faults comprises of the following:

- Design an innovative test-bench capable of re-producing low voltage motor coil arcing faults within a controlled laboratory environment.
- Develop and realize the test-bench in the Power System Simulation Laboratory, Energy Systems Research Center (ESRC).
- Identify unique characteristics associated with the arc fault current that can be utilized for the following:
    - Corroboration of the validity of the arc fault current characteristics by means of a comparative analysis of the

identified characteristics between the laboratory model and mathematical model.

    - Design algorithms, utilizing 4 distinct statistical techniques, to classify the severity of the motor coil arcing fault based on the aforementioned pre-identified unique characteristics.

- Assess the performance of each algorithm thereby thoroughly investigating the merits and/or demerits of each statistical technique in classifying the severity of the motor coil arcing fault.
- Perform comparative analysis of various classification algorithms in order to zone in on the most optimal classification technique based on a pre-identified performance evaluation matrix.
- Implement the chosen algorithm, justified as the most optimal classification algorithm, for real-time classification of motor coil arcing faults in LabVIEW.

Each of the aspects discussed in this sub-section is dealt with in elaborate detail in the relevant ensuing chapters and/or sections of this dissertation. The following section provides an overview of the organization of the dissertation with a broad perspective on the aspects covered in each chapter/section.

1.3 Organization of Report

The dissertation documenting the various aspects of the research carried out to tackle the problem defined in the previous section primarily comprises of 5 chapters.

The first of the five chapters, of which this section is a part, primarily consists of providing the reader with background information required to educate oneself with the exact nature and significance of the problem that this dissertation endeavors to address. This chapter primarily comprises of providing background information relevant to the research being discussed in the dissertation to educate the reader with the significance of the dissertation. The chapter also serves to set the foundation in terms of elaborating o the conceptual explanation of the arcing fault phenomenon and its significance in the residential, commercial and industrial power systems. Furthermore, the chapter outlines the objective and the motivation behind the research pursued for the dissertation and clearly defines the problem being encountered in the dissertation.

The second chapter aims to address the first 2 important research aspects spanning the dissertation, namely low/medium voltage switchgear arcing faults. The initial sections of the chapter focus on providing a basic overview of the problem at hand and the proposed approach to be utilized for the detection of low/medium voltage switchgear arcing faults. The following section focuses on the design and development of the hardware required to re-produce switchgear arcing faults like those in actual field conditions. This section presents all the design details associated with the development of the hardware keeping in mind that the production of the arcing fault would take place in a controlled laboratory environment.

The testing and data acquisition procedures adopted in order to record the switchgear arcing fault current signature are discusses in detail followed by the deign f the detection algorithm including the identification of key and/or unique characteristics

utilized for the detection algorithm. The methodology employed to corroborate the validity of the arcing fault current signature with contemporary low/medium voltage arcing fault models via simulation methods is also presented. The entire procedure is repeated for the detection of medium voltage switchgear arcing fault. The chapter concludes with the discussion and analysis of the results associated with the application of the arcing fault detection algorithm on the test-bench developed in the laboratory for both low and medium voltage switchgear arcing faults.

The third chapter deals with the crucial aspect of hardware development associated with the second major aspect of research pursued in this dissertation, namely the motor coil arc fault. As mentioned earlier, unlike the switchgear arcing fault, the problem defined for the motor coil arcing fault focuses more on classification of the severity of the arcing fault instead of mere detection of the presence of arcing fault. In order to do that, the development of the test-bench associated with the re-production of the motor coil arcing fault assumes great significance. This is so since it not only has to be accurate enough to produce an arcing current that corroborates with its mathematical counterpart but also flexible enough to accommodate short varying degrees of the motor coil in order classify the severity of the motor coil arcing fault. This chapter focuses on various design alternatives considered, tested and developed in the laboratory in order to come up with a test-bench design that would meet the criteria discussed above. All details associated with the motor coil arc fault test-bench development have been elaborated upon in this chapter.

The fourth chapter deals with the design and development of novel algorithms

associated with the classification of severity of motor coil arcing faults. The chapter initially discusses the mathematical background associated with each statistical technique identified as a key component for various algorithms for motor coil arc fault classification. The chapter continues to elaborate on the application of each of the statistical technique and the methodology employed to develop the algorithm to be simulated based on each of the statistical technique being employed to classify the severity of arcing faults. The results associated with each of the classification technique are assessed in terms of a comparative analysis in order to evaluate the performance of each of the algorithm in its effectiveness to classify the severity of arcing faults.

The fifth chapter is the concluding chapter of the dissertation and focuses on drawing inferences from the results of the switchgear and motor coil arc fault detection and/or severity classification algorithms developed. The effectiveness of selective algorithms in detecting and/or classifying arcing faults has been showcased. The concluding chapter also spans potential research areas for which the research documented in this dissertation can serve as a foundation or reference basis.

CHAPTER 2

SWITCHGEAR ARCING FAULT

As mentioned earlier, the deregulation of the power industry being in full swing and ever-growing competitiveness in the distribution sector calls for the transition from preventive to predictive maintenance. Switchgear forms an integral part of the distribution system in any power system set-up. Keeping in mind the switchgear arcing faults, the transition mentioned above applies most of all to the switchgear industry. The issue of arcing faults and the widespread concern surrounding the consequences of arcing faults has gained significant ground over the last decade or so. One of the major consequences of this growing concern is the rapid strides made in the mathematical modeling of the arcing fault at low and/or medium voltage levels as discussed in the previous chapter.

As is evident from discussions presented in the previous chapter, the issue of arcing fault presents itself as rather challenging engineering problem to the power and manufacturing industry alike. Certain sections of the previous chapter focused on defining the significance of the problem associated with medium/low voltage arcing faults and the motivation behind the initiation of the research documented in this dissertation. This chapter focuses on the description of a novel methodology for the

detection of arcing faults (to ground) within low/medium voltage switchgear. As mentioned above, the arcing fault differs from other short-circuit phenomenon in that the current levels need not necessarily be high enough for traditional protective equipment to be effective. This approach revolves around identifying the characteristics unique only to the arcing fault and developing a detection strategy employing these unique characteristics. Contrary to traditional detection techniques, higher order harmonics serve as a better indicator in the case of arcing faults to ground. Differential protection concept employing higher order harmonics is utilized for the detection of arcing faults to ground in low/medium voltage switchgear.

Individual laboratory test-benches are designed and set-up for both low and medium voltage testing in the Power Systems Simulation Laboratory at Energy Systems Research Center (ESRC). In the case of medium voltage testing the simulation approach is adopted and data is gathered via hall-effect sensors and data acquisition in LabVIEW during the arcing phenomenon. This data is analyzed to model the medium voltage switchgear arcing fault to ground as a non-linear device and the harmonic differential concept is tested via simulation. The validity of the approach is further confirmed by performing practical laboratory tests for low voltage arcing utilizing harmonic differential approach. The approach provides the right balance between sensitivity to internal faults and discrimination against external faults by the use of both magnitude and phase differential. The description of the concept, medium/low-voltage test-benches, simulation model, results and plots are provided in the pertinent sections of the chapter.

2.1 Relevant Research

As mentioned in the previous chapter, a majority of the research associated with arcing faults in low/medium voltage switchgear during the 1980s and early nineties has been geared towards the re-enforcement of the mechanical aspects associated with the switchgear in order to minimize the damage following the occurrence of the fault. The previous chapter along with the discussion also provides ample literature reference associated with the developments in terms of preventive maintenance for switchgear arcing faults. As mentioned in the opening stages of this dissertation, such action classifies as preventive maintenance in comparison to novel early warning and sophisticated detection approaches presented in this dissertation which endeavors to transition to predictive maintenance.

Having said that, some arc low/medium voltage switchgear arcing fault detection research has been documented during the last decade or so. A discussion in [41] cites the commercial availability of several switchgear arc monitors which can be used to detect the presence of arcing faults in switchgear and respond quickly to isolate the power source, The first of these arc monitors refers to a photocell type arc monitor with a response time of 1ms coupled with modern breaker interrupting times to disconnect the power source within 30ms. [42] elaborates in detail on the monitor based on the photo-cell concept wherein one of the most striking and fastest physical variables associated with arcing is utilized for the detection of the fault conditions. [42] detects the light produced during the arcing conditions by means of specially developed light

sensor spheres facing each cladded compartment of the switchgear panel. These light sensor spheres exhibit uniform sensitivity in all directions of the hemisphere [42].

"The light is conveyed by fibre-optics light conductor to an evaluator and converted into a digital signal by photodiodes and AID converters. The signal is evaluated using an algorithm that incorporates auxiliary signals so as to permit unambiguous differentiation between an arc and any interference signals in order to achieve maximum reliability even where light interference signals are involved. The new arc detection system for type-tested medium- voltage switchgear makes it possible to minimize the potential duration of an arc and hence its destructive effect, resulting in enhanced safety for the switchgear environment" [42].

The other type of arc monitor comprises of utilizing a pressure switch thereby employing the change in pressure due to release of various gases during arcing fault conditions to detect the presence of switchgear arc fault conditions [41]. [43] presents a detailed discussion associated with the utilization of pressure based monitor to detect the presence of arcing faults in switchgear. The approach presented in [43] endeavors to keep in mind that the arc monitor much respect selectivity and discrimination against external faults while trying to minimize damage during internal faults. The approach primarily utilizes an array of pressure sensors installed at various locations in the switchboard. These pressure sensors are activated by a pressure wave which seems to occur during the 1st 20 msecs of the arcing fault. The activation of the pressure sensors instantaneously trip the circuit breakers feeding the fault thereby isolating and mitigating the arcing fault thereby minimizing damage [43]. While this approach does

endeavor the detection of arcing fault, the underlying objective is still preventive in nature trying to minimize damage associated with arcing fault.

A case in point furthering the cause of transition from preventive to predictive maintenance is presented in [44]. Documentation in [44] seems to suggest that while re-enforcement actions such as the use of un-insulated conductors, substantial relief flaps, presence of double-skin on enclosures to prevent burn through during arcing fault, high integrity sealing of all chambers to prevent "leakage" and suitable ducting for release of exhaust gases may reduce the damage during the presence of arcing fault, they do not reduce the likelihood of arcing fault or increase the chances of detecting the arcing fault to prevent the damage [44]. The value of the proposed approach utilized to detect switchgear arcing faults utilizing higher-order harmonic differential approach assumes great significance in the wake of such references.

[45] presents an on-line condition monitoring system associated with 12kV voltage switchgear. The on-line condition monitoring system aims to monitor the conditions of the bushings, the temperature rise of the detachable contacts and the mechanical performance of the switchgear. The proposed approach documented in [45] basically aims to monitor the over-all "health" of the switchgear in terms of its operational condition.

As would be evident from the discussion presented in the section above, apart from the developments in re-enforcing the mechanical aspects and enclosure associated with the switchgear, developments on the detection front seem to focus more on utilizing the physical properties of the arc such as light emission and pressure release

through gases. The novelty associated with the approach presented in this dissertation lies in the utilization of electrical properties in the arcing fault current, namely the higher-order harmonics, in conjunction with differential approach to develop an early warning system. Furthermore, the proposed approach and the associated results presented at relevant sections of this dissertation seem to indicate great potential in terms of accurate detection of arcing faults in switchgear thereby allowing the first step towards predictive maintenance in the switchgear industry.

2.2 Medium voltage switchgear arcing fault detection

The discussion in this section of the chapter primarily revolves around the design, development and implementation of a novel approach for detecting the arcing fault in the medium voltage switchgear. The following aspects are discussed in elaborate detail during the course of the discussions presented in this section:

- Design & development aspects associated with laboratory test-bench capable of producing medium voltage arcing faults in order to replicate actual field conditions;
- Identification of characteristics unique to the arcing fault and the design of a novel approach to detect the presence of arcing faults at medium voltage levels, if any;
- Operational testing and acquisition of medium voltage arcing current data under controlled laboratory environment;

- Utilization of the acquired arcing current data to model a medium voltage arcing fault on a small-sized sample 18-bus radial distribution system in order to evaluate the performance of the proposed algorithm under simulation environment;
- Comparative analysis of the arcing fault modeled above with contemporary mathematical models for arcing faults based on the unique pre-identified characteristics;
- Demonstration of effectiveness of proposed approach to detect medium voltage arcing faults by simulation results;

2.2.1 Approach Overview

This sub-section provides a basic overview of the approach outlined for the detection of medium voltage arcing faults through the utilization of actual hardware testing and/or simulation techniques. The medium voltage switchgear arcing fault to ground is simulated by producing an arc via an arcing device at about 15kV level. An induction motor load is connected in parallel to the arcing device to simulate normal loading conditions in the distribution system. An auto-transformer and a 120V/15kV single-phase step-up neon transformer are employed to obtain the required voltage levels for the arcing device. Hall-effect sensors are employed to pick up the line current during the arcing phenomenon. In order to simulate actual field conditions, the hall-effect sensors have to be placed on the high voltage side of the step-up transformers to capture actual arc fault current signatures.

The proposed conceptual approach to detect the presence of arcing faults in medium voltage switchgear revolves around the utilization of the differential protection principle, albeit with some modifications. The principle of traditional differential protection employs the fundamental current magnitude and phase angle of the incoming and outgoing currents to detect the presence of anomalous and/or short circuit conditions in the network under question. The differential protection principle as applied for the detection of the medium voltage arcing faults differs from its traditional counterpart in that it utilizes a characteristic unique to the arcing faults as the base input. As would be evident from some preceding sub-sections, while one cannot "order an arcing fault", thereby adding to it diverse nature, irrespective of the nature, voltage level and the model of the arcing fault being analyzed, the arcing current contains higher-order harmonics due to the very physical nature of arcing phenomena. It is this unique characteristic, namely the higher-order harmonics that are utilized as the unique characteristics to be employed as the base input for the proposed differential approach. In other words, a higher-order harmonic differential approach is proposed for the detection of the medium voltage arcing faults.

The hall-effect sensor information is employed for the implementation of the afore-described differential scheme which is primarily utilizing the higher order harmonic magnitude and phases to detect the presence of arcing fault. The methodology adopted for implementing the approach is split into two phases namely the simulation phase (medium voltage arc testing) and laboratory test bench phase (low voltage arcing). As would be evident, the simulation phase would be the focus of discussion in this section

since it deals with the detection of medium voltage arcing fault with the test-bench phase being discussed in ensuing sections of this chapter. However, both done, it allows for comprehensive testing of the higher harmonic differential approach adopted for switchgear arc detection.

The simulation approach employed for the case of medium voltage arc detection is discussed in its entirety in this section. The hall-effect sensors are placed on the high/secondary side of the 120V/15kV single phase step-up transformer. The output signal from the hall-effect sensor is monitored and recorded via data acquisition using LabVIEW. This signal provides great insights into the characteristics of the arcing fault to ground current. Based on the harmonic analysis performed on this signal, a non-linear source producing exactly the same harmonics in terms of magnitude and phase is modeled to represent a switchgear arcing fault to ground in a sample 18-bus distribution system. A comparative analysis of the arcing fault model developed in the laboratory with the contemporary mathematical models for arcing faults is also discussed. The arcing fault is then modeled as a non-linear source placed at strategic locations in a sample 18-bus radial distribution system with the non-linear source having the same harmonic characteristics as derived from the harmonic analysis of the arcing current signaled acquired from the laboratory test-bench. The sample 18-bus system is then simulated with the non-linear source (arcing fault) at internal and external locations with respect to harmonic current differential scheme applied at one particular location. Simulations are performed with and without the power factor correction capacitors to compare the performance of the differential scheme under conditions as close to the

field conditions as possible. The ensuing sub-sections discuss the test-bench, switchgear arc fault (to ground) modeling, simulation process and results in their entirety.

2.2.2 Hardware Development

2.2.2.1 Test-Bench: Design & Development

In order to test and showcase the performance of the higher-order harmonic current differential scheme for medium voltage switchgear arcing fault (to ground) with precision, an accurate laboratory model for arcing fault was developed.

As mentioned earlier, a dedicated test-bench was set up in the Power Systems Simulation Laboratory at Energy Systems Research Center for this purpose. A basic schematic of the test-bench is shown in Figure 2.1. As is evident from the schematic, 208V three-phase supply is used to feed the three-phase induction motor which represents the normal loading on the system. 20A circuit breakers are employed to isolate the main power supply from the test-bench. Single pole double throw switches are employed to bring the arcing device (connected in parallel to one of the phases) into play to replicate the arcing phenomenon in the actual switchgear. As can be seen from the schematic, the arcing device is connected on the secondary side of autotransformer and 120V-15kVstep-up neon transformer.

Figures 2.2, 2.3 and 2.4 depict the actual laboratory test-bench developed in Power Systems Simulation Laboratory at ESRC. Figure 2.2 below provides a complete overview of the testing facility showing the normal load (3-phase induction motor, protective equipment) arcing and data acquisition facilities.

In actuality, the hall-effect sensors being employed for the current differential should be connected at the locations of *CT1* and *CT2* in the schematic. In the event of an arcing phenomenon in that case, the current passing through hall-effect sensor #1 (CT1) would comprise of the load current for the 3-phase induction motor and the arcing currents. Depending on the nature and magnitude of the impedance of the load, the current seen by CT2 would also include the load current and some arcing currents.

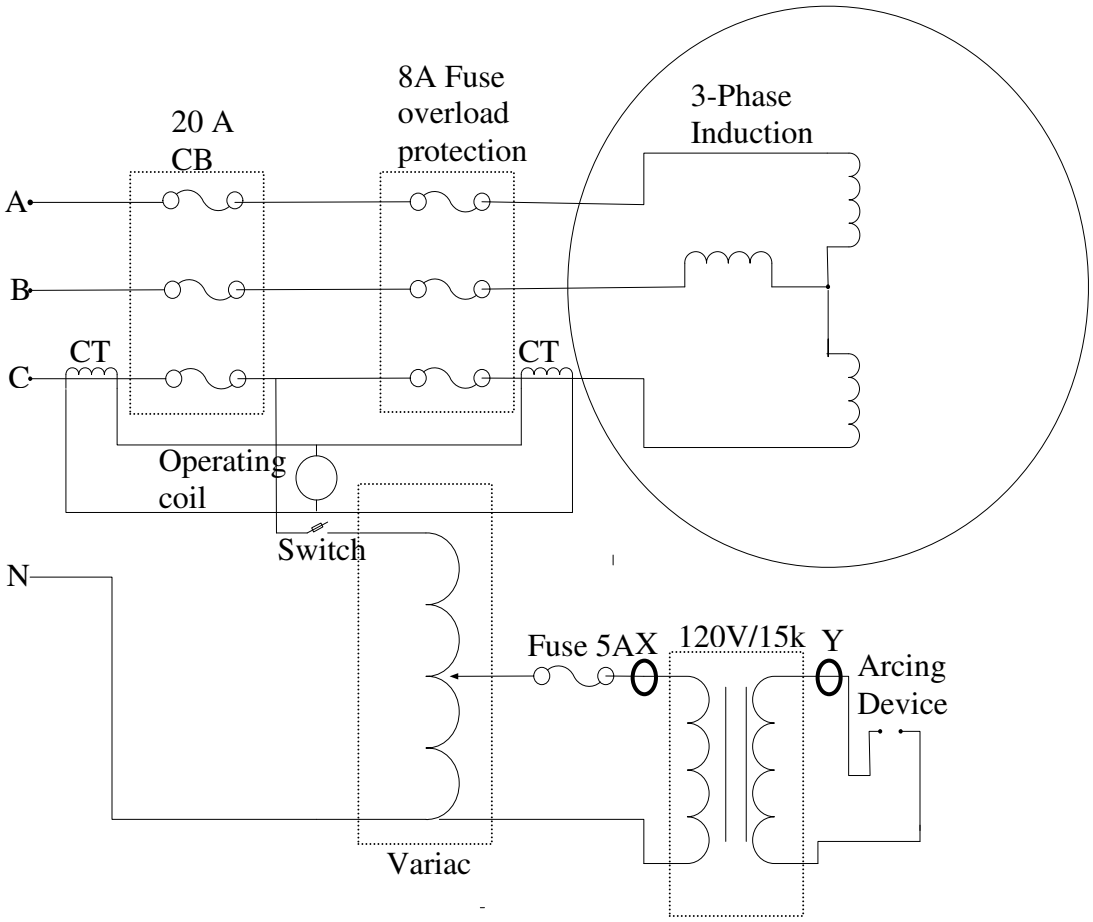

(X: Primary Side Hall-Effect Sensor Y: Secondary Side Hall-Effect Sensor)

Figure 2.1: Schematic for Medium Voltage Switchgear Test-bench

The load currents would get cancelled out in the differential set-up, and the arcing components of the arcing current would be extracted out for possible arcing and/or partial discharge detection. In either case, the current seen by the two CT's would have different phase angles. Depending on the impedance of the arcing fault, either magnitude or phase angle differential could be employed for fault detection.

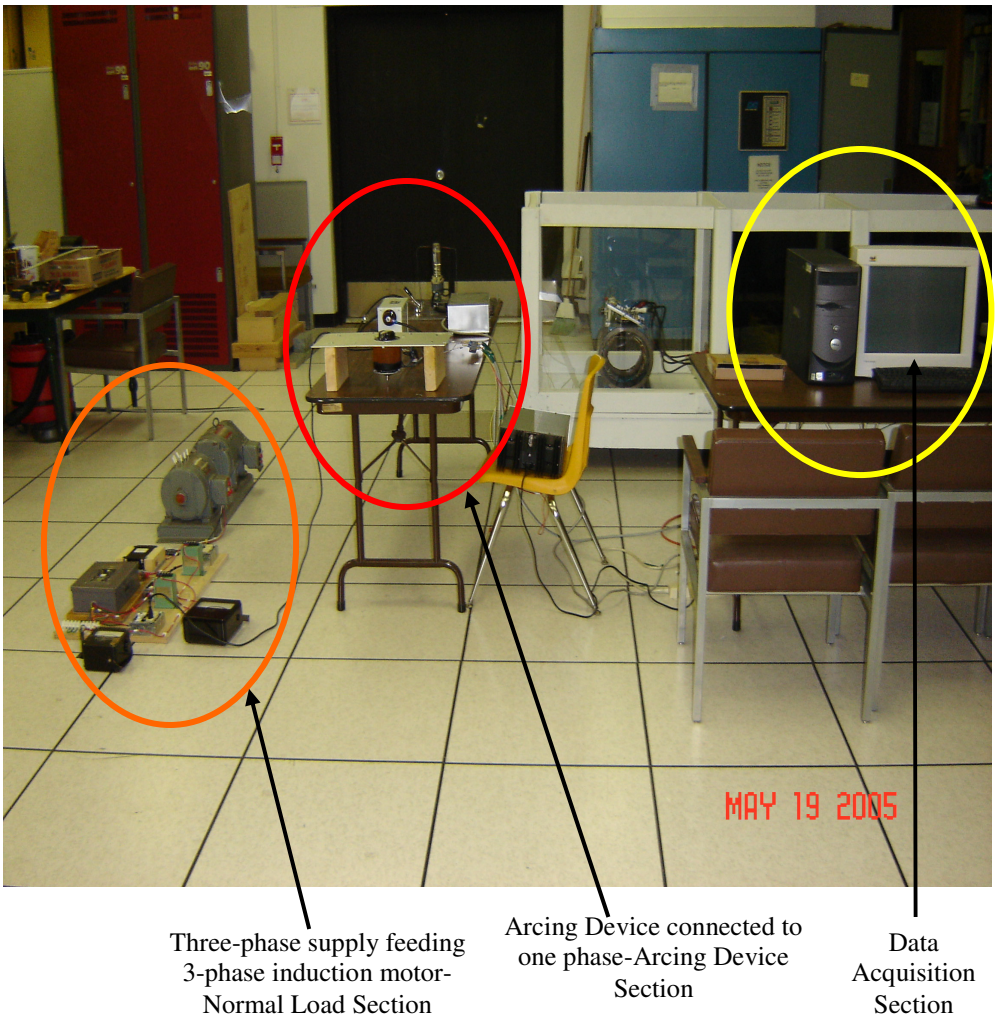

Figure 2.2 Complete Overview of the Test-Bench developed in Power System Simulation Laboratory

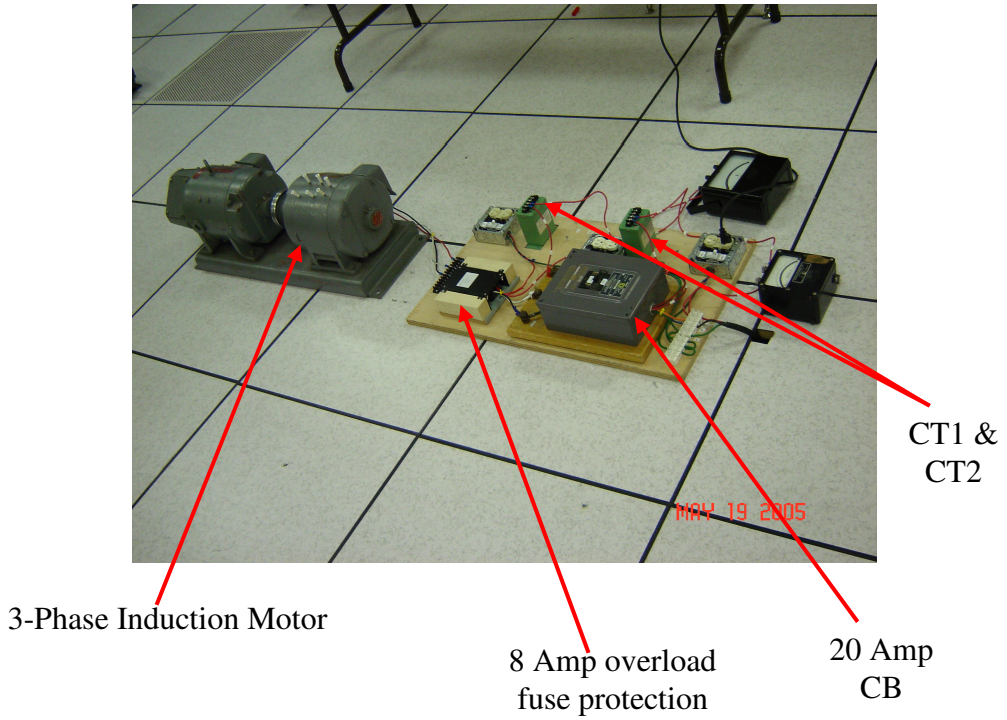

Figure 2.3: Normal Load Section: CT's and Protective Equipment

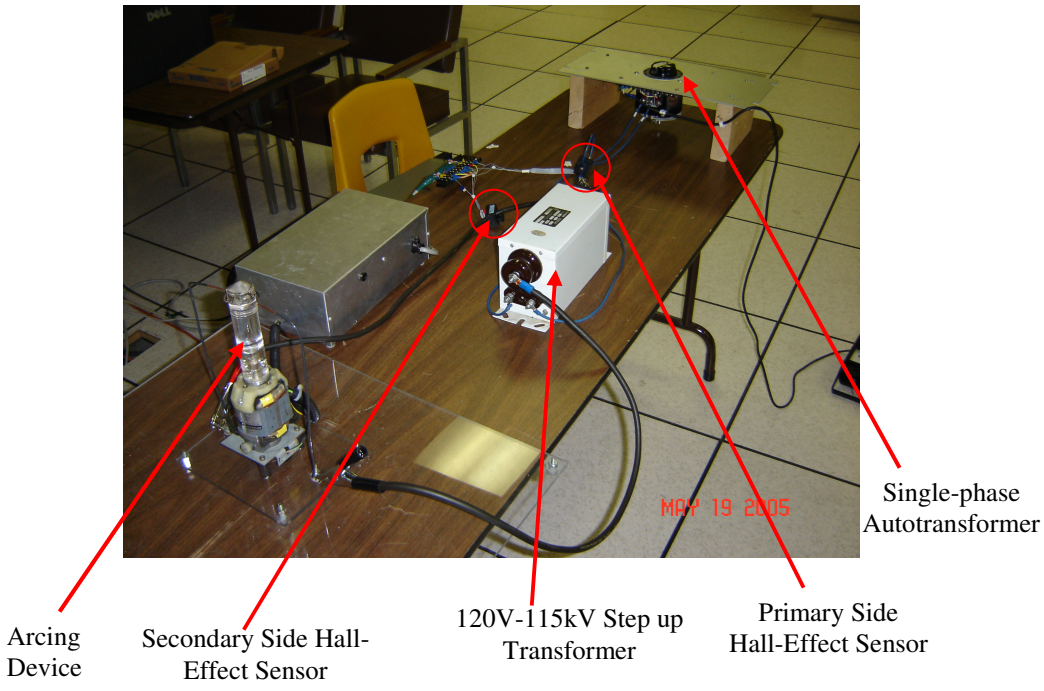

Figure 2.4: Medium Voltage (15kV) arc fault generation test-bench set-up

However before carrying out any comprehensive tests on the afore-described test-bench, simulation approach was utilized to verify the conceptual validity. For this purpose, hall-effect sensor #1 was placed close to the location of the arcing fault (on the secondary side of the transformers) to observe the harmonic content of the arcing current. The second hall-effect sensor on the other hand was placed on the line side (primary side of the transformers) to observe the effect of the transformers on the harmonic contents of the arcing current. This configuration of hall-effect sensor connections is clearly shown in Figure 2.3.

As can be seen from Figure 2.1, in order to emulate actual field conditions the harmonic current differential scheme should be incorporated on the line side. This scenario is replicated in the simulation process wherein a sample 18 bus system is analyzed in the presence of a non-linear harmonic source the behavior of which very closely represents that of the arcing fault in terms of harmonic composition. With hall-effect sensors placed on the primary and secondary side of the step-up transformer, the data for the arcing fault current is acquired and stored using LabVIEW. The objective behind this exercise is to be able to gather enough information about the composition of the arcing current in terms of harmonics to be able to model a non-linear load to represent the arcing phenomenon for simulation purposes.

It would be evident from the above discussion that the test-bench utilized for the generation of medium voltage arcing fault is designed to replicate actual field conditions as accurately as practically feasible within the confines of the laboratory environment. Apart from accuracy, aspects such as robustness and flexibility in design

to allow the replication of various arcing fault phenomenon as occurring in actual field conditions are taken into account during the design of the test-bench.

2.2.2.2 Testing & Data Acquisition

The performance of the test-bench described in the preceding sub-section is tested by the generation of arcing fault at the 15kV level. The testing procedure is accompanied with the utilization of the data-acquisition set-up to acquire the arcing fault current data to be utilized for modeling of the arcing fault as a non-linear source in the sample 18-bus system and further simulation processes. As mentioned earlier, a data acquisition module was developed in LabVIEW to record the nature of the arcing current on the primary and secondary side of the transformers. The objective behind this exercise is to be able to gather enough information about the composition of the arcing current in terms of harmonics to be able to model a non-linear load to represent the arcing phenomenon in a sample 18-bus radial distribution system for simulation purposes. The primary justification for employing hall-effect sensors instead of current transducers is the ability of the hall-effect sensors to be effective over a wide range of frequency. This allows us to capture information associated with higher order harmonics that maybe present in the arcing current.

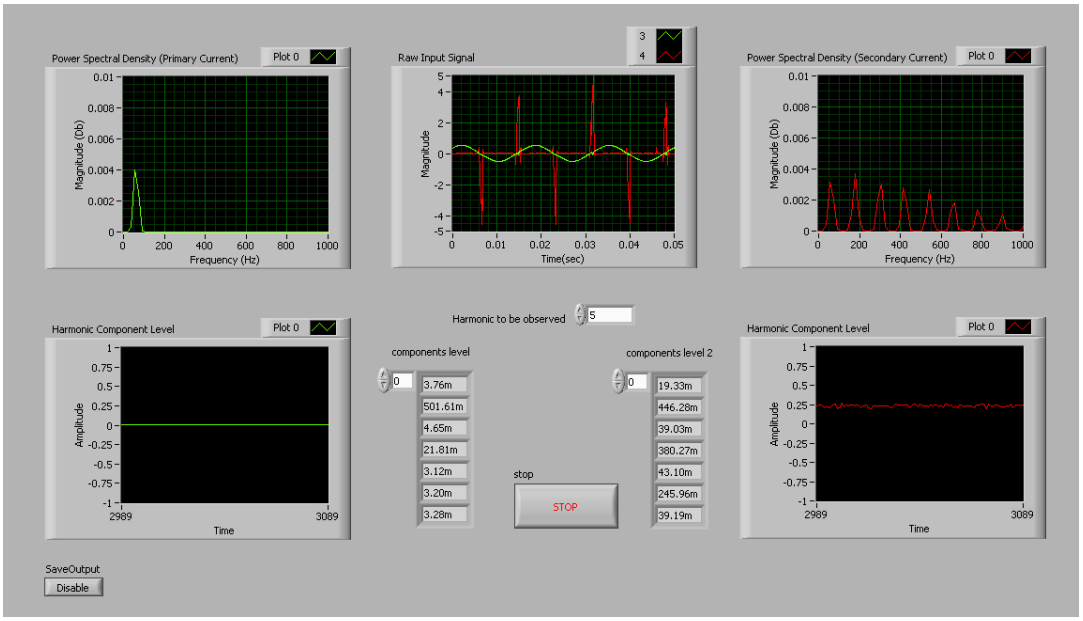

(a)

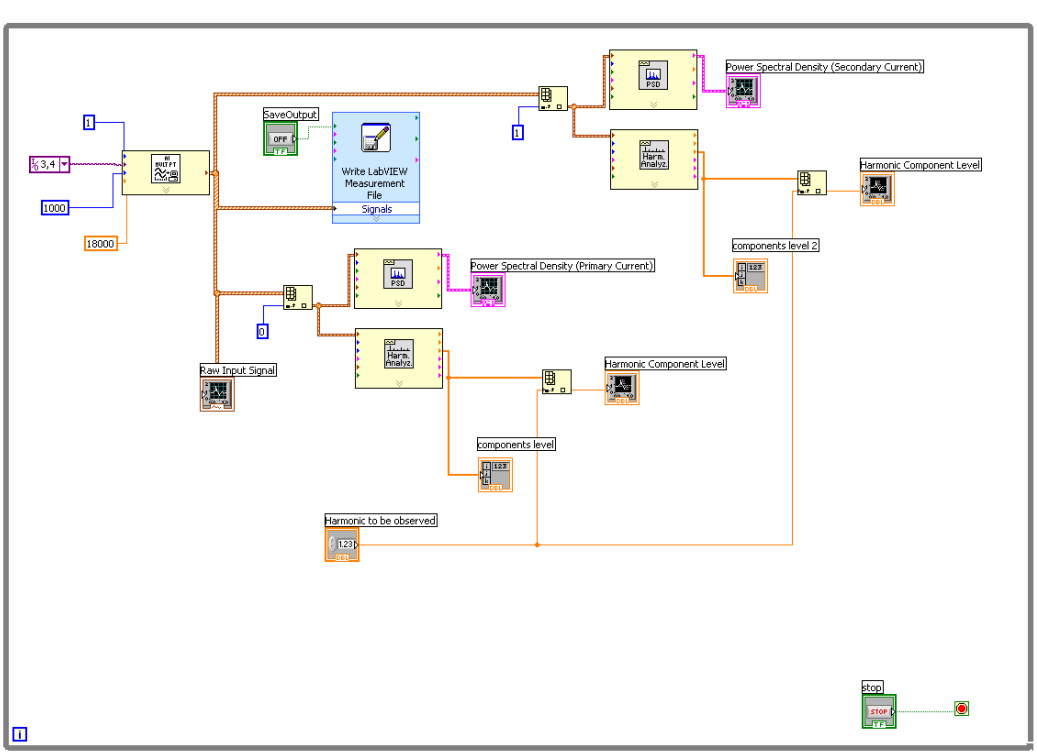

(b)

Figure 2.5 (a): Front Panel for Data Acquisition of Primary & Secondary Arcing Current (b): Block Diagram for Data Acquisition of Primary & Secondary Arcing Current

Furthermore, frequency domain analysis is performed by plotting the spectral density to observe the dominance of certain harmonics in the primary and secondary arcing current. Figures 2.5-a and 2.5-b clearly depict the front panel and the block diagram employed in LabVIEW for this purpose. As is obvious from Figure 2.5-a, the arcing current on the secondary side of the transformers clearly contains 3^{rd}, 5^{th}, 7^{th}, 9^{th}, 11^{th} and 13^{th} harmonics of significant magnitudes with respect to the fundamental component. The power spectral density of the secondary arcing current reiterates the same fact.

However, an interesting observation made through the plots in Figure 2.5-a is that the primary side arcing current contains only the fundamental component and no higher harmonics of any significant magnitudes. The same is corroborated by the power spectral density of the primary arcing current. This clearly depicts that the transformers do not allow the harmonics to pass through. However, the transformers are employed only within the laboratory to produce a voltage high enough to create an arcing situation. For an arcing fault in the switchgear in real world conditions, the arcing current would bear a stamp very close to that of the secondary arcing current. Thus the arcing current on the secondary side of the transformer bears the most significance for detection of switchgear arcing fault.

The signal is recorded in '*lvm*' format and with sampling rate for each channel set at 18000 samples/sec, the major harmonic components of the arcing current can be separated. Table 2.1 provides harmonic component breakdown for the arcing current on

the primary and secondary sides of the transformer. The magnitudes of the harmonic components are scaled with respect to the magnitude of the fundamental frequency component. The phases of the harmonic components are also relative to the phase of the fundamental frequency component.

The time domain plot depicted in Figure 2.6 is obtained by using the harmonic percentage compositions tabulated in Table 2.1. As is evident from Figure 2.6, the nature of the primary and secondary waveforms is almost identical to those obtained by data acquisition in LabVIEW. The objective behind this exercise is to corroborate the percentage harmonic composition for the secondary arcing current in particular so that these percentages can form the basis of the non-linear load modeling to be used in '*pcfloh*'.

Table 2.1 Percentage harmonic composition for primary & secondary arcing current

Hth	Freq[Hz]	%Abs Pri	relDeg Pri	%Abs Sec	relDeg
1	60	100.000	0.00	100.000	0.00
3	180	4.410	179.18	101.720	2.83
5	300	0.714	103.63	99.161	3.46
7	420	0.726	201.44	93.583	4.45
9	540	0.568	206.37	86.417	8.63
11	660	0.585	219.46	78.609	12.07
13	780	0.544	224.12	65.539	13.36
15	900	0.488	230.24	54.911	16.25
17	1020	0.426	232.88	43.288	17.30
19	1140	0.426	234.73	32.184	17.17
21	1260	0.352	233.70	21.952	12.93
23	1380	0.263	234.71	13.634	359.55

Further corroboration was obtained by performing the frequency domain analysis of the Matlab generated primary and secondary arcing current waveform. Figures 2.7 and 2.8 present the frequency domain magnitude and phase angle analysis of the primary and

secondary arcing current. As is obvious from these figures, they bear close resemblance to the figures obtained in LabVIEW thereby reiterating the accuracy of the percentage harmonic composition.

Figure 2.9 depicts the power spectral density for the arcing fault currents, based on the analysis carried out on the acquired arcing current signal in Matlab, on the primary and secondary side of the step-up transformer respectively. A comparative analysis of power spectral densities depicted in figures 2.5 and 2.9 clearly validate the data acquisition procedure via the method of elaborate harmonic analysis.

With the percentage harmonic composition of the secondary arcing current established and confirmed, thereby validating the data acquisition process thoroughly, the next step was to model the arcing fault as non-linear load with the same harmonic characteristics to be able to accurately represent an arcing condition in a sample 18-bus system utilizing the harmonic analysis software '*pcfloh*' (courtesy Dr. Mack Grady, UT Austin). Details associated with the modeling of the arcing fault as a non-linear load in the sample 18-bus radial distribution system along with comparison of the model with contemporary mathematical models for arcing faults are presented in the ensuing sections.

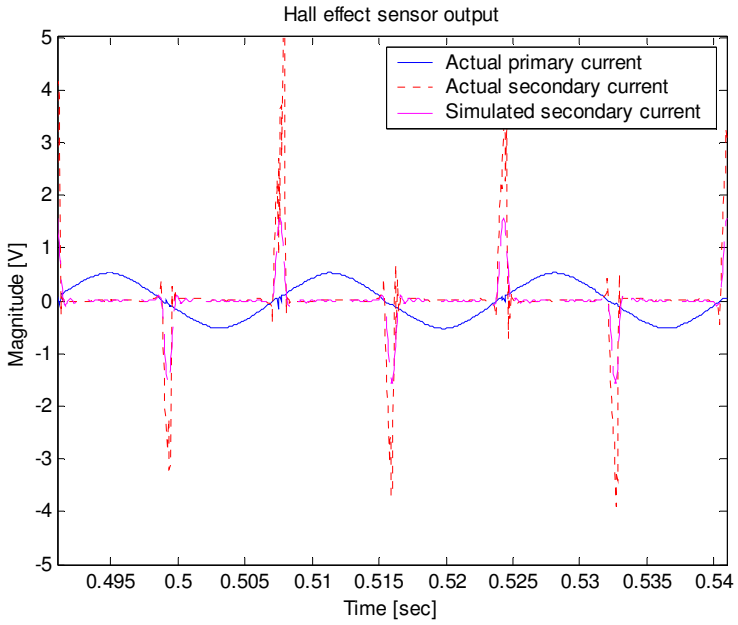

Figure 2.6: Time domain plot in Matlab to corroborate the harmonic composition of arcing current

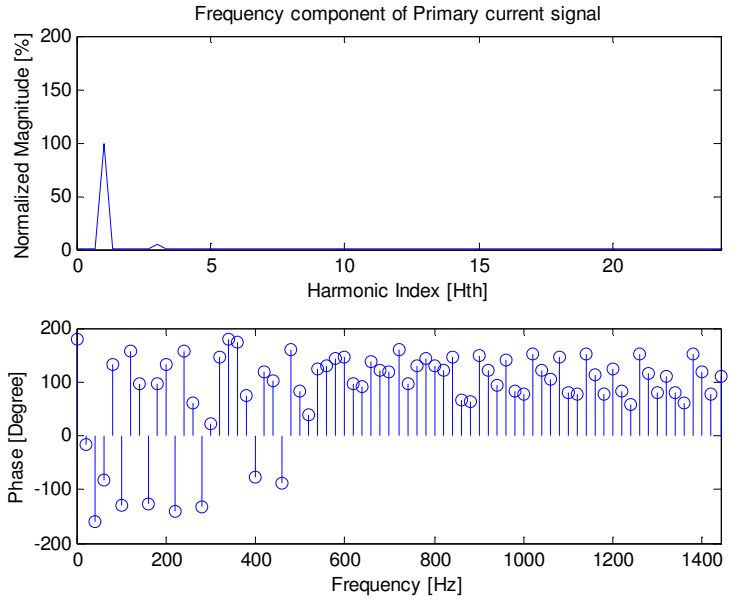

Figure 2.7: Frequency domain plots for magnitude & phase angle of primary arcing currents

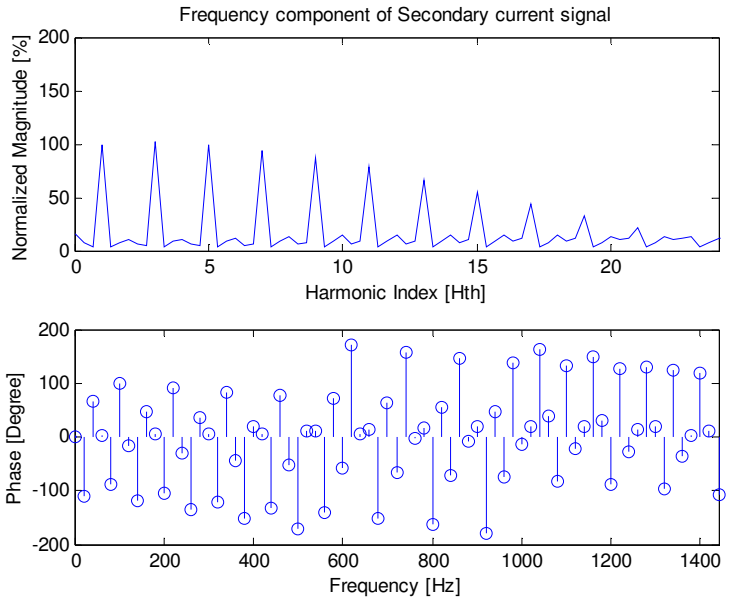

Figure 2.8: Frequency domain plots for magnitude & phase angle of secondary arcing currents

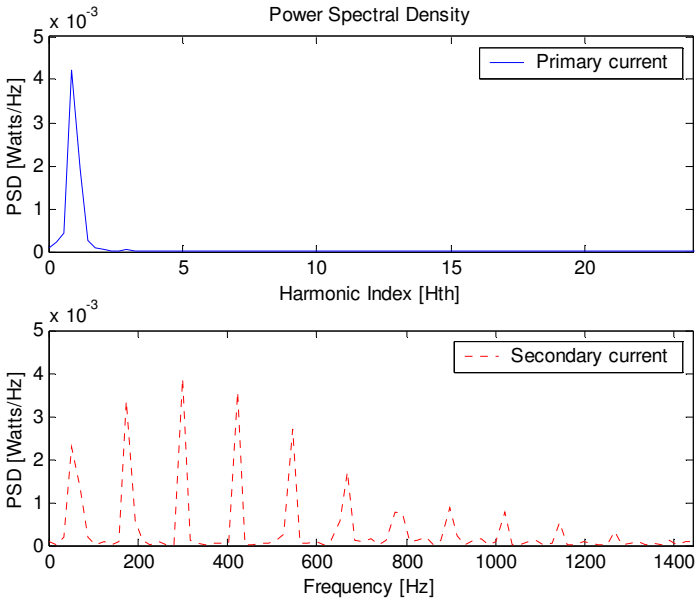

Figure 2.9: Power spectral density for the primary & secondary arcing currents

2.2.3 Modeling of Arcing Fault

With the percentage harmonic composition of the secondary arcing current known and verified, a non-linear load exhibiting the same harmonic characteristics in terms of magnitudes and phase angles (as those obtained from the harmonic analysis of the secondary arcing fault current) is designed and employed for simulation in the '*pcfloh*' harmonic analysis software. '*pcfloh*' is 500 bus power system harmonic analysis software developed by Dr. Mack Grady, UT Austin. Information about the distribution system is provided in the form of bus data files, line data files, options files and spectra files (which contains user input harmonic current injection spectral data). A sample 18 bus distribution system shown in Figure 2.10 is employed for simulation purposes in this case. Simulations are carried out for various system conditions listed below:

- All capacitors disconnected
- All capacitors connected
- All capacitors connected except for bus #5
- Line 4-5 replaced by a transformer

All the afore-described system topologies have been encompassed within the various case definitions outlined in Table 2.2. Various harmonic components (including the fundamental frequency component) of the line current between buses #4-#5 (incoming current) and buses #5-#6 (outgoing current) are monitored to observe the most ideal parameter/parameters to be chosen for current differential approach.

Table 2.2 Case Definitions for arcing fault simulation on sample 18-bus radial distribution system

Case Definition	Arc Fault Location	Internal/External Fault
BC5- no capacitors	arcing fault at bus 5	internal fault
BC6- no capacitors	arcing fault at bus 7	external fault
BC7- no capacitors	arcing fault at bus 3	external fault
BC8- with capacitors	arcing fault at bus 5	internal fault
BC9- with capacitors	arcing fault at bus 7	external fault
BC10- remove C at bus 5	arcing fault at bus 5	internal fault
BC11- remove C at bus 5	arcing fault at bus 7	external fault
TC1- Bus 4 to 5 is transformer YG-YG	arcing fault at bus 5	internal fault
TC2- Bus 4 to 5 is transformer Delta-YG	arcing fault at bus 5	internal fault

pcfloh' is designed to read column-formatted, comma-separated or tab-separated data. The input files for each of the cases mentioned above are in notepad format. The file that assumes great significance at the onset of the simulation process is the Spectra file. It is this file which decides the nature and type of the non-linear load and the harmonic composition of the non-linear load. '*Pcfloh*' provides the option of using one of the inbuilt non-linear loads by selecting an integer code however in our case the integer code chosen is 21 which signifies a user-defined non-linear load and then each harmonic order is accompanied with a magnitude percentage and phase angle. These entries basically correspond to those tabulated in Table 2.1 for the secondary arcing current. This allows the representation of the arcing phenomenon as a non-linear load on the distribution system with the non-linear load producing the same harmonic characteristics as the arcing phenomenon. As shown in Figure 2.10, the current sensors are placed on line joining buses #4-#5 and line joining buses #5-#6.

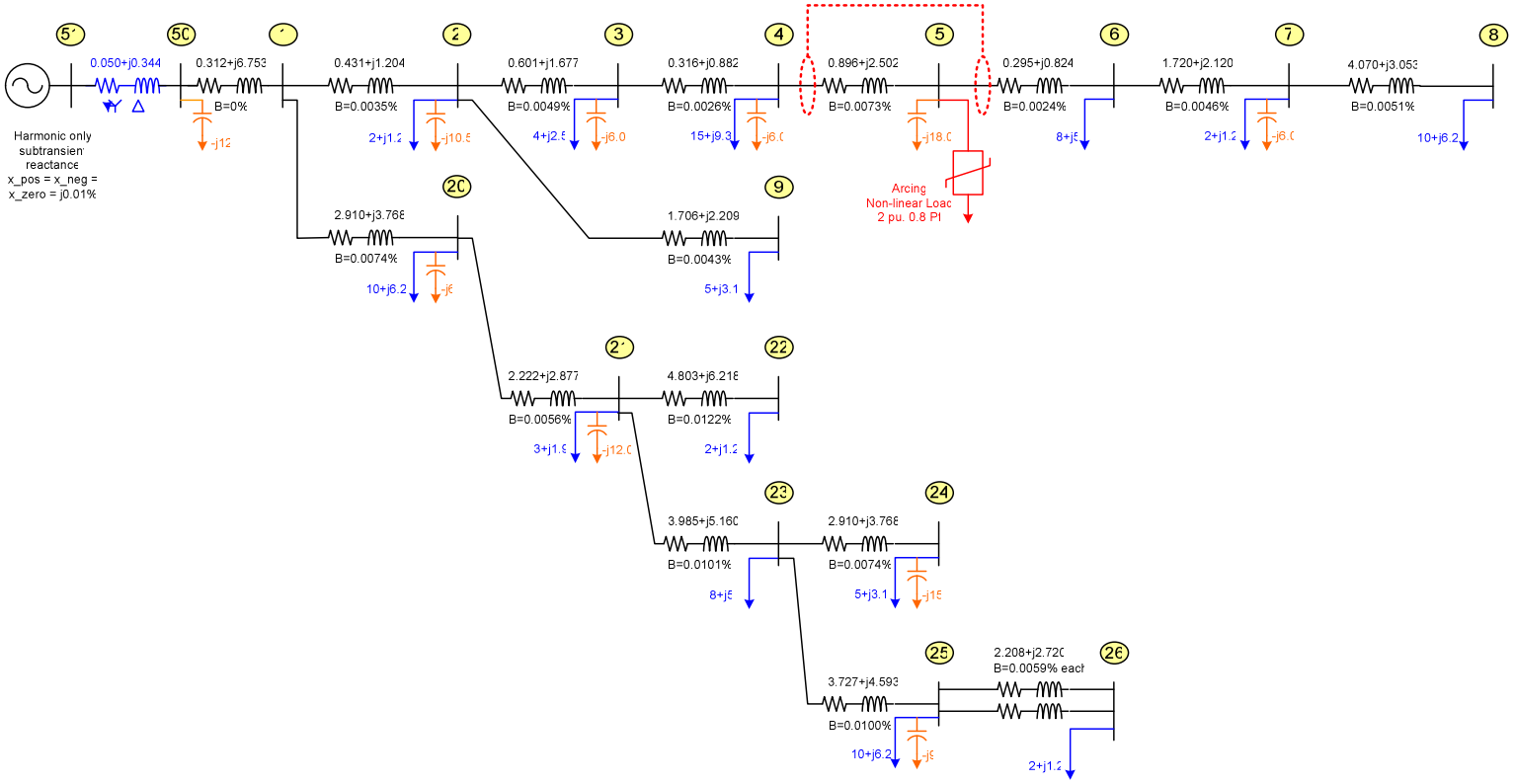

Figure 2.10 Sample 18 bus radial distribution system

'Thus any arcing fault taking place outside this area would not be within the purview of the current differential protection. Numerous cases, as tabulated in Table 2.2, are simulated with the non-linear load placed inside and outside this area to observe issues such as sensitivity to internal fault and security/discrimination against external faults. Various aspects of the current differential approach are put to test using the simulation approach. The simulation considers bus #5 as the location of the switchgear.

With the medium voltage arcing fault being modeled as a non-linear load on the sample 18-bus system as described above, various practical scenarios representing diverse operational conditions are simulated to test the validity of the approach as benchmarked against some standard performance evaluation criterion for higher-order differential protection approach. However, prior to the simulation the results of which are presented in the relevant ensuing sections of this chapter, it was necessary to perform a comparative analysis of the arcing fault developed at ESRC with the contemporary mathematical models for the arcing faults. This aspect forms the nucleus of the discussion presented in the following sub-section.

2.2.4 Simulation Results

As mentioned earlier, the performance of the proposed higher-order differential protection approach to detect the presence of arcing faults in medium voltage switchgear was evaluated by considering various operational scenarios defined in the previous sub-section. The discussion documented in this section revolves around

presenting and analyzing the results obtained from the simulation of various operational scenarios.

As discussed earlier, the primary reason for the execution of numerous scenarios, the results of which have been presented in this section, were manifold:

- Assess the successful implementation of the proposed higher-order harmonic differential approach for various practical operational conditions such as with the presence of power factor correction capacitors etc
- Perform exhaustive testing spanning varying scenarios in order to assess the robustness of the proposed higher-order harmonic differential approach
- Ensure the applicability of the proposed higher-order harmonic differential approach in the face of actual system conditions wherein the approach is adopted for detection of arcing fault a substations. For this purpose, there are additional scenarios added to the set utilized for testing wherein the line between buses 4 & 5 has been replaced by a transformer. Both variations of the transformer have been utilized for testing, in case the configuration of the transformer re-directs the harmonics produced by the arcing fault.

While numerous scenarios and/or cases have been simulated, detailed discussion of the results associated with one complete scenario (along with all cases comprising the scenario) has been presented in this section. Furthermore summary of results associated with all scenarios and/or cases defined in the previous sub-section have been presented, discussed and analyzed in this section. Detailed results associated with the remaining cases and/or scenarios have been attached in the form of appendices to this dissertation.

Case BC5

Description: Internal arcing fault: Non-linear device placed at Bus #5 with all capacitors disconnected

Figures 2.11 & 2.12 depict the currents flowing through some selected lines and voltages across some selected buses respectively for the system topology corresponding to case BC5. Table 2.3 provides details about harmonic (magnitude and phase angle) composition of each of the line currents when the non-linear load is placed on bus #5 (equivalent to an internal arcing fault). Details about the line currents between buses #4-#5 and buses #5-#6 are highlighted since these would be of prime importance when considering the current differential approach.

As can be seen from the highlighted sections of Table 2.3, all the higher harmonics do seem to exhibit the potential of being arcing fault indicators for the current differential approach in terms of the magnitude and phase angle. However it shall be seen later on in this report that as the system is modified gradually to resemble the actual conditions the choice for the parameter for current differential narrows down when both magnitude and phase angle are taken into account.

Case BC6

Description: External arcing fault: Non-linear device placed at Bus #7 with all capacitors disconnected

Figures 2.13 & 2.14 depict the currents flowing through some selected lines and voltages across some selected buses respectively.

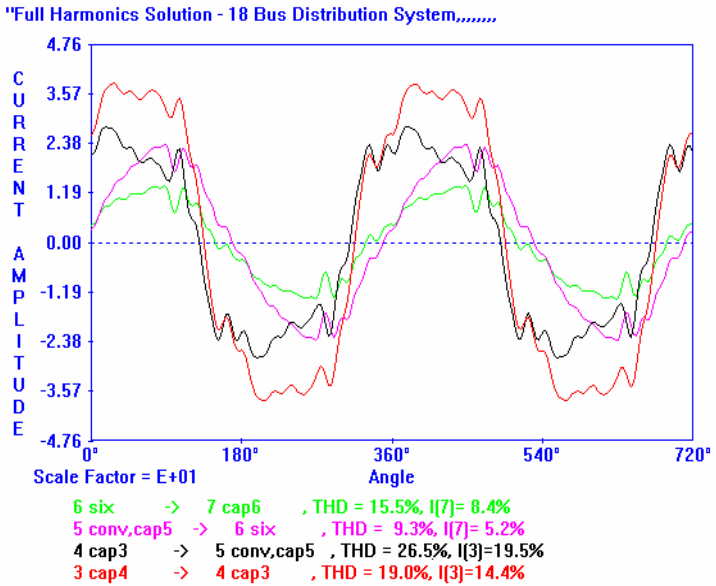

Figure 2.11: Current Plots (BC5)

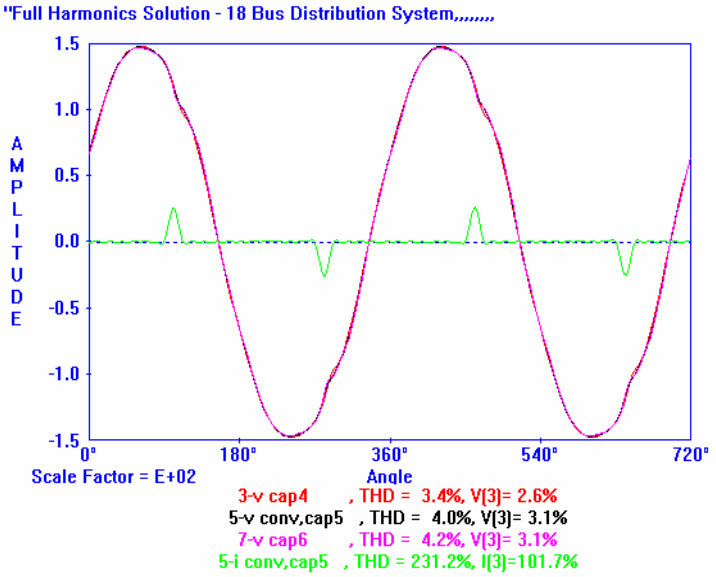

Figure 2.12: Voltage Plots (BC5)

Table 2.3: Line Current Composition for **Case BC5**

CASE BC5: Non-linear load simulation in 18-bus distribution system without any capacitors in the system : Arcing at bus #5 **(Internal fault)**														
Line	1st Harmonic		3st Harmonic		5st Harmonic		7st Harmonic		9st Harmonic		11st Harmonic		13st Harmonic	
	Mag [%]	Angle[Deg]	Mag [%]	Angle[Deg]	Mag [%]	Angle[Deg]	Mag [%]	Angle[Deg]	Mag [%]	Angle[Deg]	Mag [%]	Angle[Deg]	Mag [%]	Angle[Deg]
3to4	45.01	-6.50	2.62	149.00	2.43	-64.40	2.27	96.30	2.22	-93.00	1.72	46.90	1.38	-156.80
4to5	26.95	-6.80	2.62	149.00	2.46	-59.90	2.27	96.30	2.22	-93.00	1.81	55.50	1.47	-147.00
5to6	24.39	-6.30	0.00	0.00	0.32	-162.70	0.40	-9.40	0.00	0.00	0.46	-55.40	0.43	99.90
6to7	14.67	-6.20	0.00	0.00	0.19	-163.20	0.24	-10.10	0.00	0.00	0.28	-56.60	0.26	98.60
50to1	107.85	-6.20	2.62	149.00	2.34	-74.60	2.07	76.50	2.22	-93.00	1.50	27.30	1.16	-178.50
51to50	107.85	-36.20	0.00	0.00	2.34	-44.60	2.07	46.50	0.00	0.00	1.50	57.30	1.16	151.50
1to20	49.71	-6.20	0.00	0.00	0.32	-173.50	0.39	-25.30	0.00	0.00	0.43	-80.40	0.39	71.00
20to21	37.60	-6.40	0.00	0.00	0.24	-174.90	0.29	-27.40	0.00	0.00	0.32	-83.60	0.29	67.20
21to22	2.43	-4.90	0.00	0.00	0.02	-170.30	0.02	-21.00	0.00	0.00	0.02	-73.50	0.02	79.10
21to23	31.46	-6.40	0.00	0.00	0.20	-175.80	0.24	-28.60	0.00	0.00	0.27	-85.50	0.24	65.00

A closer observation of the magnitudes and phase angles of the highlighted sections in Table 2.4 indicates that the higher harmonics would not only provide good sensitivity for operation in case of an internal fault (case 1) but also provide good discrimination against external faults (case 2). The magnitudes and phase angles of the higher harmonics for an external fault through both the current sensors seem to be almost identical thereby not initiating the current differential in case the arcing took place outside the zone.

Case BC7

Description: External arcing fault: Non-linear device placed at Bus #3 with all capacitors disconnected

This case is simulated to corroborate the facts just discussed above for case BC6 since both cases correspond to external arcing fault while differing in the location of the external arcing fault. Figures 2.15 & 2.16 and Table 2.5 confirm the same.

The following other scenarios have been simulated with the plots and the harmonic composition tables for the line current being attached in Appendix A at the end of this dissertation:

- Scenario: With all capacitors connected
  - Case BC8: Internal Fault (Non-linear load at bus #5)
  - Case BC9: External Fault (Non-linear load at bus #7)
- Scenario: All capacitors connected except at bus #5
  - Case BC10: Internal Fault (Non-linear load at bus #5)
  - Case BC11: External Fault (Non-linear load at bus #7)

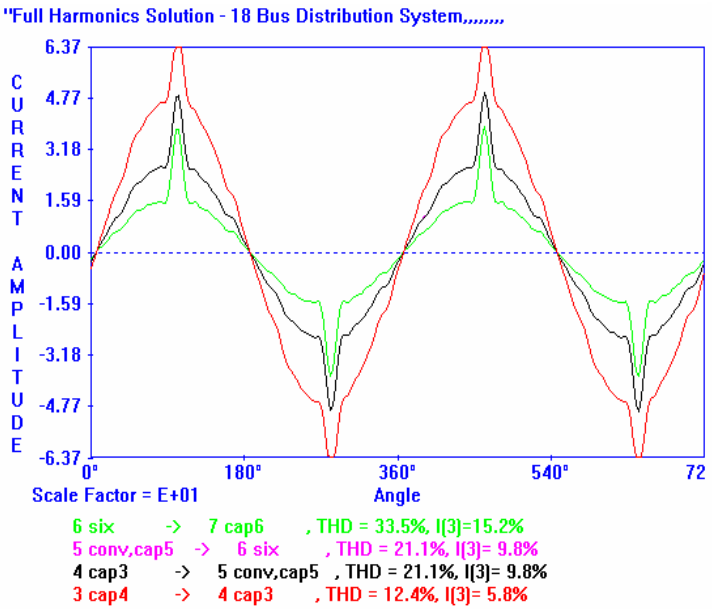

Figure 2.13: Current Plots (BC6)

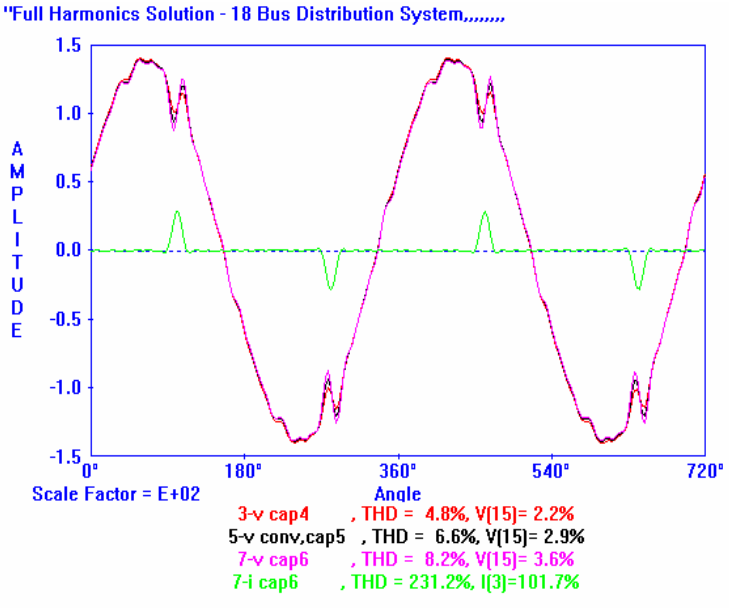

Figure 2.14: Voltage Plots (BC6)

Table 2.4: Line Current Composition for **Case BC6**

CASE BC6: Non-linear load simulation in 18-bus distribution system with all capacitor removed : Arc at Bus#7 **(External fault)**														
Line	1st Harmonic		3st Harmonic		5st Harmonic		7st Harmonic		9st Harmonic		11st Harmonic		13st Harmonic	
	Mag [%]	Angle[Deg]	Mag [%]	Angle[Deg]	Mag [%]	Angle[Deg]	Mag [%]	Angle[Deg]	Mag [%]	Angle[Deg]	Mag [%]	Angle[Deg]	Mag [%]	Angle[Deg]
3to4	45.05	-6.50	2.63	147.90	2.44	-66.50	2.22	87.40	2.24	-96.20	1.73	42.30	1.39	-162.10
4to5	26.99	-6.80	2.63	147.90	2.47	-62.00	2.28	93.40	2.24	-96.20	1.82	50.90	1.47	-152.40
5to6	26.99	-6.80	2.63	147.90	2.47	-62.00	2.28	93.40	2.24	-96.20	1.81	51.00	1.47	-152.40
6to7	17.26	-7.00	2.63	147.90	2.50	-59.00	2.32	97.50	2.24	-96.20	1.88	56.80	1.54	-145.80
50to1	107.89	-6.20	2.63	147.90	2.35	-76.70	2.08	73.60	2.24	-96.20	1.51	22.80	1.16	176.10
51to50	107.89	-36.20	0.00	0.00	2.35	-46.70	2.08	43.60	0.00	0.00	1.51	52.80	1.16	146.10
1to20	49.71	-6.20	0.00	0.00	0.32	-175.50	0.39	-28.20	0.00	0.00	0.43	-84.90	0.39	65.70
20to21	37.60	-6.40	0.00	0.00	0.24	-177.00	0.29	-30.30	0.00	0.00	0.32	-88.20	0.29	61.80
21to22	2.43	-4.90	0.00	0.00	0.02	-172.40	0.02	-23.90	0.00	0.00	0.02	-78.10	0.02	73.70
21to23	31.46	-6.40	0.00	0.00	0.20	-177.80	0.24	-31.50	0.00	0.00	0.27	-90.00	0.24	59.70

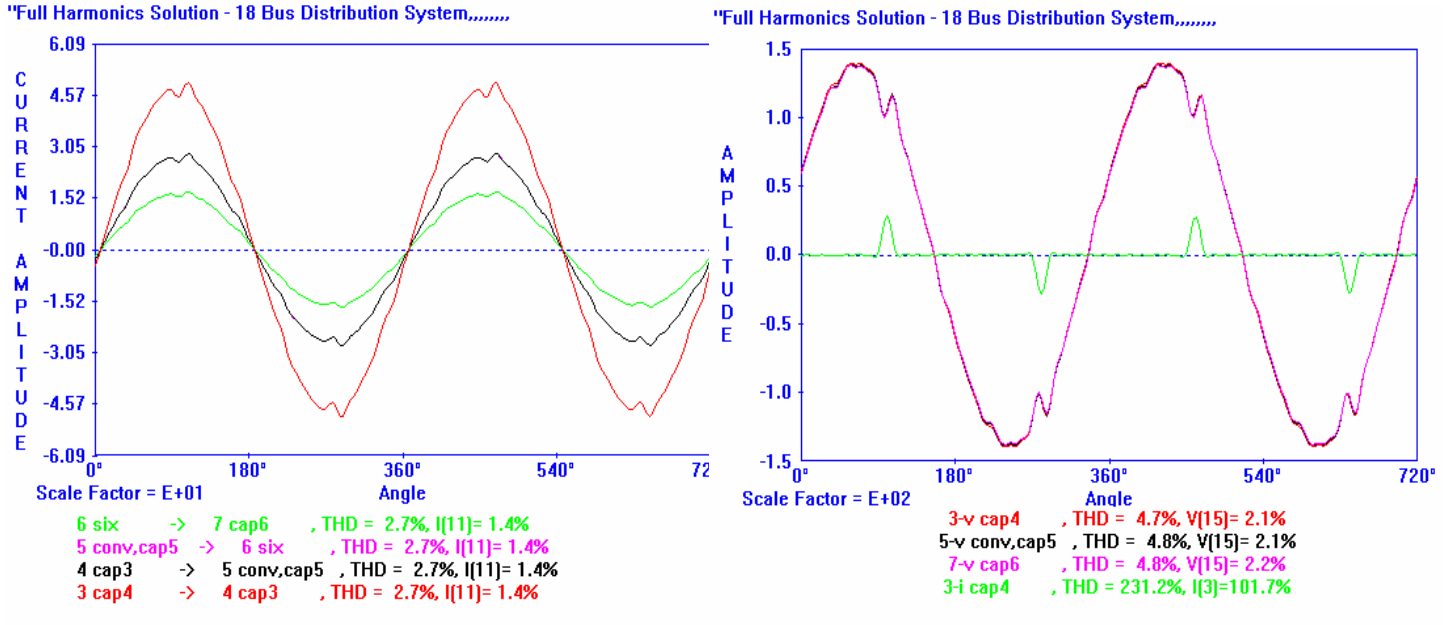

(a) (b)

Figure 2.15 (a): Current Plots (BC7) (b): Voltage Plots (BC7)

Table 2.5: Line Current Composition for **Case BC7**

CASE BC7: Non-linear load simulation in 18-bus distribution system with all capacitor removed : Arc at Bus#3 **(External fault)**														
Line	1st Harmonic		3st Harmonic		5st Harmonic		7st Harmonic		9st Harmonic		11st Harmonic		13st Harmonic	
	Mag [%]	Angle[Deg]	Mag [%]	Angle[Deg]	Mag [%]	Angle[Deg]	Mag [%]	Angle[Deg]	Mag [%]	Angle[Deg]	Mag [%]	Angle[Deg]	Mag [%]	Angle[Deg]
3to4	42.42	-6.10	0.00	0.00	0.41	-161.70	0.51	-8.30	0.00	0.00	0.59	-53.80	0.54	101.90
4to5	24.37	-6.30	0.00	0.00	0.23	-162.80	0.29	-9.90	0.00	0.00	0.33	-56.20	0.31	99.10
5to6	24.37	-6.30	0.00	0.00	0.23	-162.90	0.29	-10.00	0.00	0.00	0.34	-56.50	0.31	98.80
6to7	14.65	-6.20	0.00	0.00	0.14	-163.40	0.17	-10.70	0.00	0.00	0.20	-57.60	0.18	97.50
50to1	107.80	-6.20	2.59	149.50	2.33	-70.30	2.07	82.60	2.20	-91.30	1.50	36.90	1.16	-167.20
51to50	107.80	-36.20	0.00	0.00	2.33	-40.30	2.07	52.60	0.00	0.00	1.50	66.90	1.16	162.80
1to20	49.70	-6.20	0.00	0.00	0.32	-169.10	0.39	-19.30	0.00	0.00	0.43	-70.80	0.39	82.30
20to21	37.59	-6.30	0.00	0.00	0.24	-170.60	0.29	-21.30	0.00	0.00	0.32	-74.10	0.29	78.50
21to22	2.43	-4.90	0.00	0.00	0.02	-166.00	0.02	-14.90	0.00	0.00	0.02	-64.00	0.02	90.30
21to23	31.46	-6.40	0.00	0.00	0.20	-171.40	0.24	-22.50	0.00	0.00	0.27	-75.90	0.24	76.30

The aforesaid operational scenario is deemed necessary since the idea is to simulate arcing fault within the switchgear and the switchgear location is assumed to be bus #5. Thus it is impractical to have a capacitor at that bus. Since we are dealing with higher order harmonics the presence of a capacitor affects the results in a tremendous way since it acts as a low impedance path for the high frequency currents. This in turn could affect the performance of the current differential approach being tested.

- Scenario: All capacitors connected except at bus #5 and line 4-5 changed into transformer
  - Case TC1: Internal Fault with GY-GY transformer configuration(Non-linear load at bus #5)
  - Case TC2: Internal Fault with Delta-GY transformer configuration (Non-linear load at bus #5)

The aforesaid modification is provided since the configuration of the distribution systems is such that the switchgear follows the distribution transformer in the sub-station and hence the effect of the presence of a transformer just before the switchgear would be worth noting.

While elaborate details associated with the simulation results for all the additional cases and/or scenarios have been attached in Appendix A, Table 2.6 presented on the following page provides the summary of results in terms of the harmonic magnitudes and phase angles associated with the incoming and outgoing currents for all operational scenarios considered.

Table 2.6 Comprehensive results for all scenarios and cases

Case ID		1st Harmonic		3st Harmonic		5st Harmonic		7st Harmonic		9st Harmonic	
		Mag [%]	Angle[Deg]	Mag [%]	Angle[Deg]	**Mag [%]**	**Angle[Deg]**	Mag [%]	Angle[Deg]	Mag [%]	Angle[Deg]
BC5	From 4 to 5	26.95	-6.80	2.62	149.00	**2.46**	**-59.90**	2.27	96.30	2.22	-93.00
	From 5 to 6	24.39	-6.30	0.00	0.00	**0.32**	**-162.70**	0.40	-9.40	0.00	0.00
BC6	From 4 to 5	26.99	-6.80	2.63	147.90	**2.47**	**-62.00**	2.28	93.40	2.24	-96.20
	From 5 to 6	26.99	-6.80	2.63	147.90	**2.47**	**-62.00**	2.28	93.40	2.24	-96.20
BC7	From 4 to 5	24.37	-6.30	0.00	0.00	**0.23**	**-162.80**	0.29	-9.90	0.00	0.00
	From 5 to 6	24.37	-6.30	0.00	0.00	**0.23**	**-162.90**	0.29	-10.00	0.00	0.00
BC8	From 4 to 5	24.16	56.30	4.70	140.00	**3.22**	**-84.10**	1.83	-13.90	0.20	-124.30
	From 5 to 6	19.60	9.50	0.60	131.40	**0.51**	**-152.90**	1.01	-67.60	0.52	87.60
BC9	From 4 to 5	24.16	56.20	4.75	137.50	**3.37**	**-86.70**	2.00	-17.80	0.23	-126.70
	From 5 to 6	21.82	7.20	3.00	142.40	**2.41**	**-69.40**	1.32	93.00	1.77	-98.10
BC10	From 4 to 5	22.50	6.70	2.80	147.70	**2.50**	**-62.00**	2.80	71.70	0.60	-116.30
	From 5 to 6	20.23	8.70	0.36	139.10	**0.40**	**-130.90**	1.55	18.00	1.55	95.60
BC11	From 4 to 5	22.53	6.60	2.85	145.80	**2.62**	**-64.70**	3.06	67.80	0.70	-117.60
	From 5 to 6	22.53	6.60	2.85	145.80	**2.62**	**-64.70**	3.06	67.90	0.70	-117.60
TC1	From 4 to 5	22.42	7.00	2.76	148.40	**2.43**	**-59.10**	2.67	78.00	0.58	-113.50
	From 5 to 6	20.15	9.10	0.32	139.70	**0.30**	**-137.20**	1.29	20.70	1.56	96.90
TC2	From 4 to 5	22.42	7.00	2.43	120.90	**2.67**	**-102.00**	1.19	68.40	1.28	-137.50
	From 5 to 6	20.15	39.10	0.00	-123.40	**0.30**	**12.80**	1.29	-129.30	0.04	177.20

Note:

BC5 – no capacitors	arcing fault at bus 5	internal fault
BC6 – no capacitors	arcing fault at bus 7	external fault
BC7 – no capacitors	arcing fault at bus 3	external fault
BC8 – with capacitors	arcing fault at bus 5	internal fault
BC9 – with capacitors	arcing fault at bus 7	external fault
BC10 – remove C at bus 5	arcing fault at bus 5	internal fault
BC11 – remove C at bus 5	arcing fault at bus 7	external fault
TC1 – Line 4to5 is transformer GY-GY	arcing fault at bus 5	internal fault
TC2 – Line 4to5 is transformer Delta-GY	arcing fault at bus 5	internal fault

As is evident from the summary of results tabulated in Table 2.6, most higher-order harmonics tabulated in the above table are capable of acting as indicators when it comes to detection of arcing fault in the medium voltage switchgear. The results tabulated in Table 2.6 seem to further indicate the 5^{th} harmonic as the most suitable candidate to be utilized for the higher-order harmonic differential approach keeping in mind aspects such as discrimination against external faults and sensitivity for internal faults. While, the inferences and/or observations associated with the results are discussed in elaborate detail in an ensuing relevant section, the results for the simulation process presented in this section go a long way in establishing the validity of the proposed higher-order harmonic differential approach to detect the presence of arcing faults in medium voltage switchgear.

The discussion in the remaining sections of this chapter revolves around the application of a similar approach towards the detection of arcing faults in low voltage switchgear. In this case, the implementation of the higher-order harmonic differential approach is demonstrated on the actual hardware test-bench thereby taking the validity of the simulation results presented in the above sections to another level. Furthermore, the concluding section of this chapter discusses the key observations and analyses derived out of the simulation and/or hardware testing results.

2.3 Low Voltage Switchgear Arc Fault Detection

The discussion(s) presented in the previous section and sub-sections of this chapter revolved around the design, development and implementation of a suitable test-bench to replicate switchgear arcing fault conditions as they occur in actual field conditions, within a controlled laboratory environment. Furthermore, a novel approach utilizing the differential protection principle in conjunction with higher-order harmonics was devised to detect the presence of switchgear arcing faults in medium voltage switchgear. The approach involved the utilization of the simulation approach wherein a model for the arcing fault was simulated on a sample 18-bus radial distribution system. The model of the arc fault was based on modeling a non-linear load with the same harmonic behavior as that obtained from the arcing fault current acquired through LabVIEW during laboratory testing of the medium voltage switchgear arcing fault test-bench. As is evident from the results of the simulation presented above, the simulation approach clearly underlines the success of the approach in not only identifying arcing faults within the switchgear but also its robustness against external faults under various operational scenarios spanning all practical purposes.

This section of the chapter aims to present a discussion which would extend the application of the proposed approach to low-voltage switchgear wherein the proposed higher-order harmonic differential approach would be implemented on the arc-producing test-bench in the laboratory. The purpose of this aspect of the research is two-fold. Firstly, it endeavors to extend the validity of the proposed approach to the detection of low-voltage switchgear arcing faults. Secondly, the results presented in this section are utilized to further corroborate the conceptual validity of the approach previously established on the basis of simulation techniques presented in the previous section of this chapter.

2.3.1 Approach Overview

As mentioned above, the same conceptual approach of employing higher order harmonic currents in a differential configuration is utilized to demonstrate the detection of low voltage switchgear arcing fault to ground. While the simulation approach was employed to test the validity of the approach for medium voltage arc detection, actual laboratory testing is employed to ensure the practical feasibility of the higher-order harmonic differential approach.

Slight modifications are made to the existing test-bench thereby eliminating the instrument transformer and 15kV arcing device previously utilized for the initiation of the medium-voltage arcing fault. Arcing in this case is generated by purposely tampering the brush contact of the 120V drill motor. Provisions are made for changing the location of the arcing fault to ground dynamically in order to test the performance of the approach for internal and external faults. The data gathered from the signals of the

hall-effect sensors via LabVIEW is then analyzed graphically to gauge the success of the approach for the detection of low voltage arcing fault to ground. The proceeding sub-sections under this section present the discussion pertinent to the design and development of the test-bench, testing methodology employed and the results obtained thereof for the low-voltage switchgear arcing fault detection.

2.3.2 Hardware Development

The hardware development associated with test-bench utilized for the low-voltage switchgear arc fault initiation primarily comprised of modifying the existing set-up previously utilized for the medium-voltage arcing faults. Since arcing was now being produced at 120V the 115V-15kV neon step-up transformer was eliminated from the set-up. Furthermore, as mentioned above, a 120V drill motor with worn out brush contacts was utilized to develop arcing at low voltage. Slight modifications were also made to the data acquisition module responsible for the collection of the arcing current data at the 2 ends of the differential zone. This was done so in order to induce a certain amount of flexibility in the test-bench design to allow it to lend itself to the application of the proposed approach while testing and acquiring data simultaneously. The ensuing sub-sections go about the description of the test-bench for low voltage arc fault initiation in elaborate detail.

2.3.2.1 Test Bench: Design & Development

Figure 2.16 provides a detailed schematic for the test-bench set-up utilized for low voltage arcing fault initiation and detection. As mentioned above, slight modifications were made to the existing test-bench thereby eliminating the step-up transformer and 15kV arcing device. Arcing in this case was generated by purposely tampering the brush contact of the 120V drill motor. As can be seen from the figure, the positions of the hall-effect sensors define the zone of the harmonic current differential scheme. By providing single-pole double throw switches between, to the left and to the right of the differential zone, provisions are made for the testing of all possible scenarios by changing the location of the arcing fault to ground dynamically in order to test the performance of the approach for internal and external faults. Positions EF#1, IF and EF#2 marked on the figure indicate the location of the arcing faults with positions EF#1 and EF#2 corresponding to external faults and position IF corresponding to an internal fault. A delta connected 3-phase 208V induction motor is connected to the main supply through adequate isolation and over-loading protection equipment. This induction motor represents the normal loading on the system.

As is evident from the details of the test-bench schematic presented above, the design of the test-bench is made flexible enough to test the arcing fault within the low-voltage switchgear and both external (to the source and load) sides of the switchgear. Adequate isolation through fuses and circuit breakers has been provided in the circuit. The ensuing sub-section discusses the testing methodology employed while simultaneously validating the performance of the proposed approach for arc fault detection.

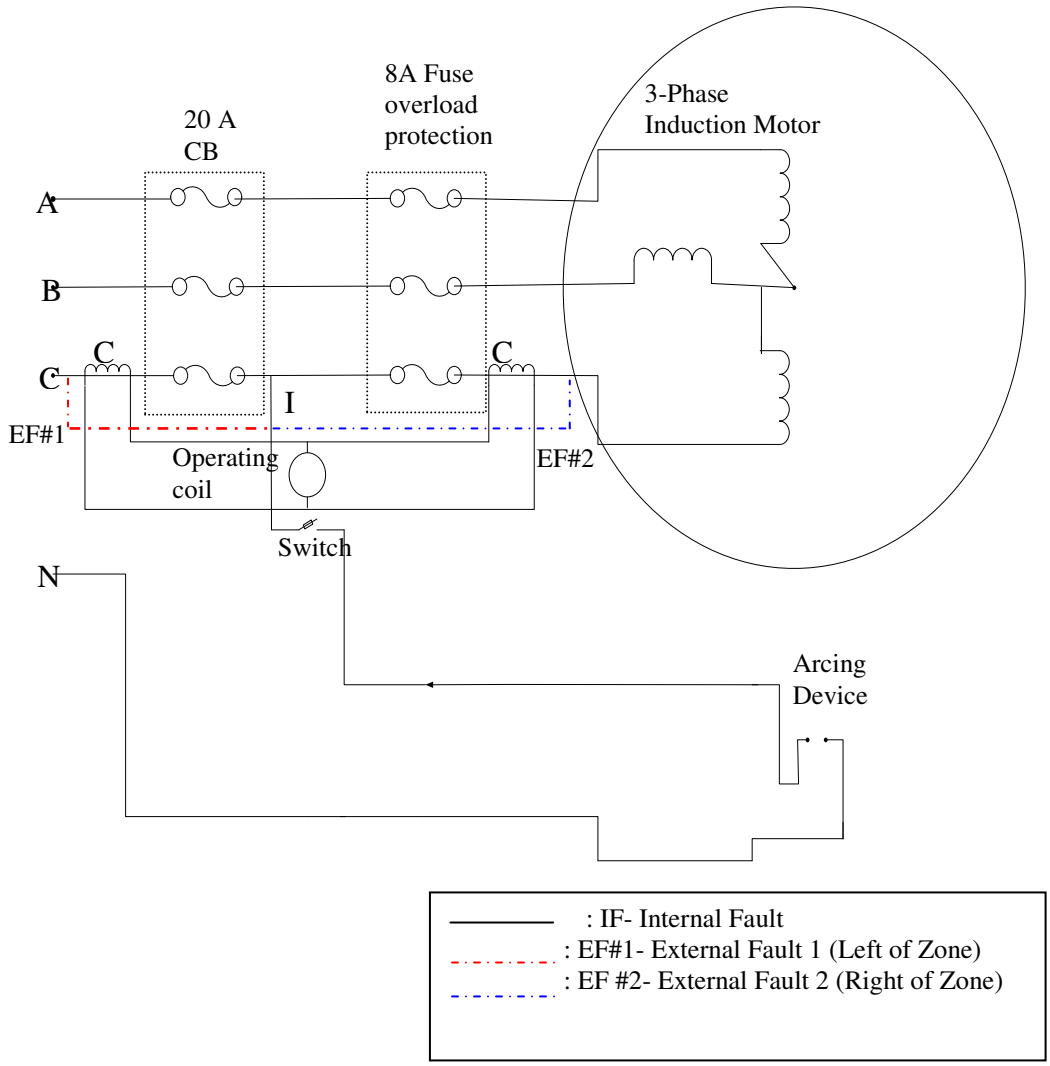

Figure 2.16: Test-Bench schematic for Low Voltage Arc Initiation & Detection

2.3.2.2 Testing Methodology

Arcing is produced by tampering with the brush contact of the drill motor rated to take 120V (line to neutral) as its input. By altering the position of the drill motor with respect to the differential zone, the arcing is created within, to the left and to the right of the zone. In each case, the current entering and leaving the differential protection zone

is monitored via the two signals from the hall-effect sensors defining the boundary of the differential zone. In accordance to ideal differential protection theory, the signals corresponding to the entering and leaving currents should cancel each other out in the case of an external fault (to the left or right) and that of an internal fault should show a significant difference.

During each of the afore-described cases the signals from the hall-effect sensors defining the differential zone are acquired into the PC via LabVIEW. Data gathered from the 2 hall-effect sensors for each of these cases, while being monitored and utilized for the application of the proposed approach, is simultaneously written into a text file using LabVIEW. While the application of the higher-order harmonic differential approach to the test-bench directly yields satisfactory results, the data written on the text file also corresponds to the signals being displayed on the front panel of LabVIEW. This data is utilized to reconstruct the actual incoming and outgoing line current signal from these text files using Matlab in order to allow for a clear analysis and display results for the dissertation. Elaborate results obtained from testing various operational scenarios described in this section have been presented in the ensuing sub-section.

2.3.3 Testing Results

The discussion associated with the results obtained from testing the performance of the proposed higher-order harmonic differential approach for the detection of low-voltage arc faults has been classified into 3 parts corresponding to 3 distinct cases tested.

Internal Arcing Fault (within switchgear) - Results

Figure 2.17 shows a comprehensive and an enlarged view of the hall-effect sensor signals corresponding to the incoming and outgoing currents for an internal arcing fault to ground. The instant of arcing is clearly labeled in the comprehensive plot. It can be seen from Figure 2.17 that before the arcing fault to ground takes place, the signals corresponding to incoming and outgoing currents are identical in magnitude and phase. The initiation of arcing fault can also be seen to be accompanied with large transients.

A closer look at the enlarged view of the two plots depicted in Figure 2.17 clearly suggests that the incoming and outgoing currents differ vastly in their harmonic components for an arcing fault lying inside the differential zone. As is also evident from the enlarged view that since the signals corresponding to the incoming and outgoing currents differ not only in magnitude but also in phase, both magnitude and phase differential scheme would be equally effective as long as the harmonic components are taken as inputs. While the sensitivity of the approach to low voltage switchgear arcing faults to ground is clearly established from plots shown in Fig. 2.17, the discrimination against external faults needs to be guaranteed. This is done so by creating arcing faults to ground outside the differential zone established on both the source and load side. The discussion on results for these 2 cases is presented below.

External Arcing Fault (Source Side) - Results

Figure 2.18 depicts the plots for the signals corresponding to incoming and outgoing currents with respect to the differential zone for an external arcing fault to ground located on the source side (left of differential zone).

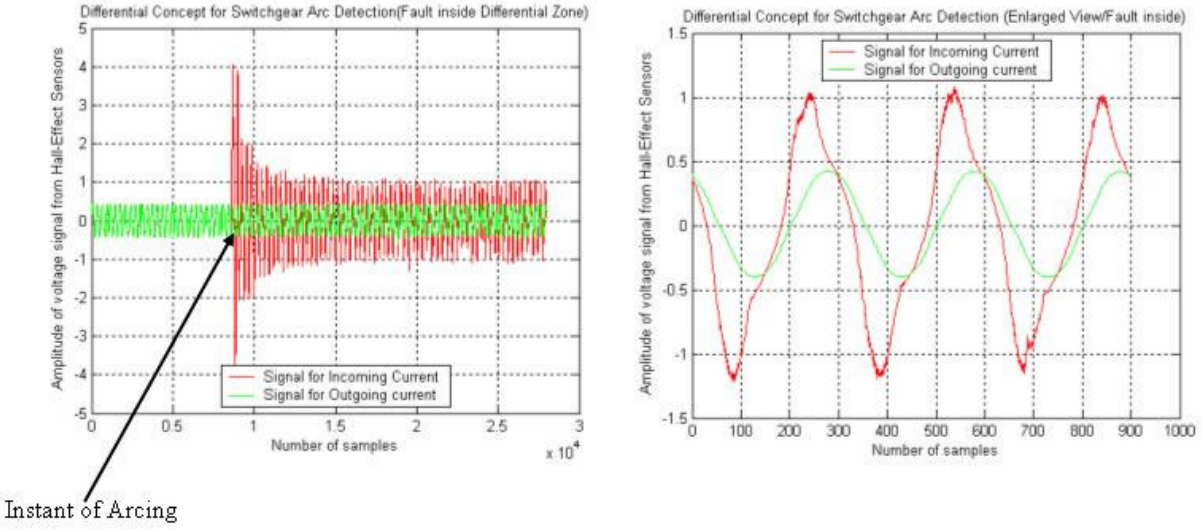

Figure 2.17: Comparative plots for current entering and leaving differential zone for an internal fault

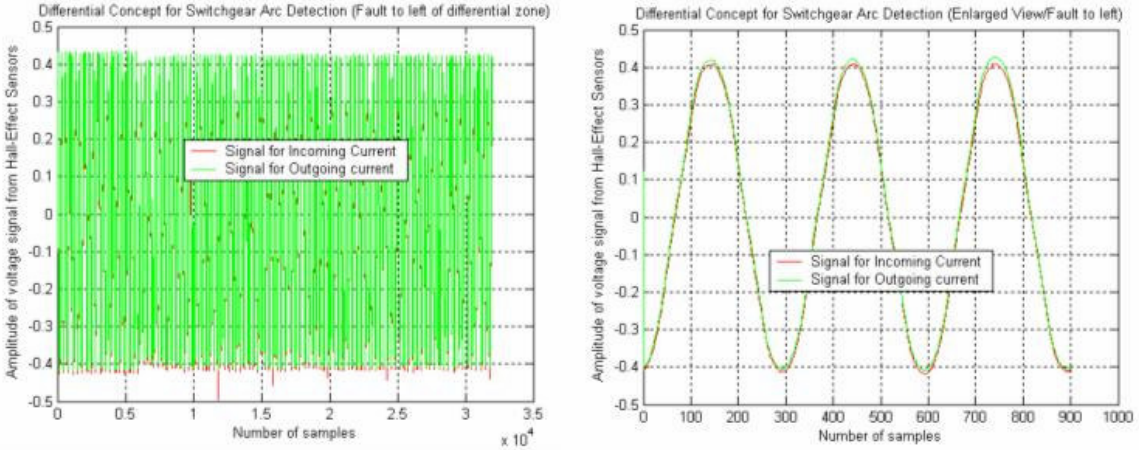

Figure: 2.18 Comparative plots for current entering and leaving differential zone for an external fault (source side of zone)

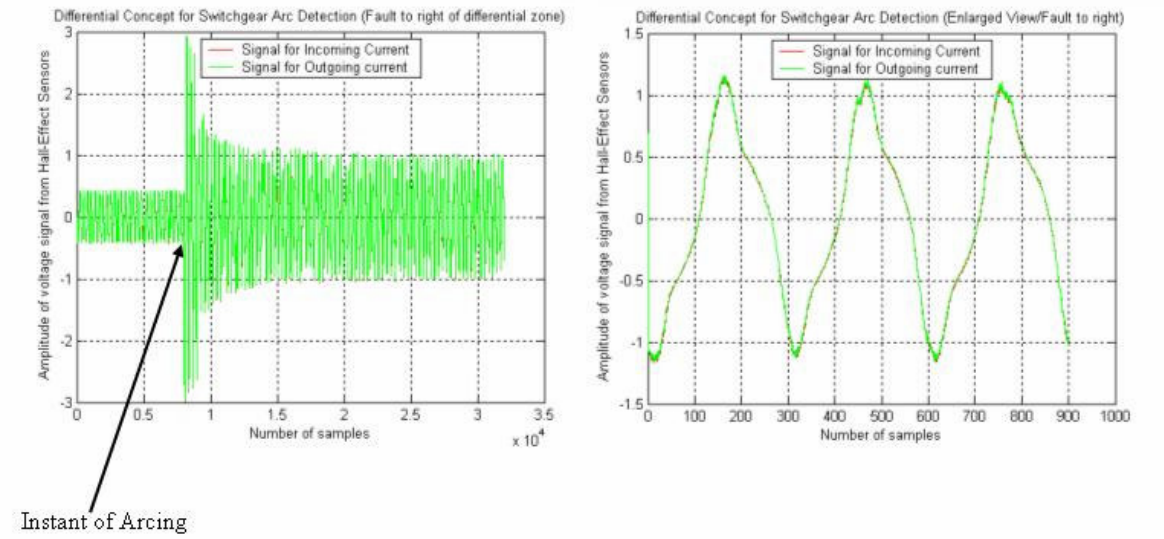

Figure: 2.19 Comparative plots for current entering and leaving differential zone for an external fault (load side of zone)

Since the arcing fault is actually taking place to the left of the pre-defined differential zone, the arcing fault current is now assumed not to be within the switchgear. In this scenario, the arcing fault current is directly drawn from the supply and hence the hall-effect sensor signals do not show any harmonic contents. Furthermore, the signals corresponding to the incoming and outgoing currents are identical in magnitude and phase and hence would get cancelled out in the differential scheme. This clearly suggests that the differential scheme would not operate for arcing faults that occur outside the switchgear on the source/supply side of the switchgear set-up.

External Arcing Fault (Load Side) - Results

The discrimination against external arcing faults, when utilizing the proposed higher-order harmonic differential approach, is more a concern when the external arcing fault does occur on the load side of the switchgear or differential zone. The nature and/or

impedance of the load type may re-direct the harmonics in such a way so as to affect the algorithm being employed for the higher-order harmonic differential approach. For this reason, the results presented in this paragraph, corresponding to the external arcing occurring on the load side assume great significance when viewed in terms of the performance of the proposed approach. Figure 2.19 depicts plots of hall-effect sensor signals corresponding to the incoming and outgoing currents for an external arcing fault located o the load side of the assumed switchgear (right of the differential zone). As can be seen from the figure, both the hall-effect sensor signals show the same harmonic components since the same arcing fault current enters and leaves the differential zone. As can be seen from Fig. 2.19, the plots of hall-effect sensor signals are identical once again in magnitude and phase for an arcing fault set-up outside the assumed switchgear. This clearly underlines the superiority of this approach as far as issues such as reliability and selectivity of operation are concerned.

2.4 Observations/Inferences

All the preceding sections documented in this chapter have endeavored to put across to the reader, the conceptual approach, hardware design aspects, algorithm development, testing and/or simulation methodology and the results associated with the detection of medium and low-voltage switchgear arcing faults. The basic underlying aspect common to both voltage levels is the conceptual design of the approach utilizing higher-order harmonics in conjunction with higher-order harmonics to detect the presence of switchgear arcing faults. While the simulation technique has been utilized

to ascertain the validity of the proposed approach at the medium voltage level, actual laboratory testing on test-benches (design of which has been elaborated upon in earlier sections) has bee utilized to establish the consistency, robustness and reliability of the proposed approach. The following 2 sub-sections dwell on certain key observations made from the analysis carried out on the results obtained from both the simulation and in-laboratory testing and the inferences that can be derived thereof.

2.4.1 Medium-voltage switchgear arc fault detection

As mentioned in the preceding sections, initially the simulation results associated with medium-voltage arc fault detection approach seem to suggest that most of the higher order harmonics would be adequately qualified to serve as input for the current differential approach. However, as the system is modified gradually to resemble the real world situation, if issues such as magnitude/ phase angle, sensitivity for internal fault, security/discrimination against external faults, selectivity etc are taken into account then the choice for the parameter may be limited and the parameter best suited could vary from system to system.

Some obvious observations/inferences that can be drawn from the results presented in section 2.1.4:

- The configuration of the transformer does not have any major impact on the line current of interest. From the results obtained from simulation, the transformer configuration would not affect the current differential approach as long as the transformer is not placed in

between the 2 current sensors that are employed for differential approach. In that case, it could affect the actual operation in terms of the harmonic current that would appear on two different sides of the winding.

- In the absence of capacitors, most of the harmonic components in line 4-5 and 5-6 provide a significant magnitude ratio and phase angle difference for an internal fault. In the case of an external fault however, all harmonic currents in line 4-5 and 5-6 have the same magnitude and same phase angle. Thus a majority of the higher-order harmonics seem to be suitable parameters for the current differential.
- The system is simulated without the zero sequence parameter for grounding impedance (series impedance from wye point of load, e.g. motor to the ground); therefore, direction of the 3^{rd}, 9^{th}, 15^{th} flows from harmonic source (non-linear load) back to swing bus. The capacitors provide additional paths for harmonics flow and tend to distort their magnitude ratio. The result shows that magnitude ratio of 5^{th} harmonic is still appreciable to detect the internal fault.
- In study cases such as TC1 and TC2 wherein the system configuration most closely resembles that of the actual system, a close look at summary results tabulated in Table 2.6 reveals that if both magnitude and phase angle are taken into account then 5^{th} harmonic current seems to provide the most suitable results required for operation of

the current differential approach of all harmonic components analyzed.

Thus after comprehensive simulation of the system, while all harmonics do qualify under the higher-order differential protection scheme, it is observed that 5^{th} harmonic component of the line current seems to provide a reliable parameter for detection of arcing fault in the switchgear. The behavior of the most harmonic components of the line current also seems to suggest that it would provide good discrimination against external faults and security against large through fault currents.

2.4.2 Low-voltage switchgear arc fault detection

The following observations/inferences can be drawn from the results presented under section 2.2.3:

- The results associated with the internal arcing fault case clearly underlines the sensitivity of the approach to faults lying within the differential zone i.e. switchgear.
- Another important pre-requisite for differential protection schemes is satisfied when clear discrimination against external arcing fault is demonstrated through the results associated with arcing on the source and load sides of the differential zone.
- The results documented in section 2.2.3 also end to corroborate the findings associated with the results for medium voltage arc fault

detection wherein both the harmonic magnitude and phase angle are found suitable foe utilization in the higher-order harmonic differential approach.

Finally, while the simulation and modeling approach is employed to confirm the validity of the approach for medium voltage switchgear arcing faults, actual hardware testing confirms the same for low voltage arcing faults. The fact that the approach clearly distinguishes between arcing fault and normal conditions using more than one yardstick goes a long way in establishing the reliability of the approach. This approach can serve as an early warning system for any developing arcing faults in medium/low-voltage switchgear thereby averting a possible safety personnel fatality. Apart from that, early detection of such a condition would prevent long durations of sub-standard power quality to the consumers. This aspect would benefit the consumers and the utility equally in this age of deregulation and competition. The successful implementation of this approach would serve as the first step in the transition from preventive to predictive maintenance in the switchgear and power quality industry.

CHAPTER 3

MOTOR COIL ARCING FAULT – HARDWARE DEVELOPMENT

While the previous chapter focused on switchgear arc fault detection, the research and discussion presented in chapters 3 and 4 focus on the detection and severity-classification of arcing faults in another very important aspect of industrial power systems, namely motor loads. Motor loads form a majority of the load portfolio in industrial power systems. Unlike the switchgear wherein mere detection of the presence of arcing fault was deemed enough, the classification of the severity of arcing faults in motors is required since the detection of the arcing fault may not be to perform necessary isolation actions. The classification of the severity of arcing faults in motor coils is based on the location and the percentage of the motor coil shorted through the arcing fault.

3.1 Background Information

Research directed towards the detection and monitoring of low and/or medium voltage arcing faults at various locations in the power system has witnessed noteworthy developments over the last decade. A sizable portion of the aforementioned research has been directed towards the development of mathematically accurate models for low/medium voltage arcing faults at various locations within the power system.

Gammon and Matthews [22] discuss the development of current-dependent arc voltage model for low voltage power system. Gammon and Matthews [1, 22] cite the common and often devastating occurrence of arcing faults in 480Y/277 V and 208Y/ 120 V systems as the motive behind their concentration on low-voltage systems. Arc fault modeling has evolved a great extent over the past decade with various models such as Mayr arc model, Cassie arc model, Habedank arc model, Kema arc model, Schavemaker arc model, Schwarz arc model and modified Mayr arc model being some of the more common models [23].

The other major focus of research in this area has been the detection of arcing faults at various power system locations by the application of waveform-analytical tools to pre-identified parameters. Some of the common parameters employed for waveform-analysis include the higher-order harmonic content of the arcing current in either time or frequency domain [24]-[25]. The time domain approaches have relied on the utilization of indicators such as positive-to-zero sequence current ratios, half cycle asymmetry and random nature of the arcing current [26]-[28]. The frequency domain analyses seem to have revolved around the utilization of the harmonic content of the arcing current or some other equivalent parameters quantizing the waveform distortion during arcing phenomenon. Certain approaches have also proposed the utilization of artificial neural networks to distinguish between arcing and normal conditions [29]-[30]. [31] discusses a novel approach involving the utilization of acoustic, infra-red and electromagnetic waves emanating from the arcing source to detect and locate the source in three-dimensional space.

More recent developments include the utilization of advanced signal processing capabilities for feature extraction in conjunction with neural networks for real-time DC arc fault detection and remedial action [32]. [33] proposes a technique for on-line detection and location of low-level arcing faults in dry-type transformers utilizing the ultrasonic, infra-red, acoustic and radio-frequency properties of the arc. A combination of the application of arc fault modeling and the subjection of network parameters obtained thereof to signal processing based feature extraction and Artificial Neural Network (ANN) to detect arcing faults for Navy IPS systems is presented in [34].

The discussion and/or references cited above are clear indicators of the fact that the previous couple of decades have heralded an era wherein research associated with the detection of arcing faults at various voltage levels and in various power system apparatuses has flourished. However, a majority of the research cited above has contributed to the mathematical evolution of the model utilized to represent the arcing fault for system modeling techniques. The work presented in few other references cited aims to utilize the modern signal processing tools to further the performance of existing methodologies for arc fault detection in power systems.

The research documented in the ensuing two chapters of this dissertation focuses on the classification of the severity of low-voltage motor coil arcing fault utilizing various statistical classification techniques. While the performance of the statistical techniques utilized is well documented, the utilization of the techniques on unique signatures based on identifying key inherent characteristics for classification of severity of motor coil arcing faults provides the novel edge to the research documented in the ensuing 2

chapters.

An elaborate test-bench, flexible enough in design to emulate motor coil arcing at various locations in the coil of varying severity, has been developed in the Power System Simulation Laboratory at Energy Systems Research Center. The design and development of the test-bench associated with the initiation of motor coil arcing fault was critical to the application of various algorithms and results obtained thereof. Various approaches to the design and development of the hardware capable of producing sustained arcing fault flexible enough to alter locations and severity and controlled enough to be performed as a laboratory experiment were tested. His chapter focuses on the various design approaches utilized accompanied with the process and rationale behind the final design. This chapter also discusses the testing and data acquisition modules developed in conjunction with the motor coil arcing fault test-bench in order to record the arcing current data for off-line analysis.

The arcing current signals obtained from the LabVIEW based data acquisition system are subjected to a filtering and subsequent feature extraction process. Statistical techniques such as Spectral Angle Mapper (SAM), Spectral Information Divergence (SID) and Linear Discriminant Analysis (LDA) are then applied to the extracted features to classify the severity of the motor coil arcing fault. The results of the classification process seem very promising in terms of the accuracy with which the various levels of arc-fault severity have been rightfully classified. The proposed approach, apart from endeavoring to elevate the arc-fault detection/monitoring research to a new level, is feasible enough for real-time implementation in the industry. The

approach while beneficial for most motor coil arcing levels would prove ideal for large motors wherein detection of the presence of an arcing fault may not be enough given the size of the motor coil winding. The discussion associated with the development of the signature patterns associated with the motor coil arcing current and the implementation of the statistical techniques for the classification of severity of arcing faults in presented in the next chapter.

3.2 Hardware Development

As mentioned above, the hardware development associated with the classification of severity of motor coil arcing faults formed a critically important aspect of the entire process. The fact that the design of the test-bench had to take into account the following factors associated with the arcing fault initiated made the design extremely critical:

- Flexible enough to allow variations in the location and severity (in terms of percentage of motor coil shorted through arcing fault) of the motor coil arcing fault to enable performance evaluation of the proposed techniques;
- Frequency of the arcing fault should be large enough to be able to capture the accurate amount of harmonic content, if applicable;
- Capability of producing sustained arcing faults at the 120V level;
- Mimic motor coil arcing fault in terms of the inductive and resistive elements associated with the motor coil;

- Robust design to allow numerous rounds of testing thereby enabling ample arcing current data acquisition;

As would be evident from the above discussion, the design of the test-bench for the initiation of the motor coil arcing fault plays an important role in the demonstrating the accuracy of results obtained from various classification techniques and hence in the accurate performance evaluation of various classification techniques. The ensuing sub-sections under this section present 2 distinct design alternatives considered for the motor coil arc fault initiation test-bench. The ensuing sub-sections also compare each of the design alternative with the evaluation parameters outlined above finally choosing one for its superior performance.

3.2.1 Test-Bench Design Alternative #1

The discussion presented in this section focuses on the first of the 2 motor coil arcing fault design alternative presented in this chapter. The sub-section discusses the design and development of the alternative in conjunction with the data acquisition module. The data acquisition module is utilized to acquire the arcing current data to make an informed decision associated with suitability of the design alternative for the purpose at hand.

The basic thought behind the motor coil arcing fault design alternative is to create a "make and break" scenario at varying voltage, speed and phase levels. Figure 3.1 provides a basic schematic elaborating on the design of the *arcing generator*. As can be seen from Figure 3.1, the schematic of the design alternative #1 primarily consists of an

outer aluminum ring housing 2 copper contacts insulated from the outer aluminum frame through insulation material (Delrin). The copper contacts are energized by the live and neutral lines of AC power supply through an inductor with the outer aluminum ring insulated through delrin to prevent short-circuit. The inner ring is mounted on the shaft of an induction/DC/synchronous motor and the inner ring s insulated from the shaft of the motor with the same insulation material. The primary reason why all three of these motors are mentioned is each of the motors provide better control over different parameters such as motor speed, torque etc which in turn could allow better control over the frequency of the arc. Provision has also been made for replacing the copper contacts on the rotating ring with inclined copper coated stainless steel inclined brushes. The rotation of the inner ring would allow the make and break of contact between the movable copper contacts/brushes and the fixed energized copper contacts mounted on the stationary aluminum ring. The advantage of using the copper coated brushes is that by adjusting the angle of the incline of the brushes the duration of the arcing could be altered for experimental purposes. The design is made flexible enough to allow for testing the arcing process under different speed conditions, different arcing instants in terms of the position in the sine wave, different durations of arcing. Furthermore a resistor-inductor circuit is provided after the lower fixed copper contact to complete the circuit with the amount of motor coil needed to be shorted through the arcing fault.

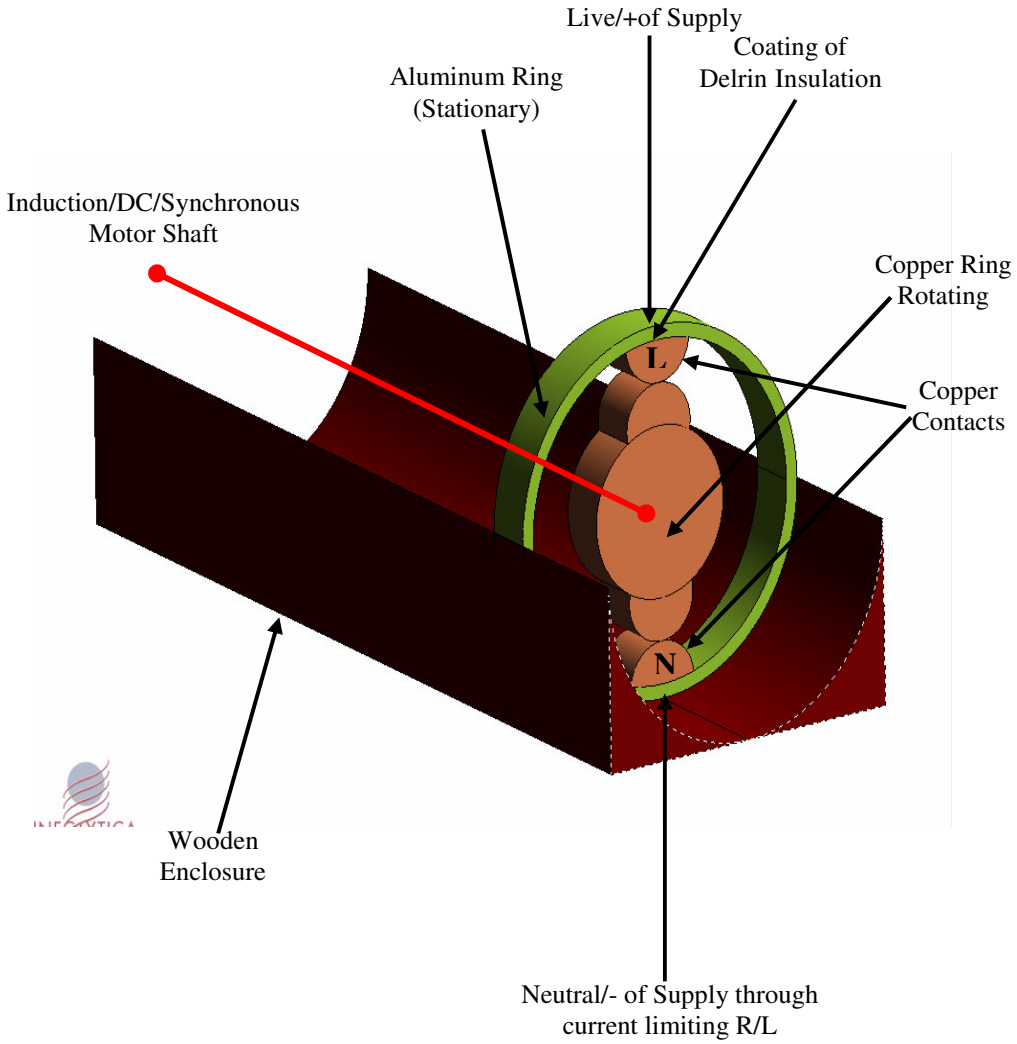

Figure 3.1: Design Schematic of *Arcing Generator* – Design Alternative #1

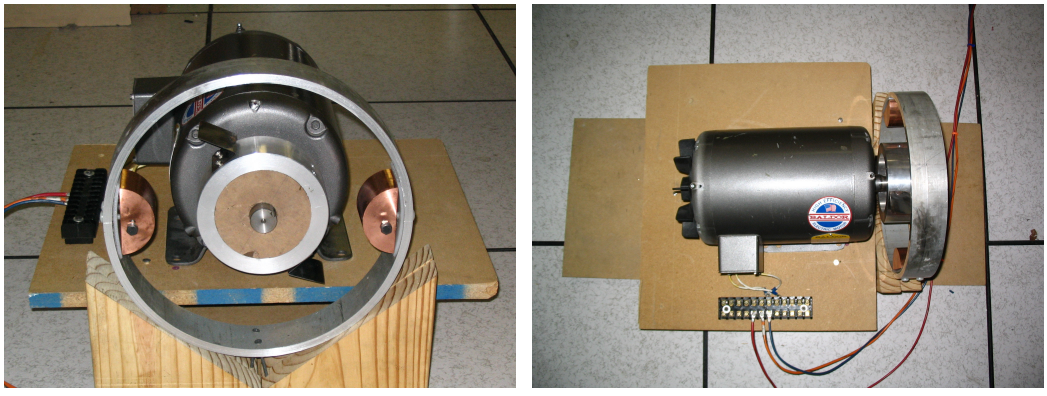

Figure 3.2 *Arcing Generator*: Complete test-bench in Power System Simulation Laboratory – Design Alternative #1

Figure 3.2 depicts the *arcing generator* complete in mechanical design and construction in the Power Systems Simulation Laboratory. Soft starting is required for the 3-phase induction motor to prevent any sudden jerk or movement since alignment of the inner ring (mounted on the induction motor shaft) is critical to the performance of the *arcing generator*. A 3-phase autotransformer in conjunction with an Adjustable Speed Drive (ASD) have been employed for voltage and hence speed control of the 3-phase induction motor, thus varying the duration and frequency of the arcing fault to ground. Hall-effect sensors are placed in the line connecting to the copper contacts on the outer stationary ring to read the arcing fault current for data acquisition using LabVIEW.

Figure 3.3 depicts the comprehensive electrical schematic with the arcing generator incorporated in conjunction with the supply and load. As can be seen from the schematic shown in Figure 3.3, the induction motor comprising the arcing generator is fed through a delta-star connected isolation transformer and an adjustable speed drive. The adjustable speed drive is used since the induction motor draws very high starting current and soft starting is an extremely important issue keeping in mind the strict alignment of the brushes with respect to the stationary copper contacts. The arcing current produces harmonics which tend to flow back into the adjustable speed drive thereby tripping the protection laid in place for the sensitive power electronic components in the drive and hence an isolation transformer is used to prevent the harmonics from entering the adjustable speed drive as shown in the schematic.

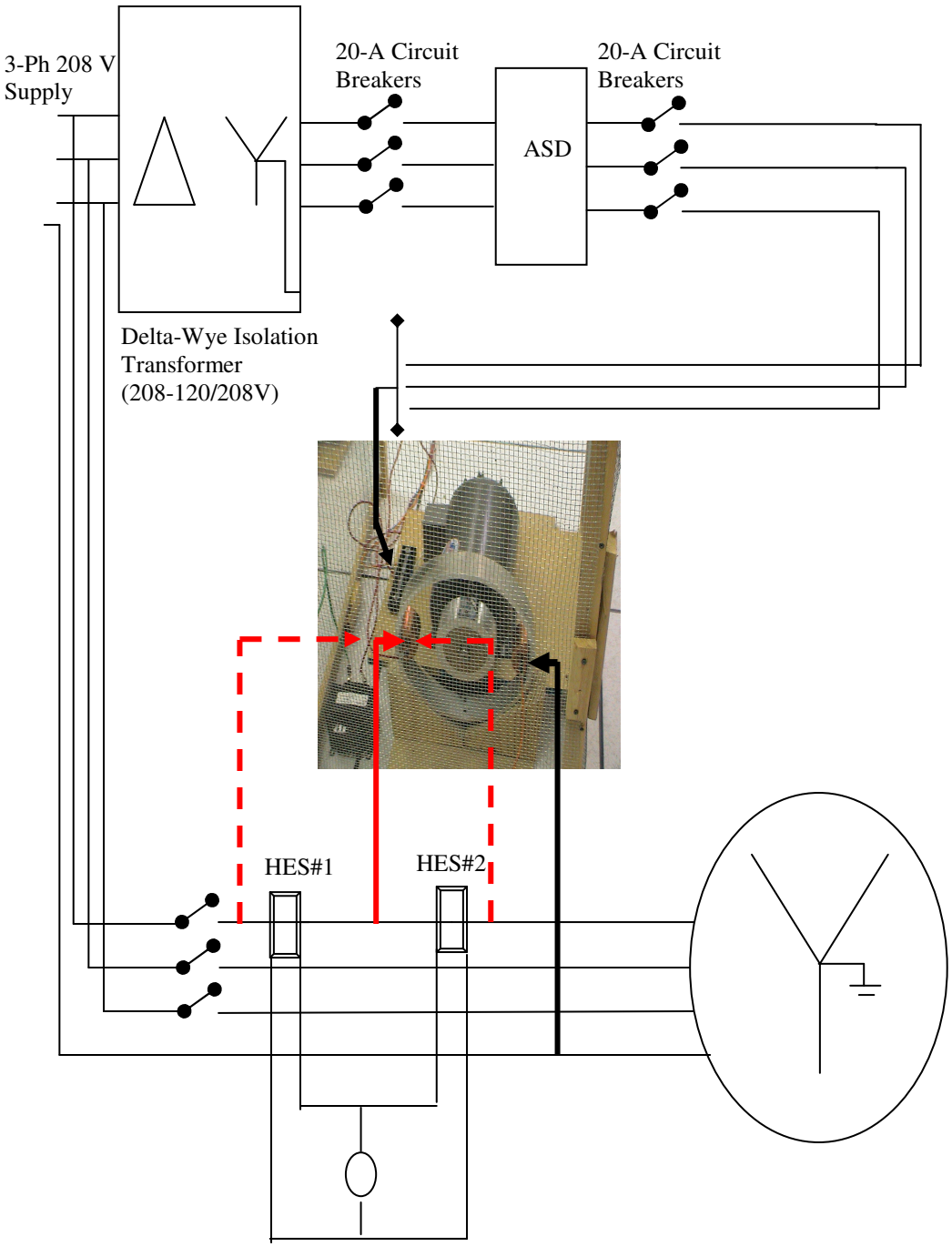

Figure 3.3: One-Line Diagram for the Arcing Generator Set-up – Design Alternative #1

The stationary copper brushes mounted on the outer ring form a part of the incomplete circuit which is terminated by varying amounts of inductance to mimic the motor coil. This circuit is completed intermittently by the rotation of the brushes mounted on the inner ring driven by the induction motor shaft. The stationary copper brushes are fed by a single phase supply as shown in the schematic.

The stationary copper contacts mounted on the outer ring form a part of the incomplete circuit which is terminated by a 100mH inductor. This circuit is completed intermittently by the rotation of the brushes mounted on the inner ring driven by the induction motor shaft. The stationary copper brushes are fed by a single phase supply as shown in the schematic.

The concept and utility of the arcing generator can now be appreciated from the fact that the single phase supply required for the arcing circuit can be taken from any location where the arcing has to be simulated. In other words, with varying amounts of inductance and/or resistance shorted through the arcing fault by terminating the arcing fault with the said inductance and/or resistance the motor coil arcing fault can be simulated at any location within the power system as depicted in the schematic.

The data acquisition module, similar to that utilized for acquiring the arcing current in the switchgear hardware design, is used in conjunction with the hall-effect sensors shown above to collect the arcing current data samples to analyze the performance of the design alternative #1 in terms of producing an arcing current to meet the criteria laid out at the onset of this section.

Figure 3.4 depicts sample plots for the arcing current data acquired via the data acquisition module applied in conjunction with the design alternative #1 designed above.

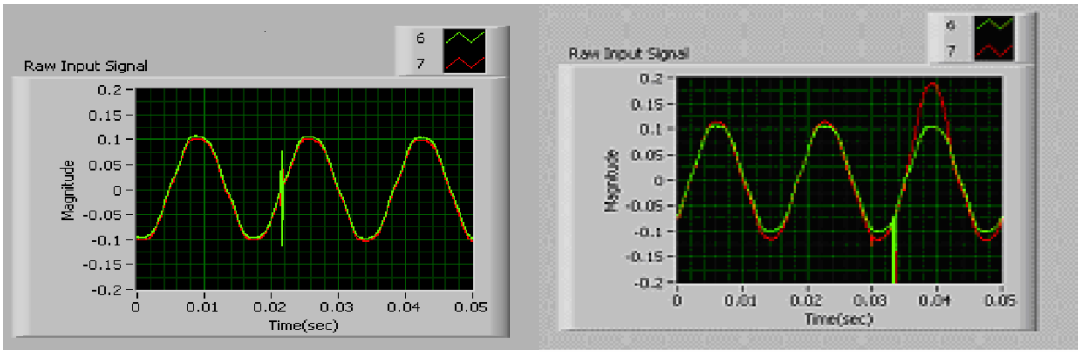

Figure 3.4: Sample Arcing Current Signals – Design Alternative #1

As is evident from the plots depicted in Figure 3.4, the arcing produced by the design alternative described above has a frequency that categorizes it as intermittent arcing more than sustained arcing. This is attributed to the fact that since the "make and break" scenario materializes only once in each revolution of the brushes the frequency of the "make and break" scenario is not large enough to mimic sustained arcing despite operating the induction motor housing the brushes at its maximum speed. Hence even at very high speeds, the arc produced by the arcing generator is an intermittent arc where in the lack of a consistent harmonic profile makes it difficult to implement any of the proposed statistical techniques since , as would be evident from the discussions in the next chapter, the signature utilized for the statistical techniques comprises of higher-order harmonics. Hence, while the design alternative #1 meets some of the criteria laid out at the onset of this section such as being flexible in terms of location of arcing fault,

the absence of the ability to provide a sustained arcing fault does not allow it to be utilized as the final design alternative. As would be evident from the discussion presented in the ensuing sub-section, all of these concerns arising from the testing results presented in this sub-section have been accounted for in design alternative #2.

3.2.2 Test-Bench Design Alternative #2

The previous sub-section focused on analyzing the results of the arcing test carried out using the arcing-generator test set-up employing varying amounts of inductance to mimic the motor coil arcing fault. Various bottlenecks in the detection of intermittent arcing (as caused by the arcing generator) were dwelled upon. The focus of the discussion presented in this sub-section revolves around the development of a new test-bench to test the arcing current pattern depending on the location of the arcing in terms of the extent of the motor coil. The sub-section discusses and describes in elaborate detail the design and development of the new test-bench devised for the afore-mentioned purpose. The design of this test-bench has been devised in such a way so as to allow for the arcing to take place at different extents of the coil in order to allow the capture the pattern of arcing current for each case thereby facilitating the study of the arcing current pattern and overcoming the shortcomings encountered in design alternative #1.

In order to study the arcing current patterns at varying arc locations with respect to the motor coil, provision has to be made for the arcing to span varying amounts of the inductive reactance of the coil. The test bench discussed in this sub-section aims to do

the aforesaid. Figure 3.5 below provides the schematic for the test bench developed in the Energy Systems Research Center.

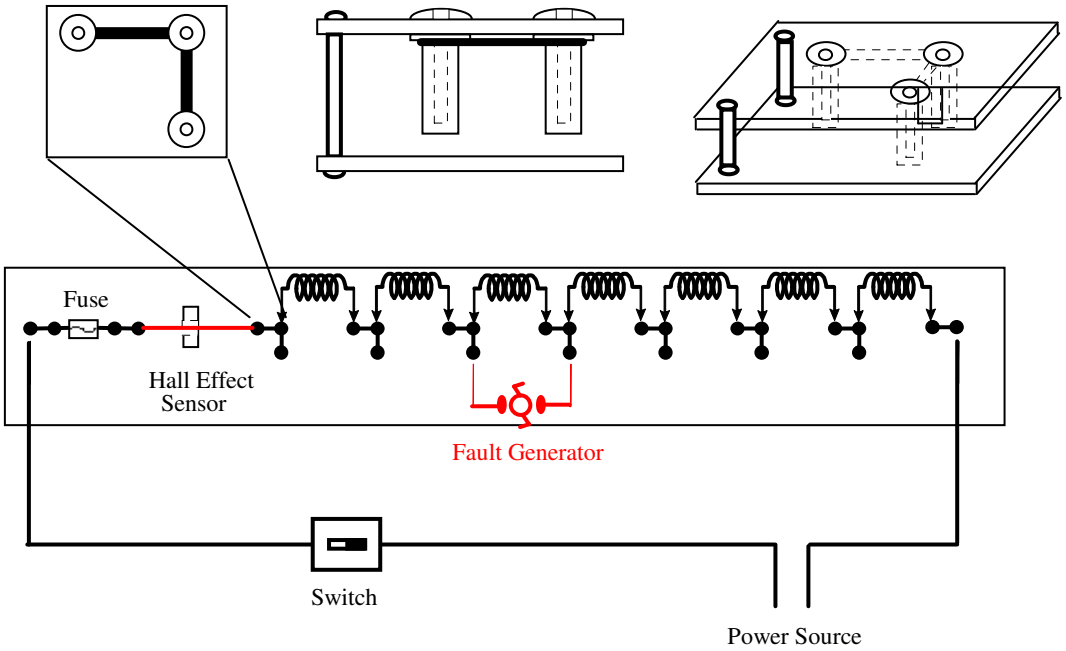

Figure 3.5: Schematic for Test-Bench for motor coil arcing – Design Alternative #2

Various design aspects such as flexibility to initiate arcing fault of varying severity at various locations, ability to vary frequency/duration of arcing fault, sophisticated data collection capability at high-sampling speeds and ease/safety of execution in laboratory environment have been taken into account. Figure 3.5 depicts the design schematic of the motor coil arcing fault test-bench. As is evident from Figure 3.5, provision is made to initiate arcing fault of varying severity by including the desired amount of inductance across the "arcing generator". The location of the arcing fault can also be maneuvered based on the location of the terminals of the arcing generator. Arcing fault current signal is acquired through the hall-effect sensor connected in series with the circuit. Provision for circuit isolation is provided by means

of an aptly sized fuse and isolation switch between the circuit and the power supply. Figure 3.6 provides a detailed view of the motor coil arcing fault test-bench with specific focus on the arc generation mechanism. As can be seen from the figure, the test-bench consists of 60 equally spaced electrically conducting screws around the perimeter of an insulated disc. The disc is mounted on the shaft of a 12V dc motor with gear drive t reach a rated speed of 30 rpm. Two variable length contacts are connected in a fashion to create a make-and-break circuit with each screw. This allows for 1800 arcing instants per minute thereby providing sufficiently frequent arcing instants. The amount of inductance appearing across the two movable contacts is the amount that would be subjected to the arcing fault.

The data acquisition module from LabVIEW has been utilized to acquire the current signal during the arcing fault of varying severity at various locations in the motor coil. A sampling rate of 18000 samples/sec has been utilized since accurate higher-order harmonic information would be utilized during the feature extraction process.

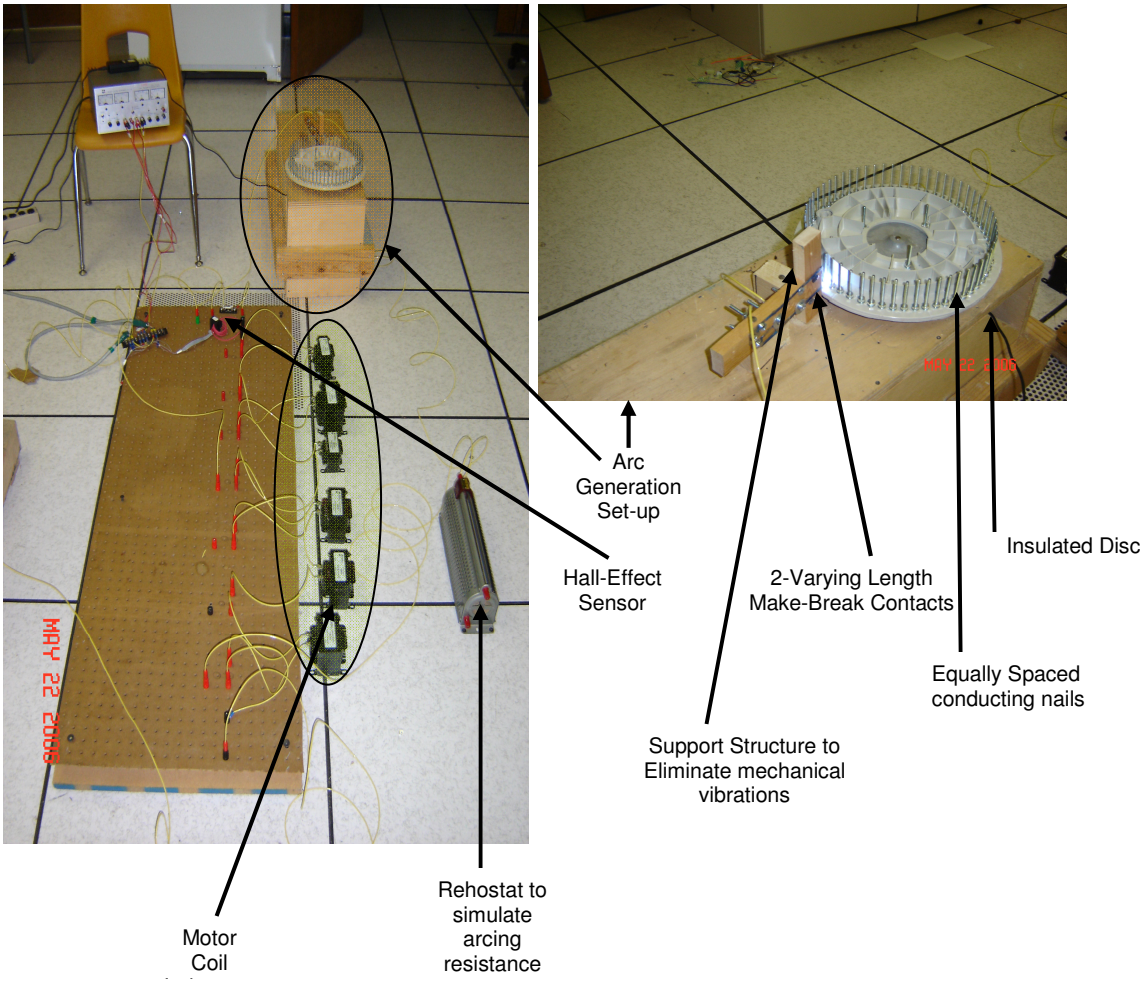

Figure 3.6: Laboratory test-bench set-up for motor coil arc-fault generation – Design Alternative #2

A glance over the elaborate description provided for design alternative #2 clearly indicates that this alternative not only manages to overcome the shortcomings of design alternative #1, but also does meet the criteria set laid out at the onset of the section. As would be evident from the results of the testing methodology presented in the ensuing sub-section, this design alternative is the preferred choice for the test-bench to be utilized to mimic the occurrence of motor coil arcing faults at the 120V level.

3.2.3 Testing & Data Collection Methodology

Since design alternative #2 was chosen as the preferred alternative the testing methodology and data collection aspects discussed in this sub-section are done with respect to that design alternative. The preliminary results associated with the testing and data collection presented in this sub-section, further corroborate the suitability of design alternative #2 for the motor coil arc fault initiation test-bench. The primary motivation behind the design and development of the motor coil arc fault generation test-bench described above is to obtain the flexibility to initiate arcing faults of varying severity at various locations in the motor coil. While doing this, the hall-effect sensor data corresponding to the arcing fault current is collected via a LabVIEW based data acquisition system.

The basic concept behind the testing methodology is to test for specific patterns of the harmonic content for the following scenarios:

- Shorting varying percentages of the motor coil
- Shorting varying percentages of the coil at the beginning, middle and end of the coil.

The idea was to discern patterns including characteristics unique to the arcing current that clearly distinguish between arcing current signal for arcing occurring across different percentages of the total motor coil inductance. Along with that, the same percentages were shorted at the beginning, end and middle of the coil to see if the location of the short does alters the aforementioned characteristics apart from the

percentage of coil shorted. Table 3.1 shown below provides a summary of the test methodology employed in this report.

Table 3.1: Test Case Definitions – Unique Characteristic Identification

Case	Shorted (mH)	Percentage	Beginning	Middle	End
1	1	1.459	Done	Done	Done
2	3.5	5.109	Done	Done	Done
3	7.5	10.949	Done	Done	Done
4	15	21.897	Done	Done	Done
5	25	36.49	Done	Done	Done
Case 3-4(a)	8.5	12.408	Done	Done	Done
Case 3-4(b)	11	16.05	Done	Done	Done
Case3-4©	13.5	19.7	Done	Done	Done

As can be seen from Table 3.1, there are 5 cases of shorting different percentages of the total motor coil inductances and each shorting case is performed under 3 different scenarios of beginning, middle and end of the coil. Since traditionally, higher-order harmonics have been a consistent occurrence in arcing faults due to the very physical nature of the arcing faults, a preliminary higher-order harmonic content analysis is performed on the data collected from the 5 test cases defined above. This is done so to ascertain whether the utilization of higher-order harmonic content in the arcing current signal for developing the feature to be subjected to the statistical techniques is justified. As can be seen from Table 3.1, the 5 cases correspond to increasing amounts of inductance coil shorted through the arcing fault. The percentage expressed in the table is expressed as a function of the total inductance included in the testing i.e. 68.5 mH. The various percentages of inductance coil is shorted at the beginning, middle and end as demonstrated by the table. These 5 cases have been initially utilized in the classification process. The cases listed as 3-4 (a), 3-4 (b) and 3-4(c) correspond to percentages of coil

shorted through the arcing fault in such a manner that all of them lie between cases 3 and 4 presented above in Table 1. Furthermore, the percentage of inductance coil shorted in case 3-4 (a) is closer to case 3, while that shorted in case 3-4 (b) is approximately in between cases 3 and 4 and finally that shorted in case 3-4 (c) is closer to case 4. These three intermediate cases have been developed to gauge the performance of various classification algorithms to unforeseen data during the occurrence of motor coil arcing fault in actual field conditions.

It is clearly evident from the testing methodology described above, that the flexibility in design associated with design alternative #1 allows the collection of data so diverse in nature and closely mimicking the occurrence of a motor coil arcing fault in actual field conditions. Furthermore, as would be evident from the results associated with the preliminary higher-order harmonic analysis showcased in the proceeding section, the arcing current signal produced from design alternative also provides the necessary unique characteristics required to extract features to be subjected to statistical techniques for the classification of severity of arcing faults.

3.3 Model Assessment – Comparative Analysis

As mentioned earlier, certain unique characteristics specific to the motor coil arcing fault current signal have been pre-identified to comprise the feature signature that would be subjected to various statistical techniques to classify the severity of arcing faults. In order to do so, the characteristics unique to the arcing fault current have to be identified based on a preliminary analysis of the raw arcing current data acquired from the test-

bench. Since traditionally, higher-order harmonics have been a consistent occurrence in arcing faults of varying nature, a preliminary higher-order harmonic analysis of the raw arcing current data was performed to assess the content of various higher-order harmonics. The discussion associated with the aforementioned higher-order harmonic analysis along with the process of feature extraction is discussed in the ensuing sub-section. Furthermore, a comparative analysis of the harmonic content of the raw arcing current data obtained from the test-bench in Energy Systems Research Center is performed with the harmonic content in contemporary mathematical models such as the Mathews model, Stokes & Oppenlander's model and Fisher's model for arcing faults in branches/coils of low-voltage systems. This discussion is presented in the final sub-section presented in this section.

3.3.1 Features utilized for arc current signature development

As mentioned earlier, based on the inferences drawn from a preliminary higher-order harmonic analysis performed on the raw arcing current data obtained from design alternative #1 test-bench, decisions associated with the feature to be utilized for statistical analysis have been made. It would therefore be fitting to first present the discussion associated with the preliminary harmonic analysis carried out on sample data acquired from the test-bench.

Figure 3.7 depicted below showcases the contents of various higher-order harmonics in the raw arcing current data for test case 5 corresponding to the shorting of

25mH of the motor coil through the arcing fault initiated via the test-bench pertaining to design alternative #2.

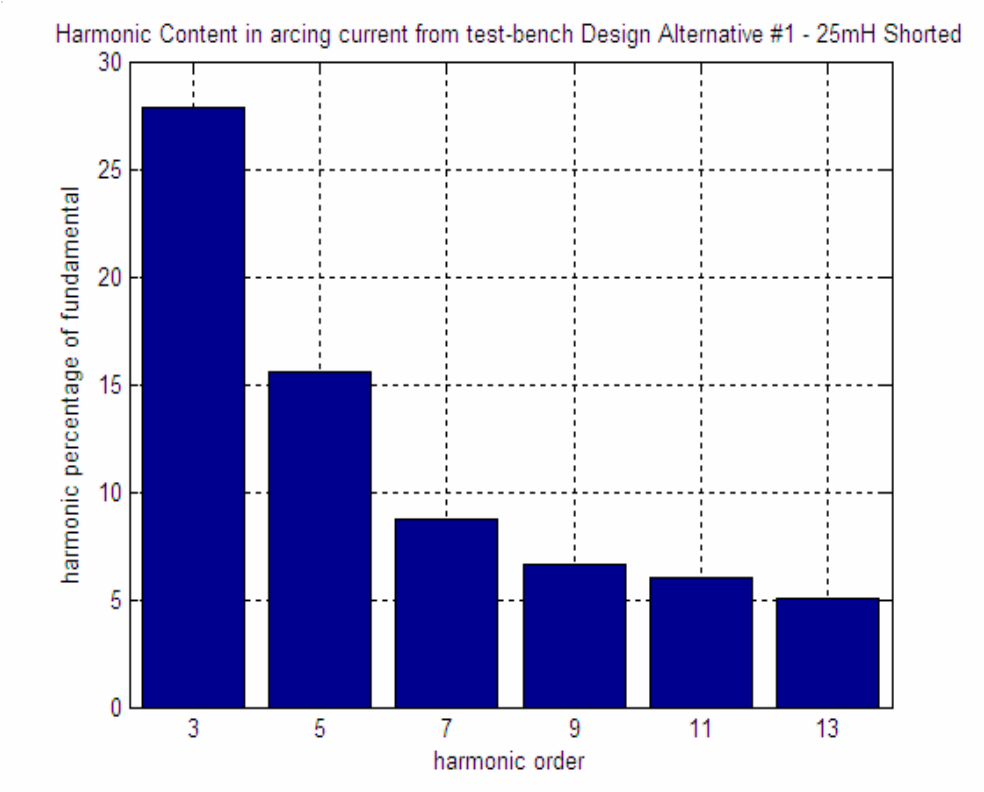

Figure 3.7: Higher-Order Harmonic Content in raw arcing current from test-bench

One of the major aspect necessary for the development of features to be subjected to statistical techniques for the classification of severity of arcing faults is corroborated from the results depicted in figure 3.7. As is clearly evident from the above figure, there are significant higher-order harmonic contents in the raw arcing current data acquired from the test-bench. The higher-order harmonics in conjunction with associated upper and/or lower sidebands would form the, what would be termed as “spectral signature” corresponding to the arcing fault for varying levels of severity.

The spectral signature vectors alluded to above are extracted from the motor coil arcing fault current data collected as described earlier. The hall-effect sensor data corresponding to the motor coil arcing fault current signal obtained from the test-bench is fed as input to a 60Hz analog notch filter. The 60Hz notch filter is utilized to eliminate the pronounced effect of the fundamental frequency component since the spectral signature to be extracted would focus on the higher-order harmonic information. The filtered signal is then subjected to a comprehensive Power Spectral Density (PSD) analysis extracting information up-to the 7^{th} harmonic and associated upper and lower side-bands. The abovementioned higher order harmonic and associated side-band information is then encrypted to obtain the spectral signature associated with associated with arcing faults of varying severities. Elaborate details associated with the application of various statistical techniques on the spectral signature vectors to classify the severity of motor coil arcing faults are discussed in the next chapter.

3.3.2 Comparative Analysis with contemporary models

Although one aspect necessary with the development of "spectral signatures" associated with each severity of motor coil arcing fault was corroborated by the preliminary higher-order harmonic analysis documented above, another aspect worth looking into is discussed in this sub-section. While it has been ascertained that the arcing current as obtained from the test-bench does contain significant higher-order harmonic content, it

would be important to analyze how this harmonic content lines up with that documented in some contemporary mathematical models for arcing faults in low-voltage systems.

[17] discusses various mathematical models associated with arcing faults in low-voltage systems. While most of the models developed and mathematically analyzed in [17] correspond to 277/480V systems, comparison with the 120V arcing fault test-bench developed in the laboratory is justified. [17] presents the mathematical model and analysis associated with Matthews model and compares key characteristics such as arc current, arc voltage and supply voltage as derived through Matthews model with more recent arcing fault models for low voltage systems such as work carried out by Fisher and Stokes & Oppenlander.

In order to compare the harmonic content depicted in Figure 3.7 with the harmonic content obtained when the motor coil configuration is simulated in Mathews model and that of Stokes & Oppenlander, the respective mathematical models were developed and simulated for the same configuration as that in the test-bench. As per [17] the arc voltage and current characteristics for the model developed by Fisher are very similar to those obtained from the model by Stokes & Oppenlander. It is for this reason that the model for Fisher is not simulated since a comparison of results with the model developed by Stokes & Oppenlander provides a clear indication of the harmonic content developed by the test-bench with contemporary mathematical models.

In order to verify the validity of the mathematical model developed, the mathematical models are first simulated with parameters exactly similar to those presented in [17] to benchmark the results associated with the arc voltage and current

for the respective mathematical models. Figure 3.8 depicts the plots for the arc current, supply voltage and arc voltage with respect to time corresponding to the Mathews model with parameters exactly similar to those utilized in [17] for arcing fault at the branch. The following differential equation has been utilized to solve for the arcing current with the system parameters utilized as listed below:

$$V_{max}\sin(wt) = Ri_{arc} + L\,(di_{arc}/dt) + V_{arc}$$

Where:

Vmax: Peak of Sinusoidal Voltage = 400V (for 277Y/480V systems)

w: System Frequency (radians/sec) = 314.159 rad/sec

R: Branch resistance (ohms) = 178.39 mohms

i_{arc}: R.M.S arc current

L: Branch inductance (Henry) = 48.86 x 10e-6 H

V_{arc}: Arc Voltage (assumed to be flat-topped 140V for Matthews model)

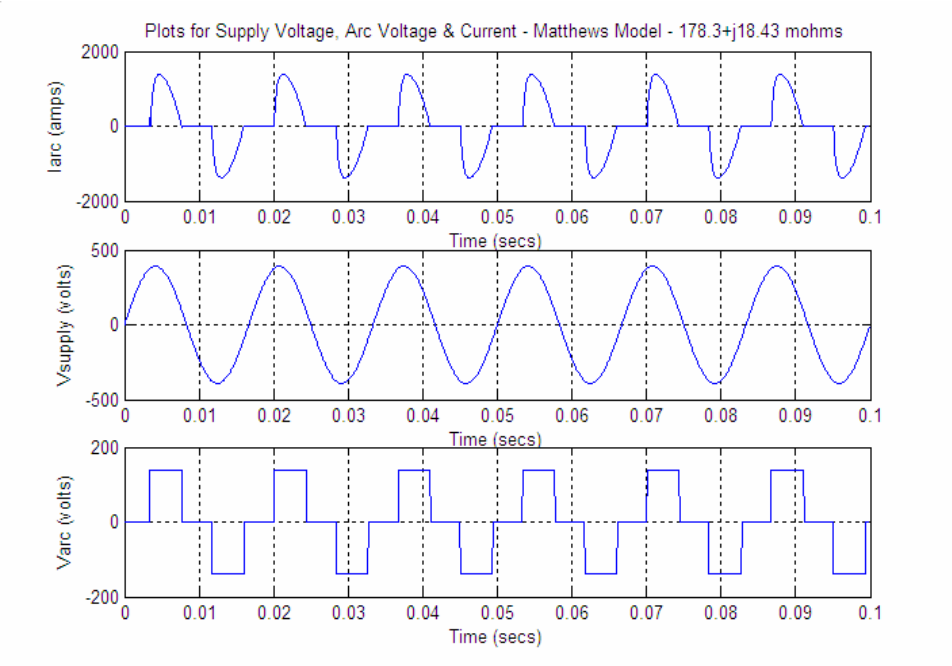

Figure 3.8: Arc Voltage & Current Plots for Z= 178.39 + j18.43 mΩ – Mathews Model

As is evident from the comparative analysis of the results presented in Figure 3.8 and its counterpart in [17] for the same system parameters, the results associated with the arc voltage and current are precisely the same thereby validating of the mathematical representing the Mathews Model to obtain the results associated with 25mH shorted through arcing fault. Figure 3.9 depicts the plots associated with the arcing current, voltage and supply voltage associated with shorting 25mH through the arcing fault in the Mathews model.

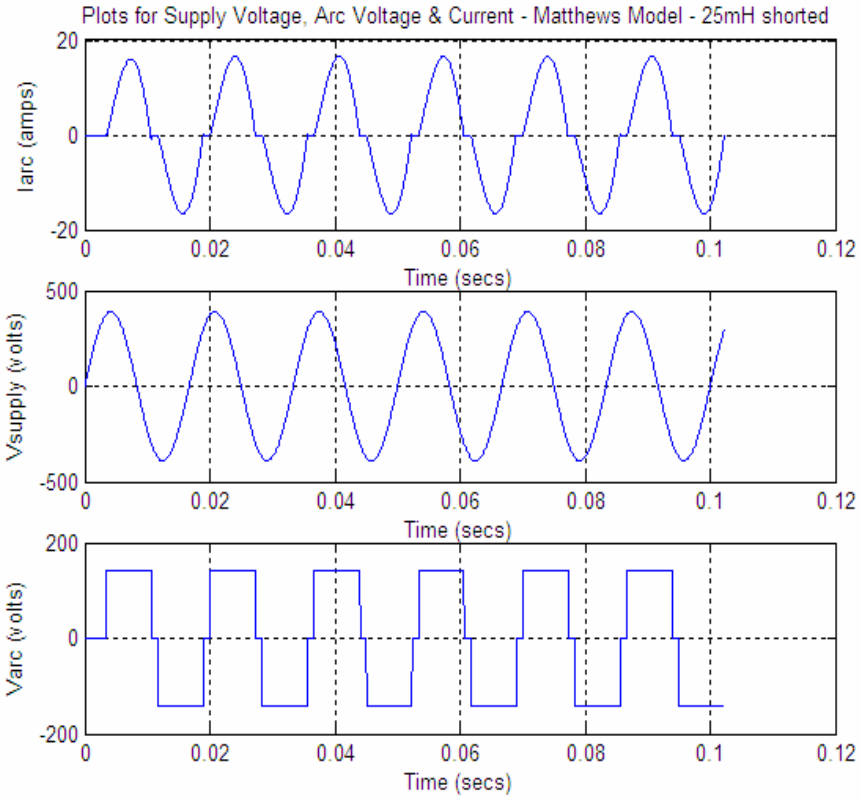

Figure 3.9: Arc Voltage & Current Plots for 25mH shorted – Mathews Model

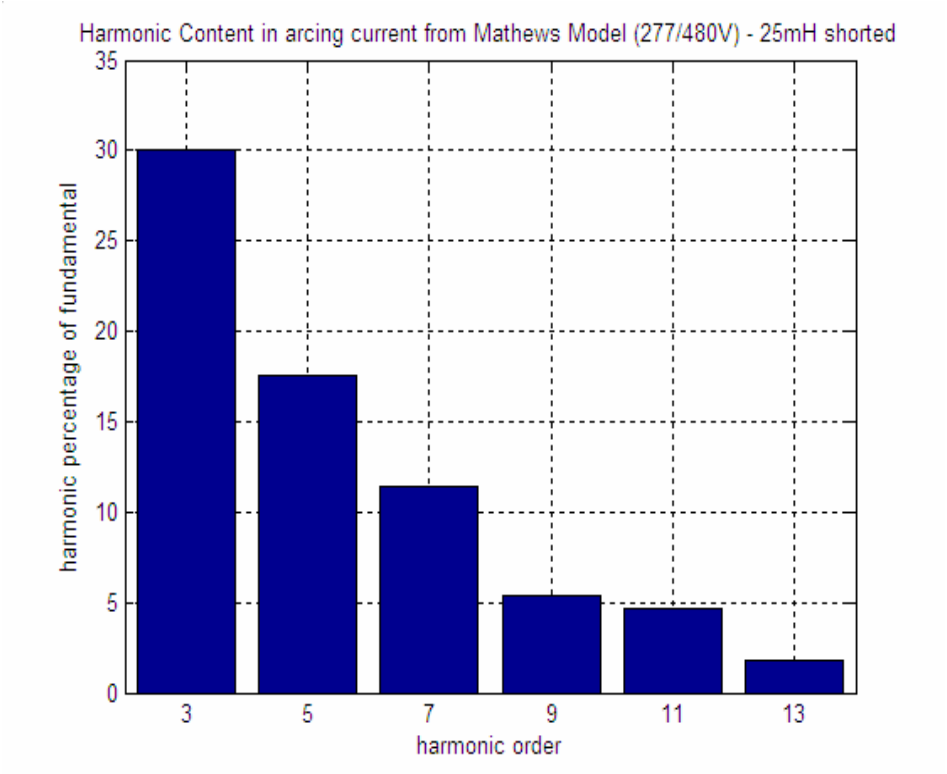

Figure 3.10: Higher-Order Harmonic Content – 25mH Shorted – Mathews Model

Figure 3.10 shown above depicts the higher-order harmonic content as present in the arcing current obtained from simulating the Mathews model for 25mH of inductance shorted through the arcing fault. A comparative analysis of figures 3.7 and 3.10 clearly indicates that the harmonic content contained in the arcing current produced from the arcing fault initiated in ESRC is very close to that simulated through Mathews model. Minor deviations between the two may arise to the difference in voltage level at which each of the arcing faults have been produced apart from inherent differences between mathematical modeling and actual hardware model. However, it is evident from figures 3.7 and 3.10 that higher-order harmonic content forms a significant part of the arcing

current signature for arcing faults at low voltage levels irrespective of the model being analyzed.

While the preceding paragraph focused on performing a comparative analysis between the harmonic content associated with the arcing current obtained from the test-bench to that obtained from simulating Mathews model for the same parameters, a comparative analysis with more recent mathematical models is the focus of discussion in the remainder of this sub-section. [17] presents a model developed by Stokes & Oppenlander which replaces the flat-topped arc voltage with an arc voltage model dependent on the arc current and the air gap characteristics. The differential equation defining the behavior of arc current for the model developed by Stokes & Oppenlander is given below:

$$V_{max}\sin(wt) = Ri_{arc} + L\,(di_{arc}/dt) + (20 + 534g)i_{arc}^{0.12}$$

Where:

Vmax: Peak of Sinusoidal Voltage = 400V (for 277Y/480V systems)
w: System Frequency (radians/sec) = 314.159 rad/sec
R: Branch resistance (ohms) = 178.39 mohms
i_{arc}: R.M.S arc current
L: Branch inductance (Henry) = 48.86 x 10e-6 H
g: air gap (meters) = 0.0254m

The differential equation defining the behavior of the arcing current according to the model developed by Stokes & Oppenlander presents more accurate results since it eliminates the assumption of the arc voltage being a constant flat topped voltage and incorporates the arc voltage dependency on arc current based on the air gap

characteristics [17]. As in the case of Mathews model, the validity of the mathematical model was first confirmed by simulating the arcing current and voltage characteristics for the same simulation parameters as those presented in [17]. Figure 3.11 presents the arc voltage and current characteristics for that simulation.

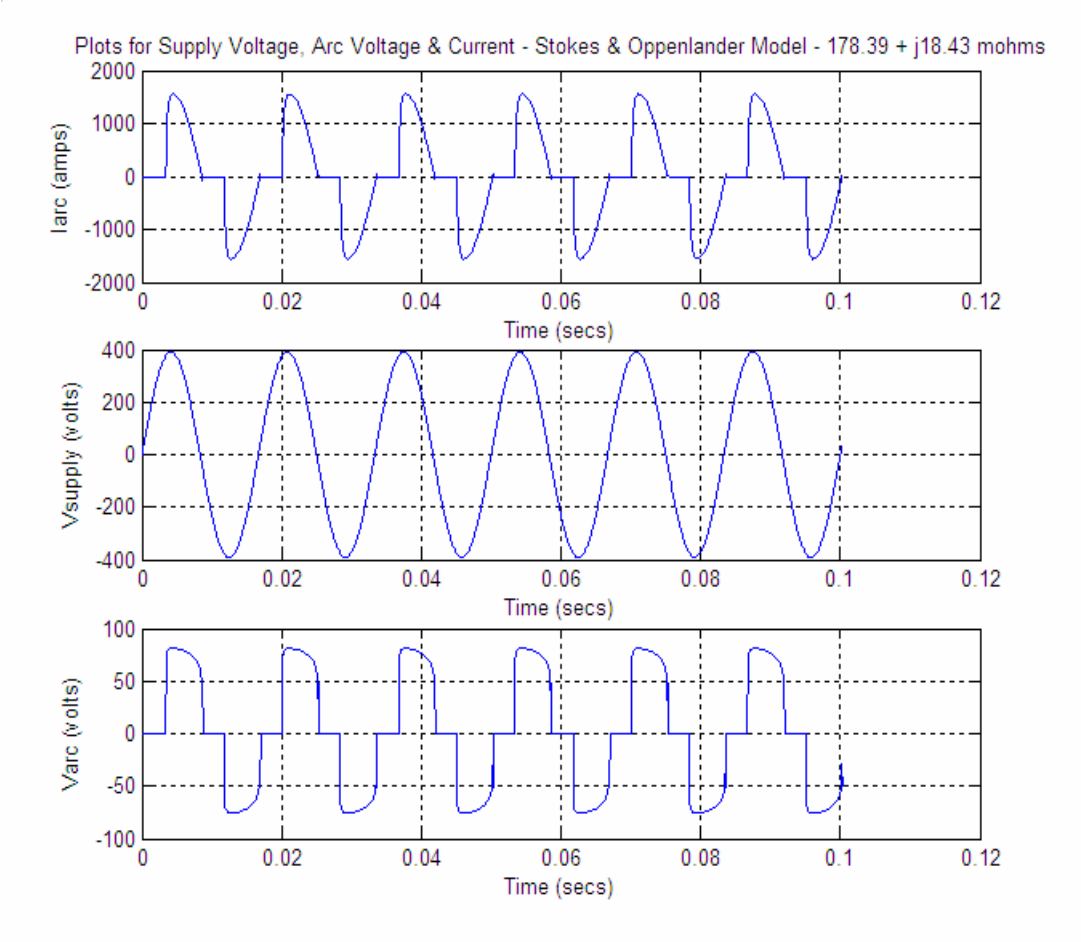

Figure 3.11: Arc Voltage & Current Plots for Z= 178.39 + j18.43 mΩ – Stokes & Oppenlander Model

As can be seen from Figure 3.11, the arc voltage and current characteristics produced from the simulation precisely resembles its counterpart for the same simulation

parameters presented in [17] thereby successfully benchmarking the mathematical model for further use with different values.

Figure 3.12 presents the arc voltage, current and supply voltage characteristics associated with shorting 25mH through an arcing fault through the model of Stokes & Oppenlander.

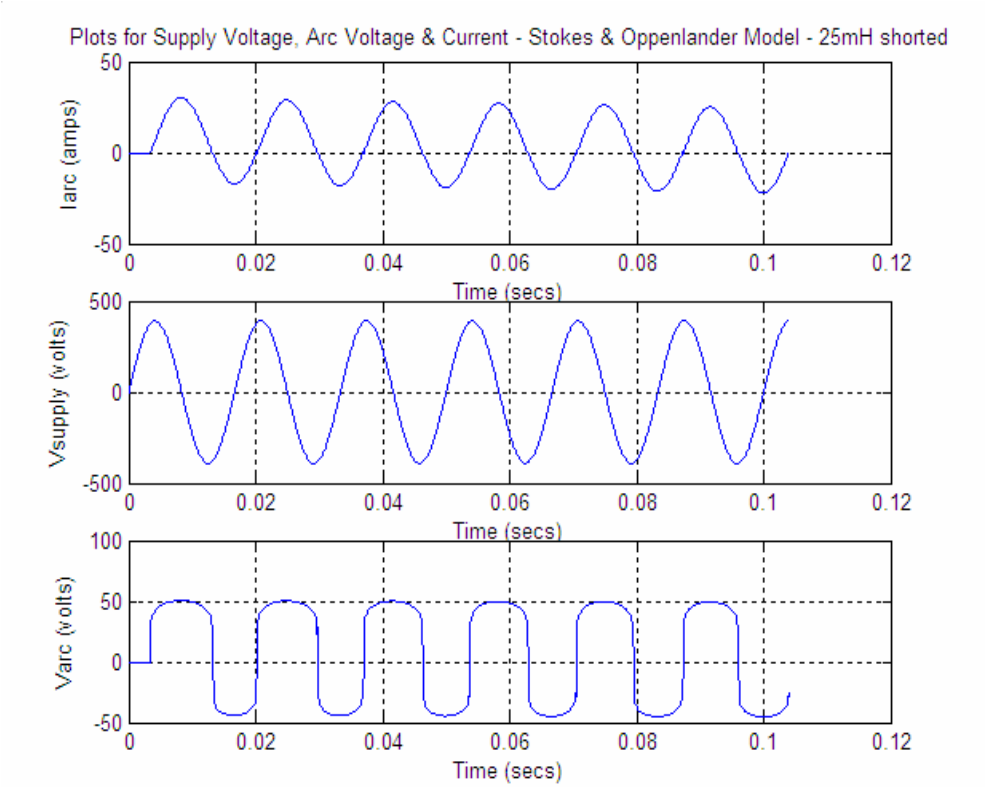

Figure 3.12: Arc Voltage & Current Plots for 25mH shorted – Stokes & Oppenlander Model

Figure 3.13 presents the higher-order harmonic content associated with the arcing current corresponding to shorting 25mH shorted through an arcing fault as simulated through the model for Stokes & Oppenlander.

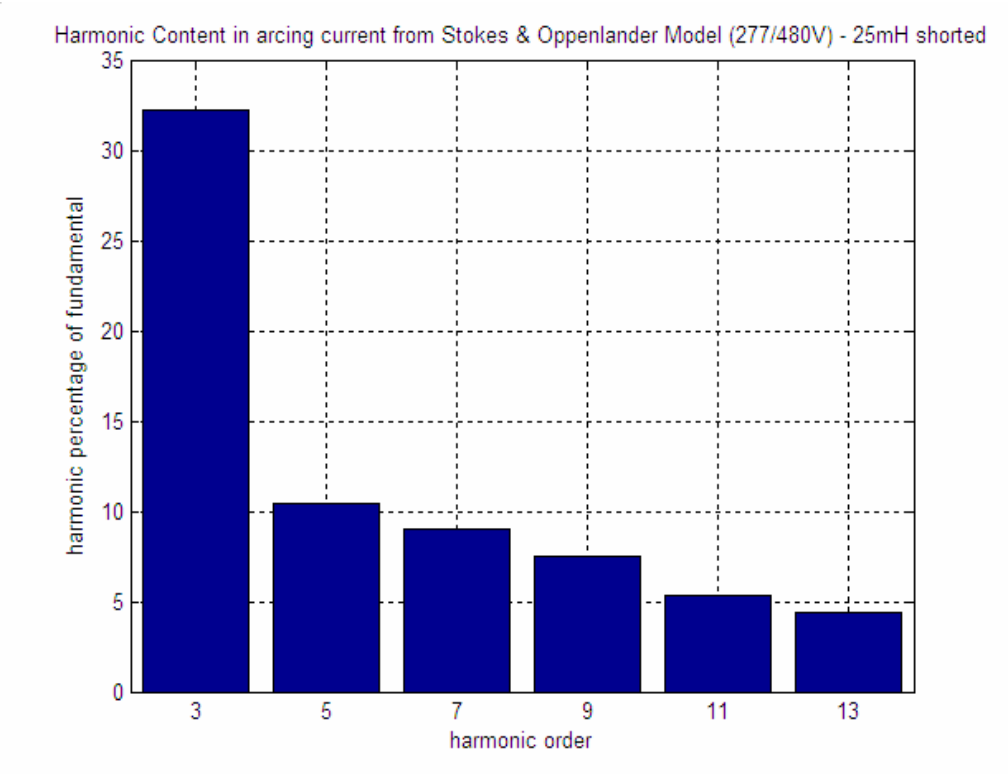

Figure 3.13: Higher- Order Harmonic Content – 25mH shorted – Stokes & Oppenlander order

As is evident from a comparative analysis of figures 3.7, 3.10 and 3.13, the higher-order harmonic content in the arcing current for shorting 25mH through a low-voltage arcing fault is of comparable magnitude with slight deviations from model to model. However, more importantly, the underlining aspect of the comparative analysis carried out is the fact that higher-order harmonic content is a significant part of the arcing current produced from arcing faults at low voltages irrespective of the model being analyzed. Hence the utilization of higher-order harmonics and associated sidebands to be subjected to various statistical techniques for the classification of the severity of arcing faults stands justified.

Thus, this chapter presents various hardware design alternatives associated with the design and development of a test-bench to mimic the initiation of low voltage motor coil arcing faults. Various aspects such as flexibility in design and the accuracy of the arcing current signature being obtained from the test-bench have been taken into account in short-listing the final design alternative. Elaborate details associated with the testing and data collection methodology associated with the final design alternative have been presented in this chapter. Finally ample rationale and justification has been provided for the selection and utilization of higher-order harmonics and associated sidebands for the statistical techniques to classify the severity of motor coil arcing faults. This is done so by comparing the higher-order harmonic content in the arcing current as obtained from the final design alternative and comparing those with that contained in the arcing current obtained by simulating contemporary low voltage arcing fault mathematical models such as Mathews model and Stokes & Oppenlander model for the same simulation parameters.

With the validity of the arcing current signature and the rationale of selecting and utilizing higher-order harmonics and associated sidebands as the unique characteristics for classification established, the following chapter focuses on the utilization of specific statistical techniques to classify the severity of motor coil arcing faults.

CHAPTER 4

MOTOR COIL ARCING FAULT – SOFTWARE DEVELOPMENT

The previous chapter focused on the design, development and implementation of hardware test-benches associated with the generation of low voltage motor coil arcing fault. Various aspects such as flexibility in design, robustness during repeated test-runs, frequency of arcing and capability of test-bench to produce varying levels of severity in arcing fault were taken into consideration during the design and development of the test-bench. The previous chapter showcased 2 design alternatives with the former falling short in terms of the design flexibility and quality of the arcing current. The 2nd design alternative was designed keeping in mind the shortcomings encountered in its predecessor. The testing methodology associated with the 2nd design alternative was presented along with various case definitions. Comparative analysis of the higher-order harmonic content in the arcing current obtained from the test-bench was performed along with the arcing current as simulated from various contemporary low voltage arcing fault models such as Mathews model, Stokes & Oppenlander model and Fisher's model with the same parameters as those in the test-bench employed. The results presented in the concluding section of the previous chapter seem to be indicative of the presence of a significant amount of higher-order harmonic content irrespective of the model being analyzed. Hence, it is justifiably concluded that the characteristics unique to the arcing current to be employed for use in the statistical analysis would comprise of

the higher-order harmonics along with associated upper and lower sidebands. Apart from that, the accuracy of the arcing current being obtained from the test-bench was compared with contemporary mathematical models such as Mathews model, Stokes & Oppenlander model and Fisher's model, utilized for modeling arcing faults for low voltage systems and the arcing current signature in terms of the higher-order harmonic content was found to be closely comparable.

With the validity and the accuracy of the arcing current being obtained from he test-bench adequately tested and benchmarked, algorithms associated with the extraction of features specific to varying levels of motor coil arcing fault and subjecting them to various statistical analyses were developed. The opening discussion in this chapter focuses on providing the reader with a basic mathematical background associated with each statistical technique employed for the classification of severity of motor coil arcing faults. It is then followed by an elaborate discussion focusing on explaining the development of the algorithm associated with the implementation of each of the statistical techniques for the classification of the severity of the motor coil arcing faults. Sections to follow then present the results associated with the application of each of the severity classification algorithms and a subsequent performance evaluation.

4.1 Background information

The classification of the severity of low voltage motor coil arcing faults is primarily explored by the application of 4 techniques in this dissertation namely:

- Spectral Angle Mapper (SAM)

- Spectral Information Divergence (SID)
- Linear Discriminant Analysis (LDA)
- Support Vector Machines (SVM)

While the primary arcing current characteristics utilized for the application of each of the aforementioned algorithms is the higher-order harmonic content and associated lower and upper sidebands, the mathematical manifestation of the spectral feature for each of the classification technique is uniquely different.

A little more elaboration on the feature extraction/selection process the output of which is utilized as input, either directly or indirectly, for each of the statistical classification techniques is necessary. The basis of the feature selection/extraction process is the computation of the Power Spectral Density (PSD) of the arcing current signal for varying levels of motor coil arc fault severity. The basic inbuilt PSD sub-vi in LABVIEW has been utilized to compute the PSD, the mathematical formulation of which is given by:

Power Spectrum $S_{xx}(f)$ of a function x(t) is:

$$S_{xx}(f) = X^{*}(f)X(f) = |X(f)|^2$$

$X(f) = F\{x(t)\}$ and $X^{*}(f)$ is the complex conjugate of $X(f)$

Depending on the number of samples in the input data sequence the built-in PSD sub-vi in LabVIEW utilizes the Discrete Fourier Transform (DFT) and Fast Fourier Transform (FFT) to compute the PSD of the data sequence. If the number of samples in the input data sequence is a valid power of 2, then the PSD of the data sequence is calculated using the FFT of a real-valued sequence by means of a fast radix-

FFT algorithm. However, if the number of samples in the input data sequence is not a valid power of 2 but factorable as a product of small prime numbers then the PSD sub-vi utilizes the DFT of a real-valued sequence to compute the PSD.

Following the computation of the power spectrum, the feature extraction process primarily comprises of extracting the spectrum amplitude information associated with 4 odd harmonics (namely the 3^{rd}, 5^{th}, 7^{th} and 9^{th} harmonics) along with their upper and lower-sideband amplitudes. In other words, if the fundamental frequency of the arcing current signal is denoted by F_s then the spectrum amplitudes associated with the harmonic and lower/upper sidebands are mathematical denoted as:

Harmonic Amplitude = Maximum Amplitude in Spectrum $\{nF_s \pm 2Hz\}$

Upper Sideband Amplitude = Maximum Amplitude in Spectrum $\{(nF_s+F_s/4) \pm F_s/12\}$

Lower Sideband Amplitude = Maximum Amplitude in Spectrum $\{(nF_s-F_s/4) \pm F_s/12\}$

Where n = order of the harmonic (3^{rd}, 5^{th}, 7^{th} or 9^{th})

There can be a significant gap between the harmonics and sidebands in terms of the maximum amplitude extracted from each of the aforementioned spectrums. In order to prevent these huge-amplitude differences to affect the detection algorithm, the extracted features are transformed to the logarithmic scale and then rescaled using a bias value. This process is mathematically formulated as:

$$20(\log_{10}(I_{PSD})) + \text{Bias}$$

As is evident from the detailed explanation associated with the feature extraction/selection process mentioned above, eventually there are 12 features (3 associated with each higher-order harmonic) extracted for each extraction process.

While the Spectral Angle Mapper (SAM) and Spectral Information Divergence (SID) utilize all the 12 features in the classification process, the LDA and SVM methodologies utilize the projected values of these 12 features to the computed principal components to classify the severity of motor coil arcing faults. The details associated with the utilization of the features are discussed in the explanation provided for the relevant classification technique.

The first three of the four techniques mentioned above are primarily statistical techniques that employ a comparative analysis between a base spectral signature and the spectral signature of interest in order to classify the spectral signature of interest into an appropriate category. While the SAM and SID techniques do not require to be trained prior to the application of various spectral signatures, LDA needs to be trained with a set of sample spectral signatures for it to classify any subsequent spectral signatures into any one of the pre-determined categories. The spectral signatures being repeatedly referred to above corresponds to a vector comprising of higher-order harmonic content and associated lower and upper sideband information associated with each class of motor coil arcing fault severity.

The Support Vector Machines, on the other hand, are primarily a set of related supervised learning methods, widely applicable to classification and regressions applications in numerous engineering disciplines. The SVMs simultaneously minimize the empirical classification error and maximize the geometric margin [35]. Support vector machines map input vectors to a higher dimensional space where a maximal separating hyper-plane is constructed. Two parallel hyper-planes are constructed on

each side of the hyper-plane that separates the data. The separating hyper-plane is the hyper-plane that maximizes the distance between the two parallel hyper-planes with the maximum distance signifying the best classification results [35].

The ensuing section presents the mathematical background associated with each one of the classification techniques mentioned above in elaborate detail.

4.2 Severity Classification Algorithms: Mathematical Background

4.2.1 Spectral Angle Mapper (SAM)

Given two spectral signatures:

$$S_i = (s_{i1}, s_{i2},\ldots\ldots\ldots s_{iL})^T \;\&\; S_j = (s_{j1}, s_{j2},\ldots\ldots\ldots s_{jL})^T$$

The SAM measures the spectral similarity by finding the angle between the two spectral signatures S_i and S_j [36]. In other words, if 2 spectral signatures are identical, the similarity measure value becomes 0. As the 2 signatures differ from each other, SAM value increases. Hence in mathematical terms SAM would equate to:

$$SAM(s_i, s_j) = \cos^{-1}((<s_i,s_j>)/\|s_i\| \|s_j\|)$$

where

$$< s_i s_j >= \sum_{k=1}^{L} (s_{ik})(s_{jk})$$

and

$$||s_i|| = (\sum_{k=1,L} s_{ik}^2)^{1/2}; ||s_j|| = (\sum_{k=1,L} s_{jk}^2)^{1/2}$$

The 2 spectral signatures here are obtained by extracting the relevant features from a base/reference current and the arcing current for a specific severity. The relevant features primarily comprise of the higher order harmonic content along with associated lower and upper sidebands.

4.2.2 Spectral Information Divergence (SID)

Given two spectral signatures:

$$S_i = (s_{i1}, s_{i2},\ldots\ldots s_{iL})^T \;\&\; S_j = (s_{j1}, s_{j2},\ldots\ldots s_{jL})^T$$

The probability mass functions corresponding to these 2 spectral signatures are denoted by:

$$P = (p_1, p_2,\ldots\ldots p_L)^T \;\&\; Q = (q_1, q_2,\ldots\ldots q_L)^T$$

where

$$p_k = s_{ik}/\sum_{k=1,L} s_{ik};\; q_k = s_{jk}/\sum_{k=1,L} s_{jk}$$

The self-information provided by s_i and s_j for a specific band k is then given by:

$$I_k(s_i) = -\log(p_k) \;\&\; I_k(s_j) = -\log(q_k)$$

The discrepancy of the self-information of band image B_k provided by s_j relative to self-information of the same band image by s_i is denoted by $D_k(s_i||s_j)$ and is formulated as [36]:

$$D_k(s_i||s_j) = I_k(s_j) - I_k(s_i) = \log(p_k) - \log(q_k) = \log(p_k/ q_k)$$

The afore-described expression represents the discrepancy in self-information for one band image B_k provided by s_i relative to s_j. The same concept when extended over the entire range of band images provides the following formulation:

$$D(s_i||s_j) = \sum_{a=1,L} (D_a(s_i||s_j))(p_a) = \sum_{a=1,L}(p_a) (\log(p_a/ q_a))$$

and

$$SID(s_i,s_j) = D(s_i||s_j) + D(s_j||s_i)$$

The spectral signature vectors referred to in the mathematical backgrounds presented above for SAM & SID classification techniques, are extracted from the motor coil arcing fault current data collected as described earlier. The hall-effect sensor data corresponding to the motor coil arcing fault current signal is fed as input to a 60Hz digital notch filter. The 60Hz notch filter is utilized to eliminate the pronounced effect of the fundamental frequency component since the spectral signature to be extracted would focus on the higher-order harmonic information. The filtered signal is then subjected to a comprehensive Power Spectral Density (PSD) analysis extracting information up-to the 7^{th} harmonic and associated upper and lower side-bands. The abovementioned higher order harmonic and associated side-band information is then encrypted to obtain the spectral signature associated with arcing faults of varying severities.

4.2.3 Linear Discriminant Analysis (LDA)

Linear Discriminant Analysis (LDA) refers to a statistical technique utilized to classify objects/patterns into mutually exclusive and exhaustive groups based on a set of pre-identified features associated with each object/pattern [37]. The critical aspects governing the performance of LDA with respect to accuracy of classification are:

- The pre-identified features utilized as basis for classification – Higher order harmonic and associated side-band information.
- The precision of training data and methodology utilized for LDA prior to training.

The mathematical objective associated with the application of LDA is to assign an object to a group with highest conditional probability thereby minimizing the Total Error of Classification (TEC). Although this does correspond to the application of Bayes Rule theoretically, the direct application of the same is not feasible for problem at hand. The mathematical formulation of the problem then amounts to [38]:

$$f_i = \mu_i C^{-1} x_k^T - (1/2)\mu_i C^{-1} \mu_i^T + \ln(p_i)$$

where

f_i: Discriminant function

x_k : Pre-identified features for all data

μ_i: Mean of features in group i

C: Pooled Co-variance matrix

p_i: Prior probability for group i

Each element in the pooled covariance matrix is obtained from the individual co-variance matrices for each group utilizing the formulation [38]:

$$C(j,k) = (1/n) /\sum_{i=1,g} (n_i) (c_i(j,k))$$

where

C(j,k): Element of pooled co-variance matrix

g: Number of groups

$c_i(j,k)$: Element of co-variance matrix for group i

n: number of objects to be classified

The co-variance matrix for individual group, i , is given by [38]:

$$C_i = ((x_i^{0})^T x_i^{0}) / n_i$$

The essence of the formulation mentioned above lies in that the object k would be classified into group I having the maximum f_i. An alternative method to efficiently compute the pooled covariance matrix associated with the training/test data for each group is to subtract the group mean vectors from training/test data for each of the groups. The resulting matrix is then subjected to QR decomposition resulting in two matrices namely Q_j and R_j for group j. Q_j is the orthogonal matrix (its inverse is the same as its transpose) while R_j is the upper triangular matrix resulting from the QR

decomposition. The scaled form of R_j can be utilized to obtained the pooled covariance matrix to be utilized in the evaluation of the discriminant function to classify the test/training data points into respective groups. The LDA approach employed for the classification of severity of motor coil arcing faults utilizes the training data in conjunction with pre-assigned group labels to obtain the upper triangular matrix associated with each group to develop the over-all pooled covariance matrix. As would be evident from the discussion and the discriminant functions presented above, one of the limitations of the LDA approach is that the pooled covariance matrix must be on-singular for successful classification. This can only be assured by ensuring the absence of any under-sampled data i.e. the number of training samples should not be less than the dimensions. For this reason, Principal Component Analysis (PCA) is utilized in conjunction with the classical LDA approach to reduce the dimension of the data to overcome what is now popularly known as the Small Sample Size (SSS) problem associated with classical LDA approaches for pattern recognition. However, ample training data points were utilized for the training stage of the LDA approach utilized for the motor coil arc fault severity classification and PCA+LDA approach is beyond the purview of the work presented in this dissertation.

Hence the vectors corresponding to pre-identifiable extracted features are and appropriate groups are utilized for the execution of the training procedure. A pre-condition for the successful completion of the training procedure is for the pooled co-variance matrix obtained from the training data to be positive definite. The extracted features corresponding to the test data are then subjected to LDA analysis based on the

implementation of the formulations provided above.

4.2.4 Support Vector Machines (SVM)

Support Vector Machines (SVM) is a useful and well established tool for data classification applications. A typical classification process comprises of training and testing data which consists of some data instances [39]. Each data instance in the training data set comprises of a "target value" and some "attributes" or features. The primary objective of the SVM is to develop a model which estimates the target value of data instances for which only the attributes have been provided. It is implied that the same attributes were utilized to train/develop the model during the training period.

Let us now consider N samples of data such as:

$$\{(\vec{x}_1, y_1), (\vec{x}_2, y_2), \ldots, (\vec{x}_m, y_m))$$

Where: $\vec{x} \in \mathbf{R}^n$ and $y_i = +\backslash- 1$ are labels for the data for classification

The discussion presented in this section tends to lay the mathematical foundation associated with the utilization of SVM-technique for classification problems by utilizing a rather simple linear separable case. From there on, more complex problems such as linear non-separable case and the training of non-linear non-separable machines do result in a very similar quadratic programming optimization problem, albeit some transformations for the non-linear machines [46]. Reverting back to the rather simple linear clearly separable case, let us suppose that there exists a hyperplane that separates the positive from the negative labels and corresponding data, with the

hyperplane being termed as the "separating hyperplane". Hence the points that lie on this separating hyperplane would satisfy the equation:

$$\mathbf{w} \cdot \mathbf{x} + b = 0$$

Where,

w: Normal to the hyperplane

|b|/||w||: Perpendicular distance from the hyperplane to the origin

||w||: Euclidean norm of w

Let $d_+(d_-)$ be the shortest distance from the separating hyperplane to the closest positive (negative) example. In that case the "margin" is defined as the sum $(d_+ + d_-)$ with the same being illustrated in Exhibit 1 below.

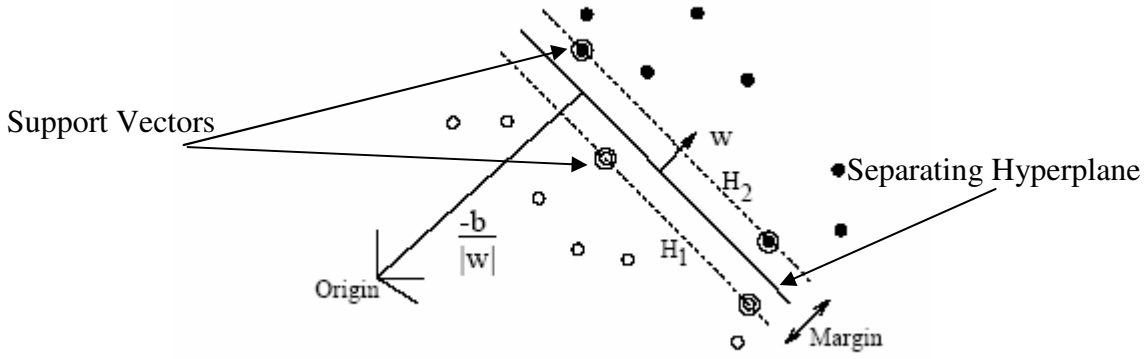

Exhibit 1: Mathematical Manifestation of Support Vector Machines [46]

For the simple linearly separable case illustrated above, the SVM algorithm simply attempts to find the separating hyperplane which maximizes the margin. Methematically, this can be formulated in the following set of constraints:

$$\mathbf{x}_i \cdot \mathbf{w} + b \geq +1 \quad \text{for } y_i = +1$$
$$\mathbf{x}_i \cdot \mathbf{w} + b \leq -1 \quad \text{for } y_i = -1$$

The above set of constraints can then be combined to form a single inequality of the form:

$$y_i(\mathbf{x}_i \cdot \mathbf{w} + b) - 1 \geq 0 \quad \forall i$$

Dwelling a littlie more in the mathematical details, the points that fall on the hyperplane labeled H1 on Exhibit 1, would seem to satisfy the following equation:

$$\mathbf{x}_i \cdot \mathbf{w} + b = 1$$

Similarly the points that fall on the hyperplane labeled H2 on Exhibit 2, would seem to satisfy the following equation:

$$\mathbf{x}_i \cdot \mathbf{w} + b = -1$$

Hence $d_+ = d_- = 1/\|w\|$ thus formulating the margin to be $2/\|w\|$.

The SVM algorithm now equates to finding a pair of hyperplanes that result in the maximum margin by minimizing $\|w\|^2/2$ subject to the constraint:

$$y_i(\mathbf{x}_i \cdot \mathbf{w} + b) - 1 \geq 0 \quad \forall i$$

The mathematical formulation associated with the implementation of the SVM algorithm is then made to under a Lagrangian switch. There are 2 primary reasons for incorporating this switch. The first of the 2 reasons is that the constraint equated above would be replaced by its Lagrangian multiplier counterparts and is much easier to handle. The second reason is that the reformulation of the problem implies that the

training data would appear only in the form of dot products between vectors which plays an instrumental role in utilizing the kernel-based approach for the non-linear case. Elaborate mathematical details associated with the discussion presented above can be referred to in [46].

The lagrangian switch results in the SVM classification problem being formulated in the following format:

$$L_P \equiv \frac{1}{2}\|\mathbf{w}\|^2 - \sum_{i=1}^{l} \alpha_i y_i (\mathbf{x}_i \cdot \mathbf{w} + b) + \sum_{i=1}^{l} \alpha_i$$

We must now minimize Lp with respect to w and b while simultaneously requiring that all derivates of Lp with respect to all $\acute{\alpha}_i$ vanish and all subject to $\acute{\alpha}_i > 0$. In the case of a linear non-separable case, an additional penalty factor is incorporated in the mathematical formulation of the SVM algorithm to allow and account for classification errors. This is done so by the introduction of slack variables thereby modifying the equations defining the pair of hyperplanes to the following format [46]:

$$\begin{aligned} \mathbf{x}_i \cdot \mathbf{w} + b &\geq +1 - \xi_i \quad \text{for } y_i = +1 \\ \mathbf{x}_i \cdot \mathbf{w} + b &\leq -1 + \xi_i \quad \text{for } y_i = -1 \\ \xi_i &\geq 0 \ \forall i. \end{aligned}$$

Thus for an classification error to occur the corresponding ξi must exceed unity. Hence an obvious way to assign extra cost for errors in the SVM optimization problem is to change the objective function to be minimized from $\|w\|^2/2$ to:

$$\|\mathbf{w}\|^2/2 + C\left(\sum_i \xi_i\right)^k$$

The parameter C is chosen by the user with a large value of C corresponding to a higher penalty for errors in the objective function.

Most of the mathematical techniques discussed in this section have pertained or directly apply to the linearly separable or non-separable case. However, most of the real world pattern recognition and/or classification problems present themselves in the form of non-linear classification problems. The adaptation of the SVM algorithm discussed above, for the linearly separable case, to account for non-linear data scatter classification was done based on a deduction drawn above that the training data appears only in the for of dot products of the vectors after the Lagrangian switch.

As mentioned earlier, the training problem is in the form of dot products of the vectors $x_i.x_j$. Let us suppose that the non-linear data was mapped to some other Euclidean space H, using a mapping that shall be termed Φ such that:

$$\Phi : \mathbf{R}^d \mapsto \mathcal{H}.$$

Then the training problem would only depend on the data through dot products in the Euclidean space H i.e. on functions $\Phi(x_i)$ and $\Phi(x_j)$. Now, if there exists a kernel function such that $K(x_i, x_j) = \Phi(x_i) \cdot \Phi(x_j)$ then we would only need to use the kernel function in the training algorithm. This is precisely the approach that is adopted to utilize the SVM algorithm for the classification of non-linear scatter spreads. The reader does have to bear in mind that the Euclidean space H is an infinitesimal space and hence working with Φ directly would not be very easy. However, if $x_i \cdot x_j$ is replaced by $K(x_i,$

x_j) everywhere in the training algorithm then the SVM algorithm will produce an SVM that exists in the infinite dimensional space.

For instance the data are vectors in R^2 and we choose the kernel function $K(x_i, x_j) = (x_i \,.\, x_j)^2$ then it is relatively easy to find a higher dimension Hilbert space H and mapping Φ from R^2 to H such that $x.y = \Phi(x) \,.\, \Phi(y)$. We choose $H = R^3$ then we have:

$$\Phi(\mathbf{x}) = \begin{pmatrix} x_1^2 \\ \sqrt{2}\, x_1 x_2 \\ x_2^2 \end{pmatrix}$$

It would be important to bear in mind that neither the mapping nor the Hilbert space H are unique for any given kernel function K. It is also important to apply the Mercer's condition to be able to determine whether a given/chosen kernel is actually a dot product in some space, a necessary condition for performing the mapping in the SVM algorithm. Detailed discussion on this aspect can be found in [46].

For the implementation of the SVM classification technique, as far as motor coil arcing fault severity classification is concerned, the OSU-SVM toolbox in Matlab has been utilized. The toolbox is widely used to create models for regression and classification using Support Vector Machines. As mentioned above, the Gaussian Kernel function was utilized for the SVM algorithm for the classification of motor coil arcing faults. There are 2 critical input parameters in one-class SVM classification, namely σ (sigma) and ν (nu). The former parameter, sigma, is utilized in the mathematical formulation of the Gaussian kernel operator of the SVM which is mathematically expressed as:

$$Exp(-||x-x`||^2\backslash(2\sigma^2)$$

This parameter σ sigma, controls the shape of the decision boundary and hence the number of support vectors in turn. If sigma is set to a higher value, a lower number of support vectors are generated along with a less complex decision boundary. On the other hand, a lower value of sigma corresponds to a higher number of support vectors accompanied with a more complex decision boundary.

The second input parameter for the one-class SVM classification, ν (nu), determines the number of training data points that would be considered as outliers. In other words, is ν is set to 0.01, it implies that about 1% of the training data points can be considered as outliers whereas if ν is set to 0.1 it implies that 10% of the training data points can be considered as outliers. Figures 4.2 and 4.3 depict the effect of the selection of σ and ν on the decision boundary and the number of support vectors for one-class SVM classification.

Since the training data sets utilized in the motor coil arc fault classification process are assumed to correspond to a healthy condition of the motor, a less complex decision boundary which manages to include all the training data is referred to a more complex decision boundary. Furthermore, since the training data points correspond to the healthy condition of the motor almost a negligible amount of training data points should be considered as outliers and hence ν is set to 0.001.

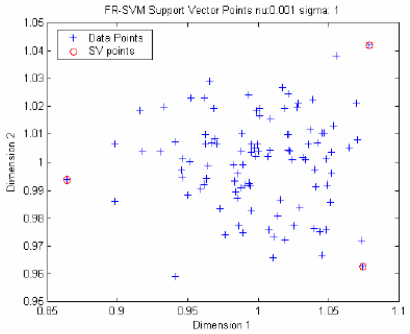

(a) nu:0.001, sigma = 1, number of SVs = 3

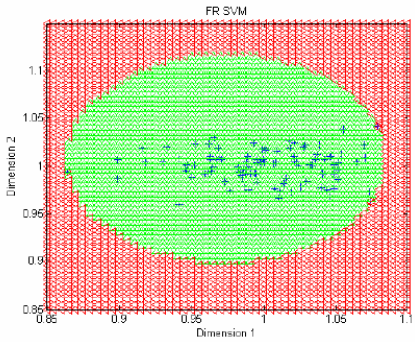

(b) nu:0.001, sigma = 1, number of SVs = 3
(green:normal, red: abnormal)

Figure 4.1: Decision Boundary & Support Vectors associated with σ = 1 & ν = 0.001

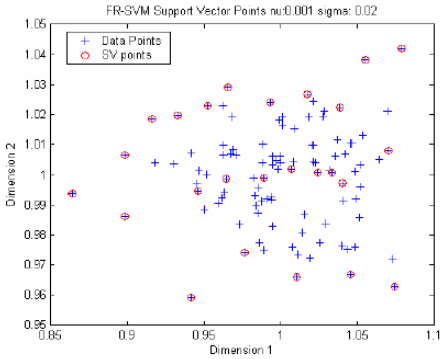

(k) nu:0.001, sigma = 0.02, number of SVs = 25

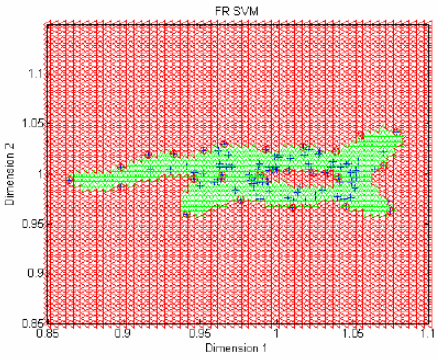

(l) nu:0.001, sigma = 0.02, number of SVs = 25
(green:normal, red:abnormal)

Figure 4.2: Decision Boundary & Support Vectors associated with σ = 0.02 & ν = 0.001

The algorithms subjecting the spectral signatures associated with varying levels of severity of low voltage motor coil arcing faults to the aforesaid classification techniques are firmly based on the implementation of the mathematical manifestations described in the above section. The details associated with the design of the algorithm and the input data associated with each of the 4 classification techniques is presented in the ensuing section.

4.3 Algorithms: Application & Simulation Methodology

The mathematical formulations associated with each of the 4 classification techniques are formulated in the form of modular algorithms in order to implement the classification techniques to classify the severity of low voltage motor coil arcing faults. The sub-sections comprising the ensuing section present the algorithms associated with the application of classification of severity of motor coil arcing faults.

4.3.1 Spectral Angle Mapper (SAM)

Figure 4.3 presents the algorithmic flowchart associated with the application of the SAM technique to classify the severity of motor coil arcing faults. As can be seen from the figure, the arcing current corresponding to varying levels of fault severity is acquired via the hall-effect sensor. The arcing fault current is then filtered to eliminate the fundamental frequency component since the 60Hz component is so prominent that it seems to suppress the effect of the higher-order harmonics which happen to be elements of interest for the classification procedure. The filtered signal is then subjected to a Fast Fourier Transform (FFT) analysis to extract the relevant higher-order harmonics and associated upper and lower sidebands to develop the spectral signature associated with the given motor coil arcing fault severity. The SAM associated with this severity and a pre-determined base spectral signature is calculated based on the mathematical formulations presented in section 4.2.1.

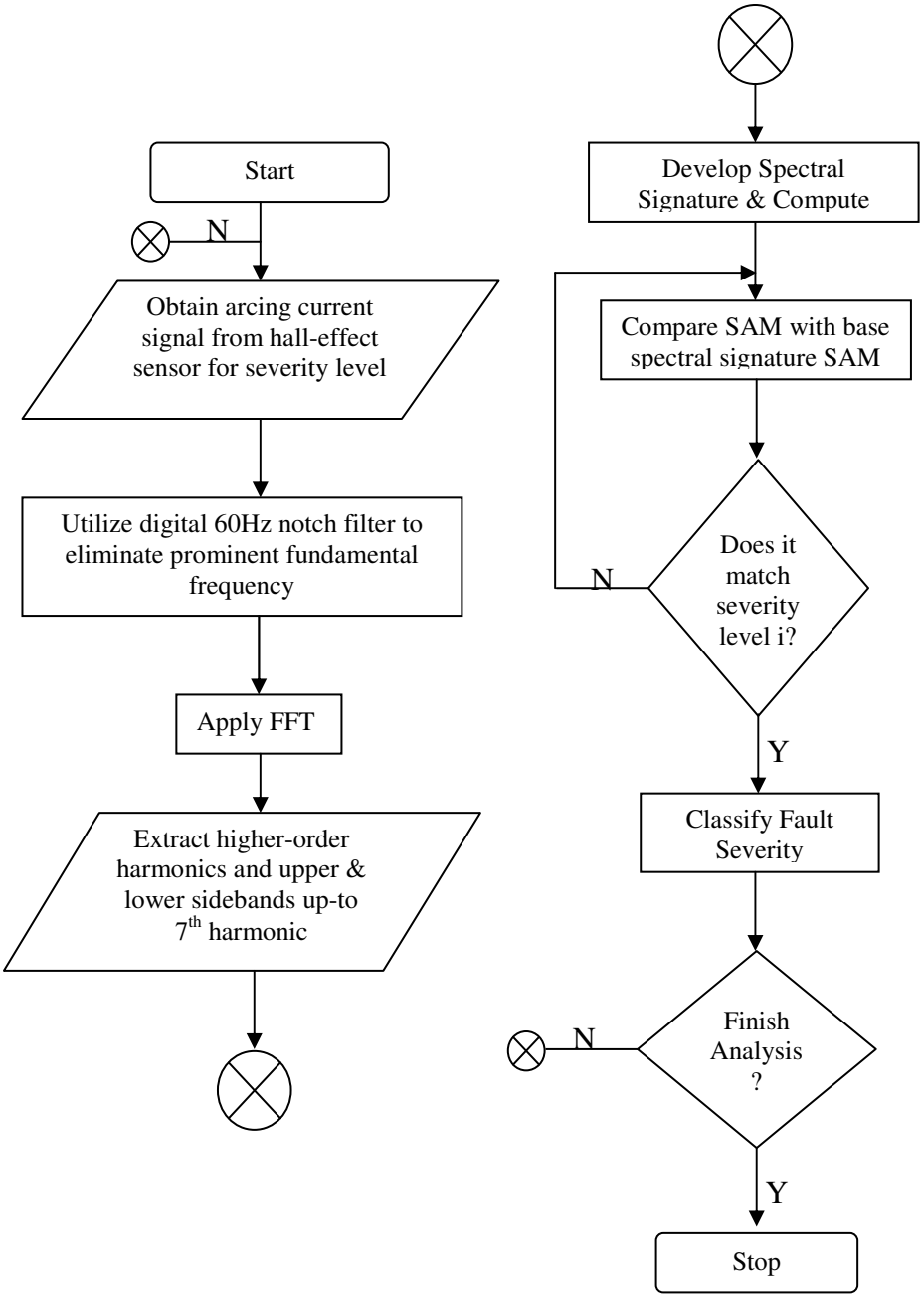

Figure 4.3: Algorithmic Flowchart representing SAM technique for motor coil arc fault classification

The SAM value as obtained for each severity level is classified based on its comparison with the SAM value associated with the base spectral signature and hence each spectral signature vector is classified into one of the many arcing fault severity levels. The results associated with the implementation of the algorithm presented in Figure 4.3 are presented in the following section.

4.3.2 Spectral Information Divergence (SID)

Figure 4.4 presents the algorithmic flowchart associated with the application of the SID technique to classify the severity of motor coil arcing faults. As can be seen from the figure, the arcing current corresponding to varying levels of fault severity is acquired via the hall-effect sensor. The arcing fault current is then filtered to eliminate the fundamental frequency component since the 60Hz component is so prominent that it seems to suppress the effect of the higher-order harmonics which happen to be elements of interest for the classification procedure. The filtered signal is then subjected to a Fast Fourier Transform (FFT) analysis to extract the relevant higher-order harmonics and associated upper and lower sidebands to develop the spectral signature associated with the given motor coil arcing fault severity. The SID associated with this severity and a pre-determined base spectral signature is calculated based on the mathematical formulations presented in section 4.2.2.

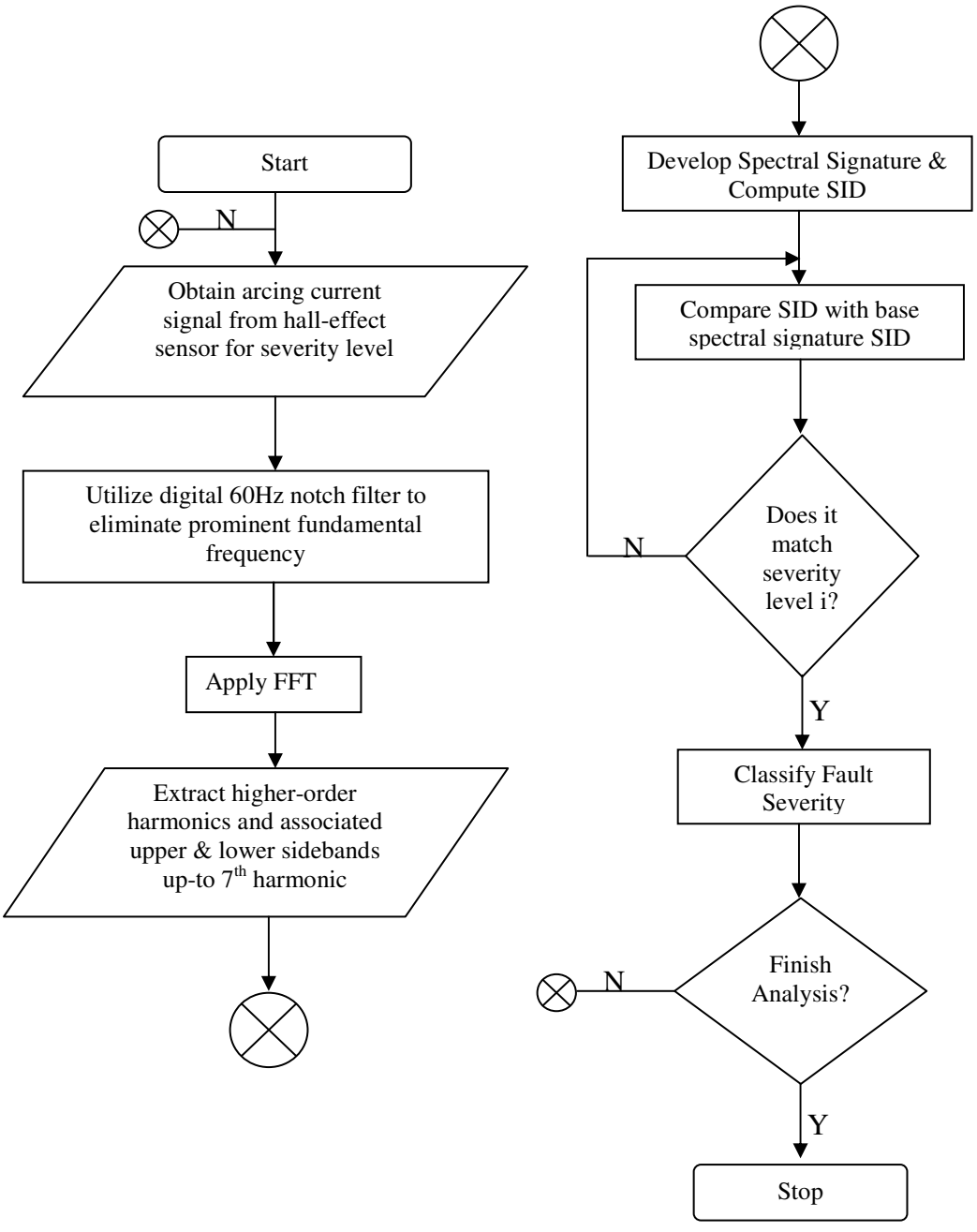

Figure 4.4: Algorithmic Flowchart representing SID technique for motor coil arc fault classification

The SID value as obtained for each severity level is classified based on its comparison with the SID value associated with the base spectral signature and hence each spectral signature vector is classified into one of the many arcing fault severity levels. The results associated with the implementation of the algorithm presented in Figure 4.4 are presented in the following section.

4.3.3 Linear Discriminant Analysis (LDA)

As mentioned earlier, the classification based on the LDA technique differs from the SAM/SID classification techniques in that the LDA technique requires prior training to identify/classify the spectral signature to belong to any of the pre-trained classes. In other words, as would also be made evident by the results presented in the proceeding section, the SAM/SID classification techniques possess the capability of classifying severity levels lying in between any 2 pre-identified severity levels also. However, since the LDA technique relies on classifying the spectral signature in one of the classes that it has been trained for, the spectral signature for any other severity levels will not be classified accurately unless the LDA model is trained to classify that severity level.

Figure 4.5 depicts the algorithmic flowchart associated with the implementation of the LDA technique for the classification of severity of motor coil arcing faults.

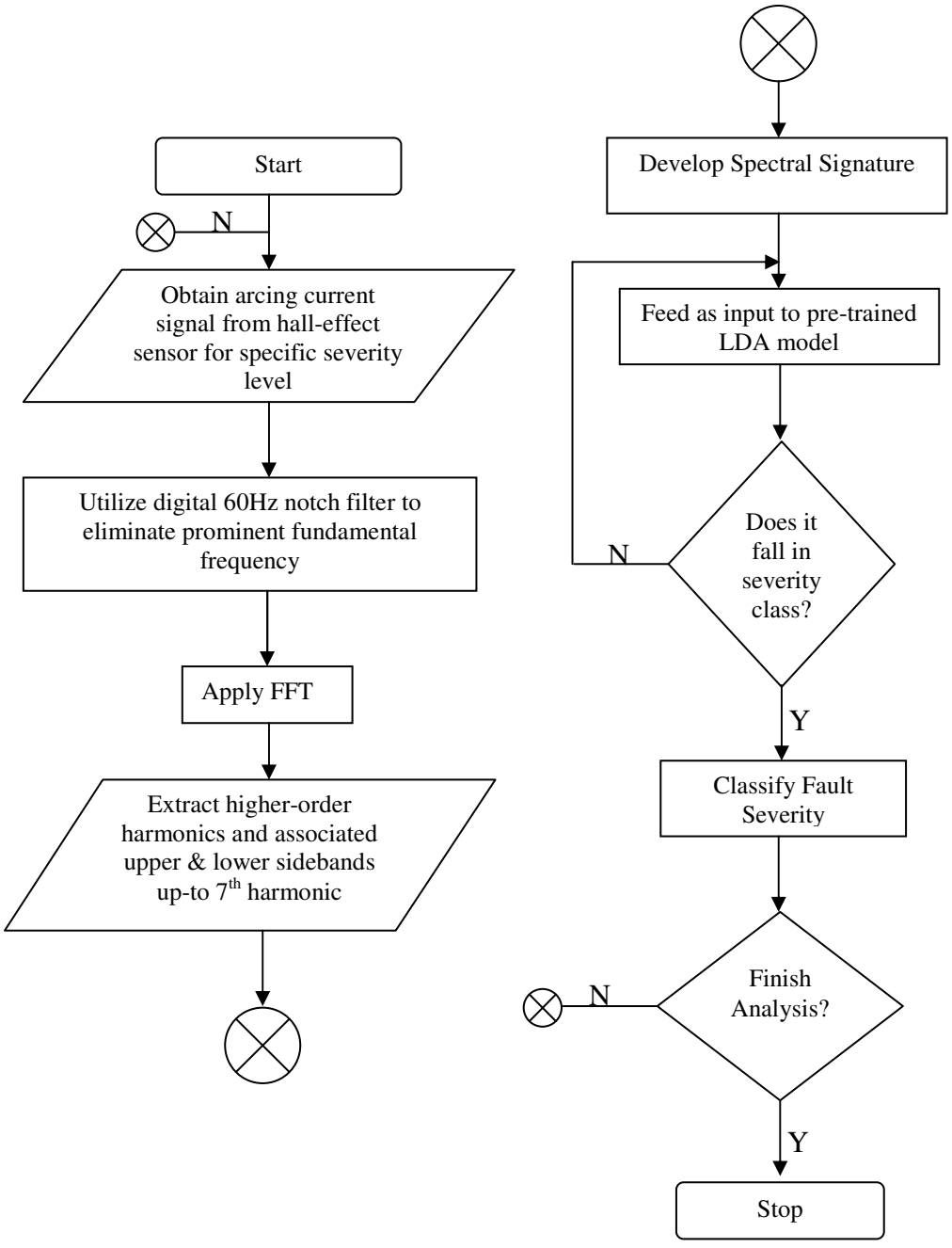

Figure 4.5: Algorithmic Flowchart representing LDA technique for motor coil arc fault classification

4.3.4 Support Vector Machines (SVM)

The mathematical and algorithmic details associated with the 1-class SVM classification technique were discussed in detail in section 4.2.4. The training data consisting of the feature space extracted for various classes of arc fault severity (as described in earlier sections of the dissertation) and the labels associated with the class are utilized to construct the SVM classifier in the OSU-SVM toolbox. The SVM classifier provides the critical SVM parameters such as the Lagrangian multipliers, the bias and the number of support vectors derived out of the training process. These SVM parameters are then utilized to classify the test data that also does consist of the samples of the extracted feature space corresponding to varying levels of the motor coil arc fault severity. When the training data corresponded to the healthy condition of the motor coil, the 1-class SVM classification is found to be capable of performing anomaly detection, as would be evident from the results presented in the proceeding sections. Figure 4.6 depicts the block diagram for the SVM classification.

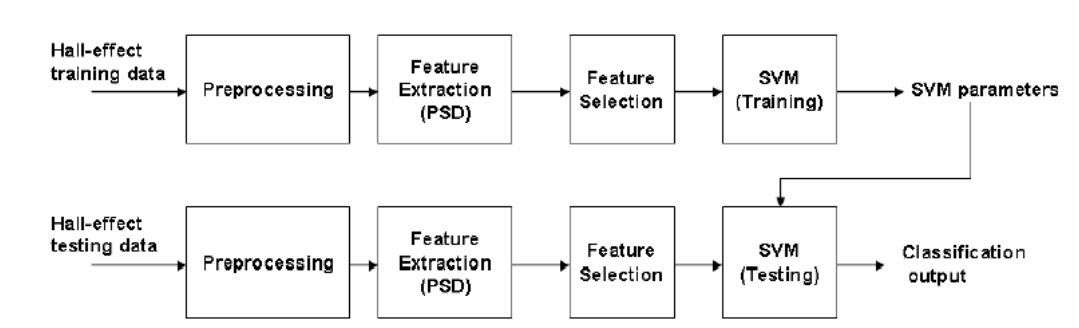

Figure 4.6: Block Diagram for SVM Classification Algorithm

As is evident from the block diagram presented in figure 4.6, the training data corresponds to various cases of the motor coil arcing fault severity current acquired through the hall-effect sensors. The SVM parameters, namely σ and ν, for each class are determined based on the training data and then utilized on the test-data fo each severity level.

4.4 Algorithms: Simulation Results

The discussion presented in the previous section focused on presenting the methodology and the algorithmic logic associated with the implementation of the algorithms, the mathematical formulation for which has been provided in earlier sections. This section focuses on presenting the results associated with the classification of severity of motor coil arcing faults via the application of each of the 4 classification techniques dwelled upon in the previous sections.

4.4.1 Spectral Angle Mapper (SAM)

Figures 4.7 and 4.8 depict the classification results when Spectral Angle Mapper (SAM) is utilized to classify the severity of the motor coil arcing fault. Figure 4.7 depicts the classification results corresponding to arcing data for the original 5 cases presented in Table 3.1. As can be seen from figure 4.7, the SAM values corresponding to any one arcing case are within close proximity of each other. Furthermore, the SAM values corresponding to 2 different arcing cases are clearly segregated in terms of their SAM values. Figure 4.8 underlines the flexibility and robustness of the approach when

subjected to data corresponding to unforeseen arcing cases. The data presented as cases 3-4(a), 3-4(b) and 3-4(c) in Table 3.1 has been utilized to analyze the performance of the proposed statistical measure in the case of unforeseen data during arcing phenomenon in actual field conditions. The data corresponding to additional arcing cases presented in Table 3.1 correspond to percentages of arcing coil between those presented in case 3 and 4 shorted through arcing fault. As is evident from Figure 4.8, the SAM values corresponding to ach of these 3 additional cases lie between those corresponding to cases 3 and 4. Additionally, the SAM values for each of the 3 additional cases are in conjunction with the percentage of coils shorted through the arcing fault for each case.

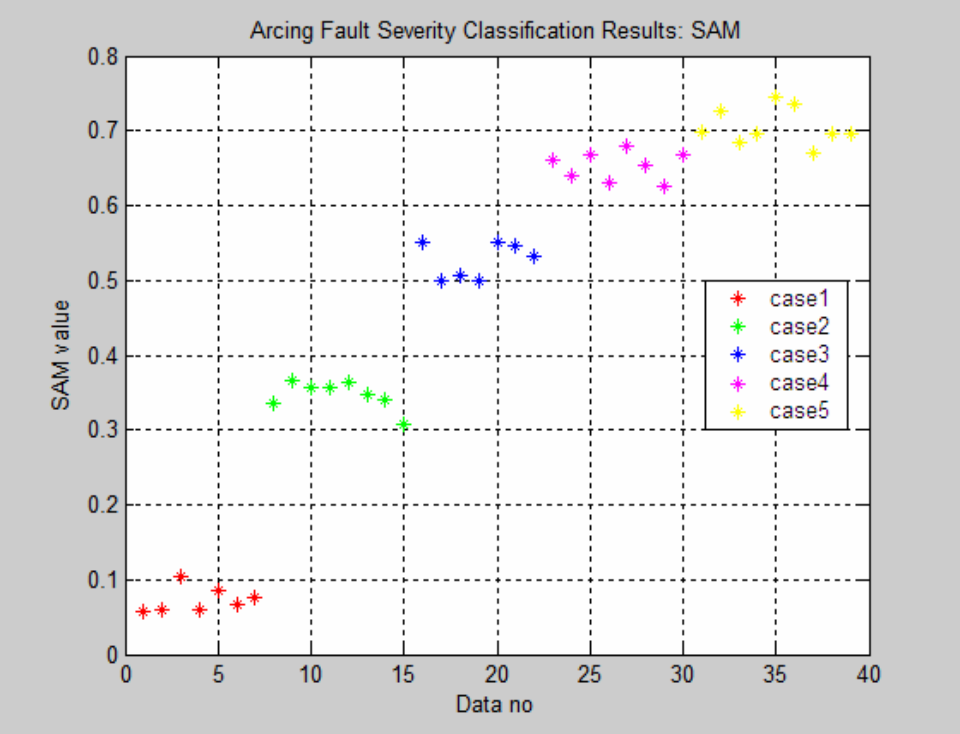

Figure 4.7: Classification Results using SAM: Original Cases

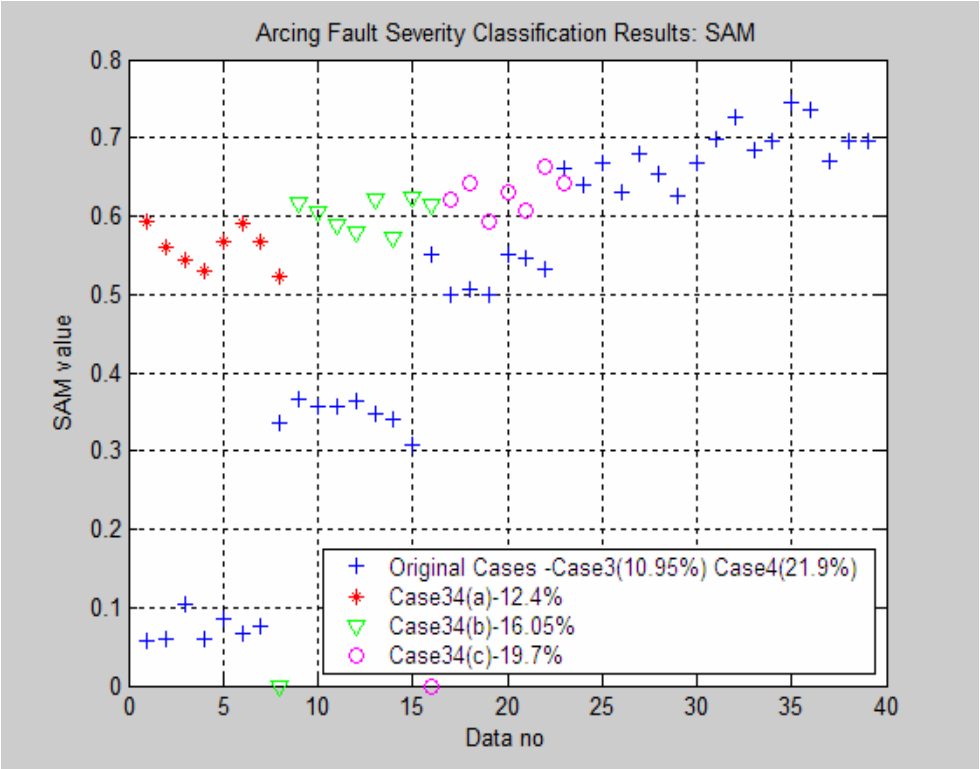

Figure 4.8: Classification Results using SAM: Additional Cases

As is evident from the results showcased in figures 4.7 and 4.68, the SAM statistical classification technique performs adequately in classifying the severity of motor coil arcing faults for the 5 severity cases shown in Table 3.1 developed by means of experimental set-up. As can be seen from the results presented in Figure 4.5, the SAM values corresponding to any one severity class clearly fall in a specific region with ample and clear segregation from SAM values corresponding to other severity classes. Furthermore, the SAM values also tend to indicate a pattern in terms of

monotonically increasing SAM values with increasing percentages of the motor coil shorted or with increasing levels of severity of the motor coil arcing fault.

The robustness of the approach is also demonstrated through the results presented in figure 4.8, wherein the classification results for unforeseen severity levels have been showcased. As is evident from figure 4.8, the classification results corresponding to intermediate severity levels in between cases 3 and 4 are found to have SAM values in between cases 3 and 4. Case 34-a corresponds to severity levels between cases 3 and 4 but closer to case 3 and the SAM values associated with the spectral signature of case 34-a lie between those for cases 3 and 4 and closer to case 3 SAM values. The same applies to SAM values associated with cases 34-b and 34-c with each of them lying between cases 3 and 4.

4.4.2 Spectral Information Divergence (SID)

Figures 4.9 and 4.10 present the classification results when Spectral Information Divergence (SID) is utilized to classify the severity of the motor coil arcing fault. As in the case of SAM, figure 4.9 presents the classification results corresponding to the original arcing cases while figure 4.10 presents the performance of the SID approach when incremental cases representing unforeseen arcing conditions. As can be seen from Figure 4.9, SID approach is equally adept at classifying various cases corresponding motor coil arcing faults. The performance of SID approach when incremental cases are utilized is also equally satisfactory when compared to SAM. The classification of the incremental cases between cases 3 and 4 is accurate in terms of SID values and trend.

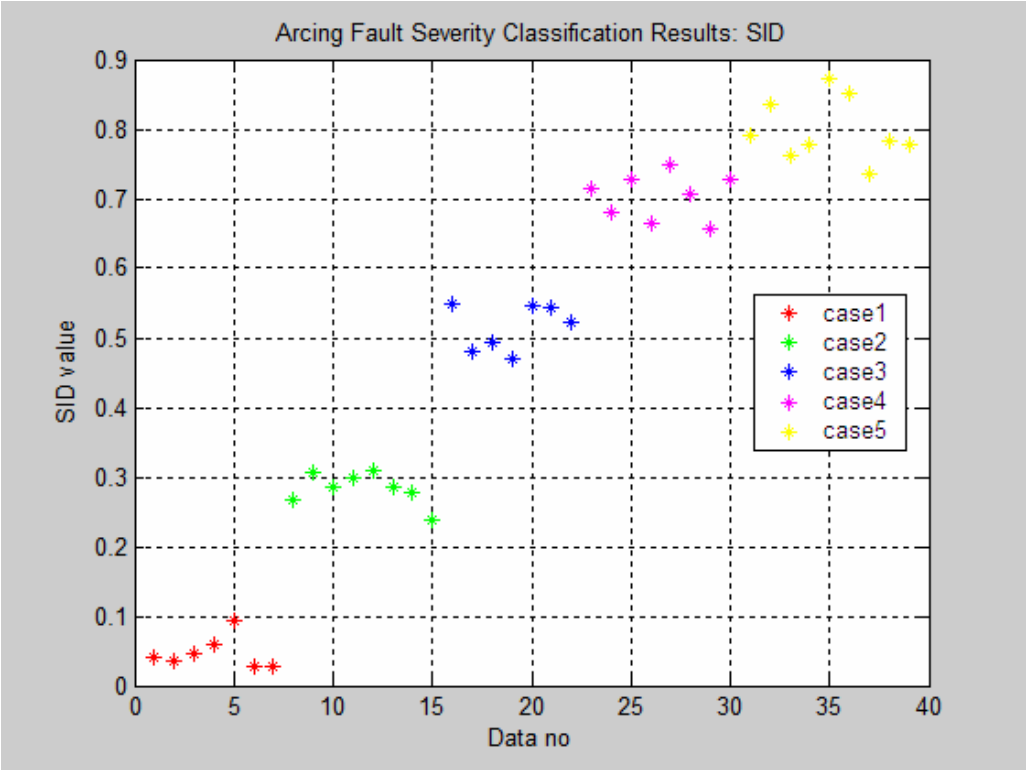

Figure 4.9: Classification Results using SID: Original Cases

4.4.3 Linear Discriminant Analysis (LDA)

Figures 4.11 and 4.12 present the classification results when Linear Discriminant Analysis (LDA) is utilized to classify the severity of the motor coil arcing fault. Figure 4.11 depicts the output of the LDA algorithm on the training data utilized to train the LDA to recognize the pattern corresponding to each arcing fault case. As would be expected, the classification of the training data is near perfect thereby corroborating accurate training of the LDA algorithm. Figure 4.12 presents the performance of the LDA algorithm on actual test data corresponding to the 5 original arcing fault cases presented in Table 3.1. As can be seen from Figure 4.12, the classification results obtained from the LDA algorithm are very accurate in terms of correctly identifying the

extent and severity of the motor coil arcing fault.

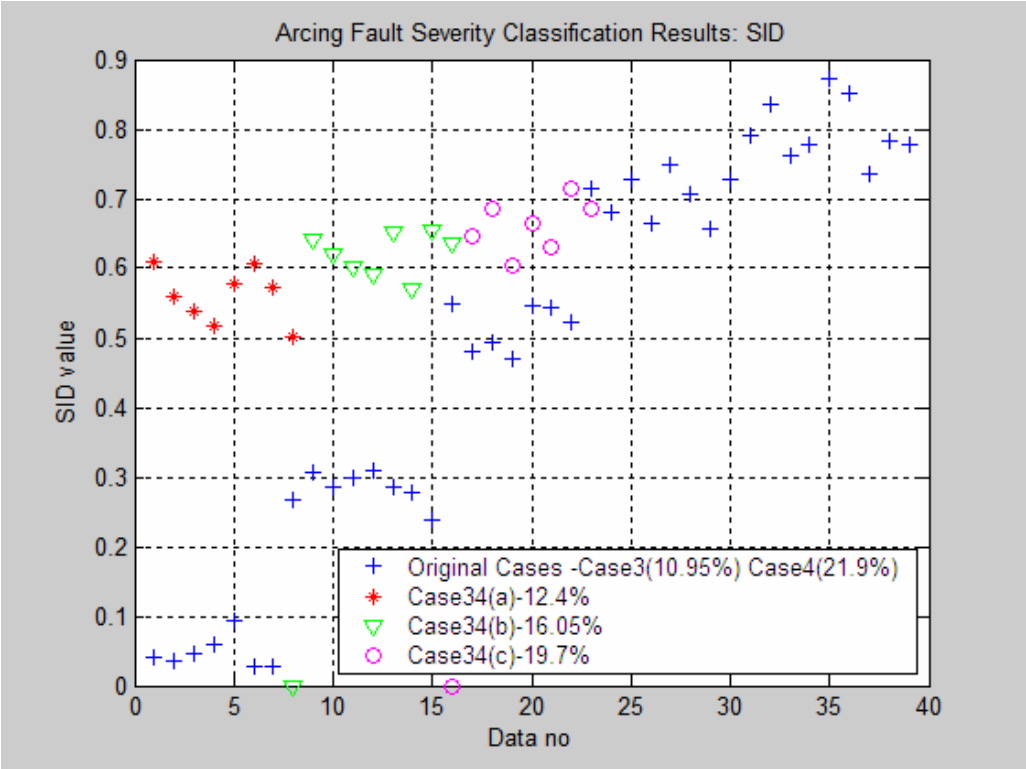

Figure 4.10: Classification Results using SID: Additional Cases

However, unlike SAM and SID approaches wherein additional test data was accurately classified, the LDA approach does not appropriately classify additional arcing fault data unless trained in prior. Figure 4.13 presents the classification results pertaining to the original and additional arcing fault cases after the LDA algorithm was trained for the additional cases. As can be seen from Figure 4.13, the LDA based classification results for additional cases are very accurate after the LDA algorithm has been trained to recognize the pattern corresponding to the additional arcing fault cases. The incremental arcing fault severity for which the LDA algorithm would need to be trained would depend on the resolution of arcing fault severity classification desired for

a particular application. However, with the appropriate data, the results depicted in Figures 4.11, 4.12 and 4.13 clearly indicate the success of the LDA algorithm in accurate classification of the severity of motor coil arcing faults. Figure 4.11 depicts the classification results pertaining to the training data while Figure 4.12 depicts the classification results pertaining to the training and test results. Figure 4.13, on the other hand, extends the applicability of the LDA algorithm by depicting the results for classification of test data with some additional classification samples.

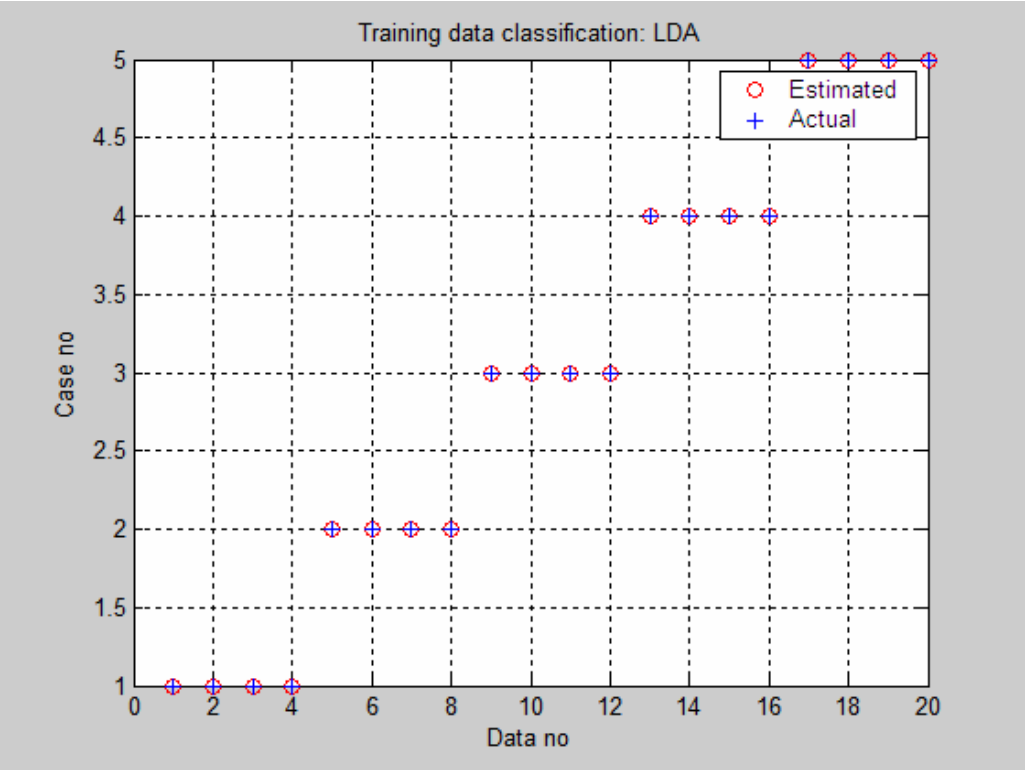

Figure 4.11: Classification Results using LDA: Training Data

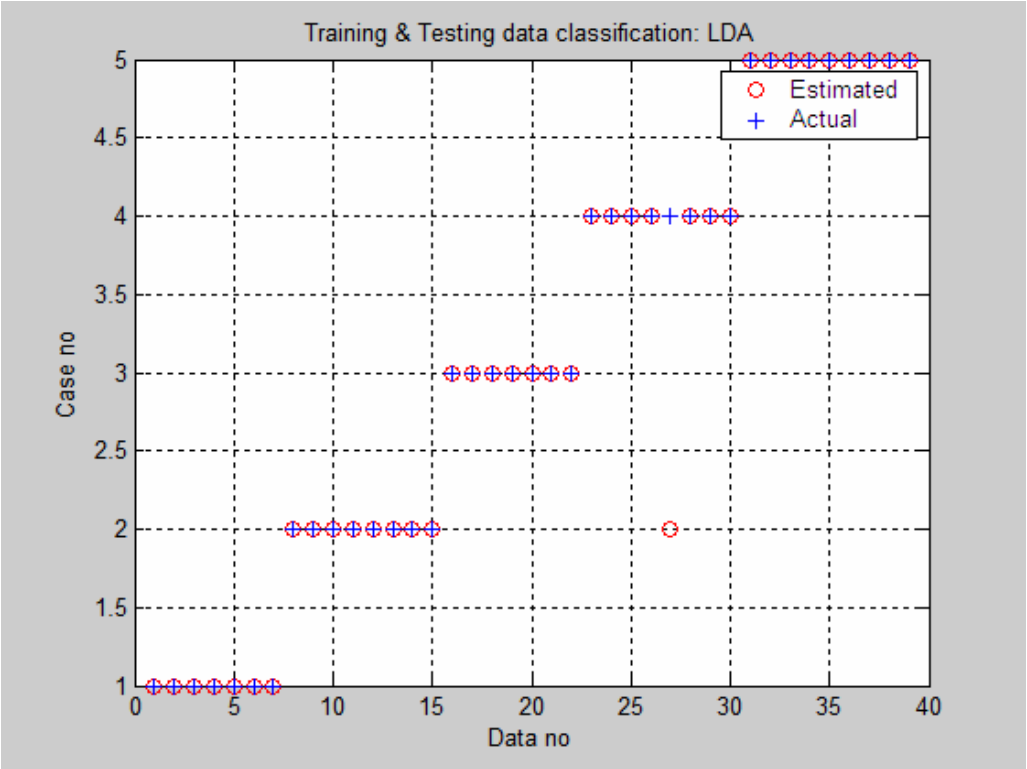

Figure 4.12: Classification Results using LDA: Training/Test Data

4.4.4 Support Vector Machines (SVM)

Figure 4.14 presents the results associated with the utilization of 1-class SVM technique for anomaly detection in motor coil arcing conditions. The 1-class SVM is an unsupervised classification algorithm. For demonstration purposes, the data files corresponding to spectral feature extraction of arcing current under normal operating conditions are utilized for training purposes.

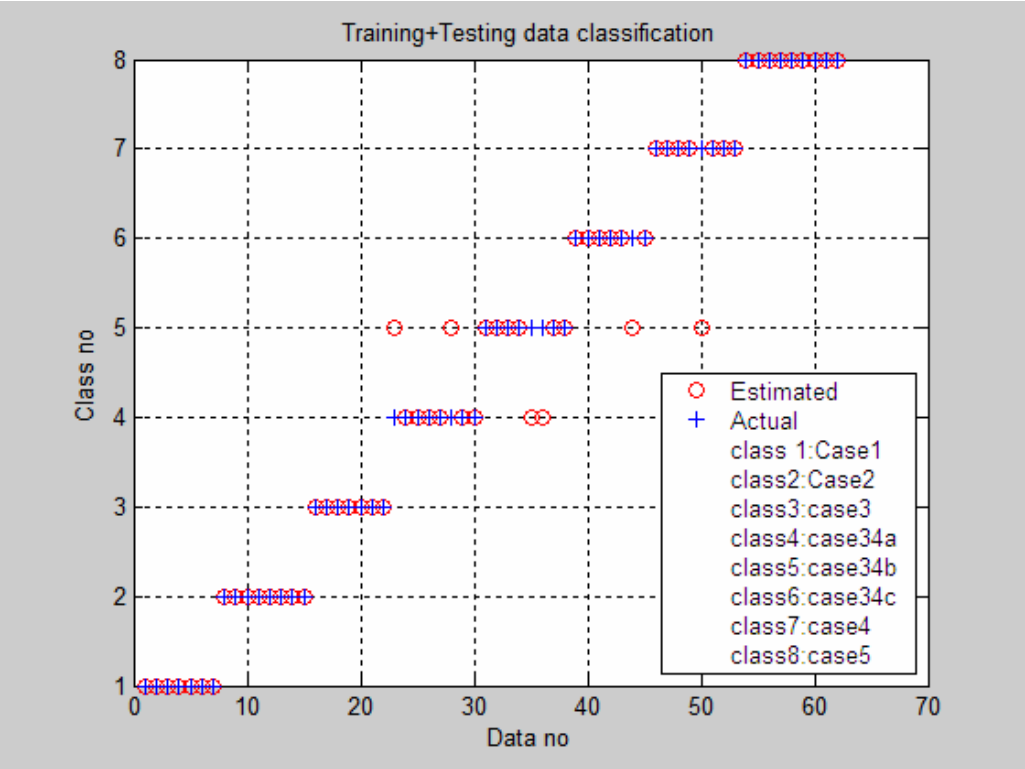

Figure 4.13: Classification Results utilizing LDA: After LDA trained for additional test data

For testing all data files corresponding to cases 1 through 5, as tabulated in Table 3.1, have been utilized. As is evident from figure 4.14, while the data corresponding to normal operation is labeled 1 corresponding to healthy conditions, the data corresponding to cases 1 through 5 is labeled -1 corresponding to abnormal conditions.

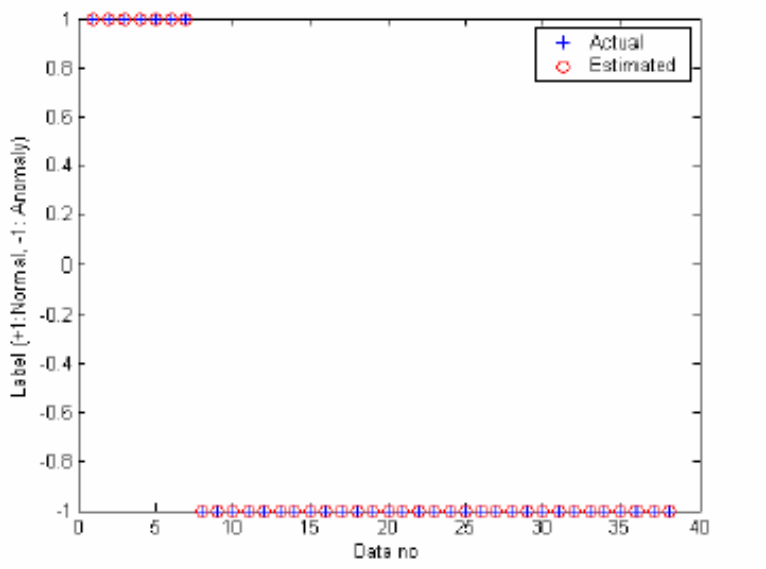

Figure 4.14: 1-Class SVM Results for Anomaly Detection

Figures 4.15 (a) and (b) depict the comprehensive SVM classification results, as obtained from the iterative expansion of the 1-class SVM process, for the training and testing data. As is evident from the results showcased in figures 4.15 (a) and (b) , the SVM classification process does perform adequately well in classifying the severity of motor coil arcing faults.

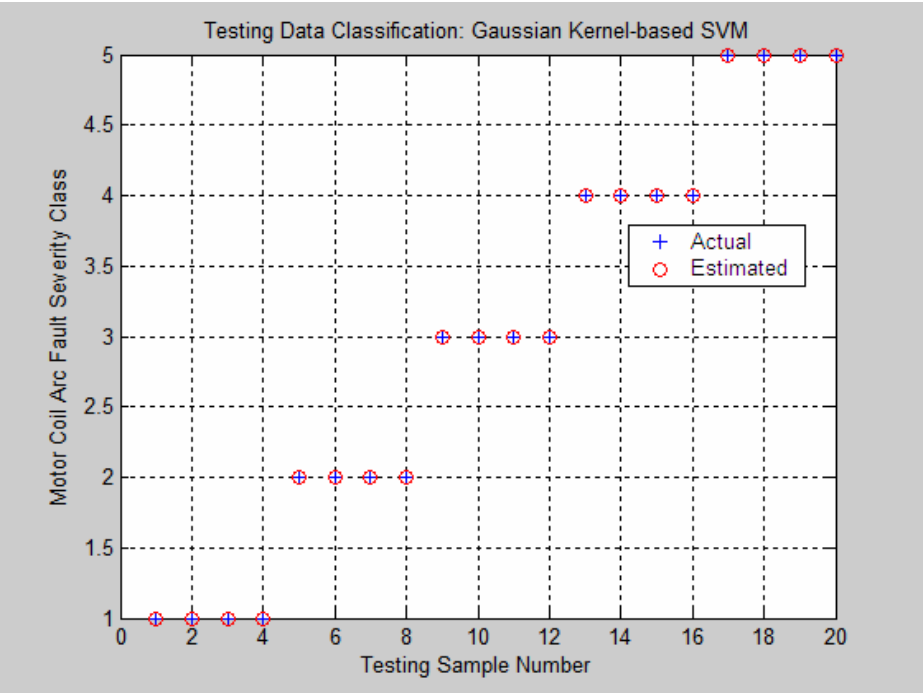

(a)

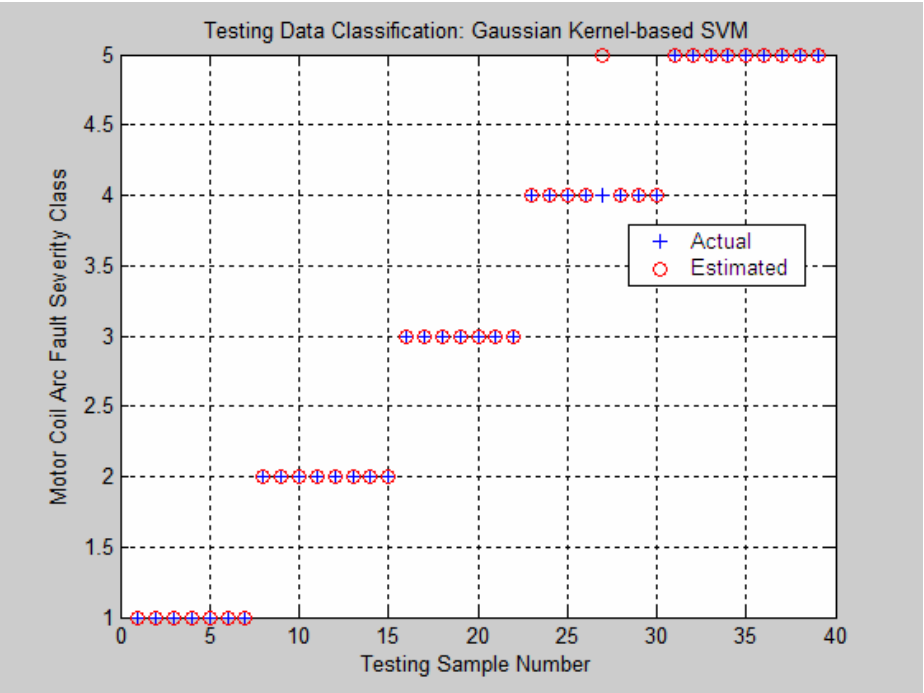

(b)

Figure 4.15 (a): SVM Classification results for Training Data (b): SVM Classification results for Actual Testing Data

4.5 Performance Evaluation & Comparative Analysis

As is evident from the classification results presented in section 4.4 above, various classification techniques provide adequate performance in terms of classification accuracy while being accompanied by advantages and disadvantages.

Table 4.1 presented below aims to summarize a comparative analysis associated wit each of the 4 classification techniques presented above on the basis of some common performance evaluation criterion.

Table 4.1: Comparative Analysis of Performance Evaluation – Classification Techniques

Performance Criterion	**Classification Technique**			
	Spectral Angle Mapper (SAM)	**Spectral Information Divergence (SID)**	**Linear Discriminant Analysis (LDA)**	**Support Vector Machines (SVM)**
Complexity	Moderate	Moderate	Moderate	High despite introduction of Lagrangian multipliers
Robustness	Relatively robust – Classifies unforeseen data accurately	Relatively robust - Classifies unforeseen data accurately	Dependent on prior-knowledge based training data	Dependent on training data & choice of kernel function for non-linear case
Accuracy to unforeseen data	Adequate	Adequate	Contingent on prior training	Contingent on prior training
Classification Errors	Negligible	Negligible	Negligible	Dependent on number of support vectors & ability to handle non-separable case (i.e. C parameter)
Suitability for real time application	Suitable	Suitable	Suitable	Complexity of implementation reduces suitability
Classification layers	Continuous	Continuous	Discrete	Discrete

Table 4.1 - continued

Performance Criterion	Classification Technique			
	Spectral Angle Mapper (SAM)	**Spectral Information Divergence (SID)**	**Linear Discriminant Analysis (LDA)**	**Support Vector Machines (SVM)**
Mathematical Limitations	Distinct Spectral signatures required	Distinct Spectral signatures required	Pooled Covariance matrix should be non-singular Suffers from SSS problem	Choice of suitable Kernel function & handling of non-separable cases
Computing Time	Order of 4-7 seconds for 11X39 matrix of test data	Order of 4-7 seconds for 11X39 matrix of test data	Order of 10-16 seconds for 11X20 matrix of training data and 11X39 matrix of test data	Order of 40-90 seconds – may not be suitable for real time applications

As is evident from Table 4.1, the results associated with the 4 classification techniques presented during the course of the discussion presented in this chapter, underline the various advantages and disadvantages associated with the techniques respectively. The choice of the classification technique would depend on the application associated with the classification of low-voltage motor coil arcing fault severity. The ensuing chapter aims to conclude the discussion comprehensively put forth in this dissertation by providing a summarized discussion associated with various important research contributions provided by the dissertation accompanied with scope for future work in this area of research.

CHAPTER 5

CONCLUSIONS/RECOMMENDATIONS

As would be evident to the reader of the dissertation by now, the discussion presented in this dissertation focused on the design, development and implementation of medium/low-voltage arcing fault detection and/or severity classification algorithms. Two major components of the medium/low-voltage power system networks, especially in industrial environments, were focused upon during the arc fault detection and/or severity classification algorithm development and implementation, namely the switchgear for low and/or medium voltage and the motor coil for low-voltage. The discussion presented in the first half of the dissertation tends to focus on the design and development of hardware and simulation based approaches to substantiate the higher-order harmonic differential approach for detection of arcing faults in medium and/or low-voltage switchgear. The discussion presented in the second half of the dissertation pertains to the design and development of low-voltage motor coil arcing fault severity classification techniques utilizing statistical and pattern recognition techniques such as SAM, SID, LDA and SVM. Each of the relevant sections concludes with adequate results substantiating the approach adopted. This chapter aims to summarize the observations made from the results presented in various sections to draw inferences and/or conclusions associated with the implementation and performance of various approaches discussed during the course of the dissertation.

5.1 Conclusions: Switchgear Arcing Faults

To summarize, a higher-order harmonic differential approach to serve as an early warning detection system for the presence of medium and/or low-voltage switchgear arcing faults was proposed in this dissertation. While the simulation-based approach was utilized to demonstrate the technical soundness of the proposed algorithm for the detection of medium voltage switchgear arcing faults, actual laboratory based test-bench accompanied with real-time implementation of the higher-order harmonic approach was utilized to underline its effectiveness in actual field conditions. The approach primarily aims to utilize the inherent presence of higher-order harmonics during the arcing phenomenon to isolate the arcing fault conditions from normal operation.

The medium voltage switchgear arcing fault detection was based on the collection of arcing current data obtained by producing arcing fault at the 15kV level in a laboratory test-bench developed at ESRC. The higher-order harmonic content in the arcing current data is utilized to model a non-linear source producing an exact same harmonic pattern on a sample 18-bus radial distribution feeder for simulation purposes. The non-linear harmonic source is taken to be the arcing fault location in the sample distribution system. The higher-order harmonic differential approach for both magnitude and phase differential is applied for numerous variations in the system topology to test the performance of the approach under various practical conditions. Results do tend to indicate that more than one higher-order harmonic and sometimes a combination of 2-higher order harmonics serve to comprise the differential scheme in either magnitude or phase or both.

The effectiveness of the higher-order harmonic differential approach in terms of actual field implementation is underlined by the hardware-based laboratory implementation of the higher-order harmonic differential approach to detect low-voltage switchgear arcing faults. Elaborate descriptions associated with the test-bench utilized for the initiation of the low-voltage arcing fault have been presented at relevant sections of the dissertation. Hall-effect sensors in conjunctions with adequate signal processing and data acquisition devices are utilized to acquire the incoming and outgoing current signals with respect to the low-voltage switchgear. The higher-order differential approach is tested for source-side and load-side external arcing faults as well as internal arcing faults to demonstrate the versatility and robustness of the approach.

In summary, the following observations can be made from the simulation and test-bench based implementation of the proposed higher-order harmonic differential approach to detect low/medium-voltage switchgear arcing faults:

- The higher-order harmonic differential approach seems to exhibit good sensitivity for internal arcing faults whilst maintaining adequate discrimination against external faults.
- The results associated with the application of simulation-based higher order harmonic differential approach tend to underline the robustness of the approach keeping in mind the accurate performance of the approach under varying system topologies such as with/without voltage support capacitors etc.
- The results associated with the implementation of simulation-based approach also tend to indicate that more than one higher-order harmonic

can be utilized in magnitude or phase differential form for the early warning detection system for switchgear arcing faults.

- The application of the proposed approach on a test-bench based laboratory proto-type tends to underline the fact that the approach an lend itself to actual field implementation.
- The application of the proposed higher-order harmonic differential approach is also accompanied by a relatively small response time keeping in mind the time taken for the arcing faults to assume potentially hazardous or damaging proportions.
- The proposed approach provides the initiative for the transition from preventive to predictive maintenance in terms of the switchgear industry.

5.2 Conclusions: Motor Coil Arcing Faults

The discussion presented in the second half of the dissertation focuses on the classification of the severity of low-voltage motor coil arcing faults. The initial part of the discussion focuses on the selection of the appropriate design alternative to be employed for the initiation of low-voltage motor coil arcing fault within the controlled laboratory environment. Furthermore, certain sections in this part of the dissertation have been devoted to the comparison of the arcing fault current produced from the chosen design alternative with its contemporary mathematical counterparts. The higher-order harmonic content in the arcing current produced in the laboratory is compared with that contained in arcing current signatures produced from the simulation of contemporary mathematical models. Mathematical models from Mathews, Stokes & Oppenlander and Fisher have

been modeled with parameters similar to those utilized in the laboratory. The comparative analysis is utilized as justifying argument for the selection of higher-order harmonic-based features selected for utilization in all severity classification techniques. 4 techniques, namely, SAM, SID, LDA and SVM have been utilized for the severity classification of low-voltage motor coil arcing faults.

While the first three of these, SAM, SID and LDA are primarily statistical techniques, SVM is more of a pattern recognition technique based on similar lines as neural networks. It differs from neural networks in the manner in which it "learns" to identify various patterns. Mathematical realizations and formulations associated with each of these 4 classification techniques have been presented in the relevant section in the dissertation. Results associated with the severity classification as classified by each of the 4 classification techniques are presented followed by performance evaluation and comparative analysis based on pre-selected performance evaluation criterion.

Some of the observations and/or inferences that can be drawn fro the results presented by the 4 classification techniques are:

- SAM & SID are primarily trend identification tools which utilize the higher-order harmonic content in the features extracted to classify the severity of the low-voltage motor coil arcing fault.
- SAM & SID tend to produce better results associated with the classification of unforeseen data without prior training in comparison to LDA.

- LDA performs adequately well in terms of classifying the severity of motor coil arcing faults based on the comprehensiveness with which it is trained.
- SVM has been utilized initially as a one-class, unsupervised learning based, classifier for anomaly detection. It performs reasonably well in terms of detecting abnormal or faulty conditions without classifying the severity of motor coil arcing faults.
- The one-class SVM-based classifier has been extended to multi-class SVM classifier for the classification of severity of motor coil arcing faults. The results associated with the classification using multi-class SVM though accurate do require rigorous and lengthy training samples and properly chosen boundary complexity and kernel.
- The ease of implementation associated with SAM & SID in conjunction with the absence of any training seems to lend itself well to the real-time applications associated with the classification of severity of motor coil arcing faults.

5.3 Recommendations/Future Work

While some ground breaking research odes characterize this dissertation especially in the less trodden path of low/medium voltage switchgear and motor coil arcing fault detection and/or severity classification, the author does feel that the results documented herein have opened some new research avenues. The successful implementation of the test-bench based higher-order harmonic differential approach for

the detection of low-voltage switchgear arcing can be utilized as a precursor for the development of a real-time, remote, web-enabled early warning system for switchgear arcing faults. Some research in that direction is already underway at Energy Systems Research Center (ESRC) with some promising preliminary results. Furthermore, the successful testing of such a proto-type in actual field conditions would usher in an era of the predictive maintenance so long desired by the switchgear industry.

On the low-voltage motor coil arcing fault severity classification front, while the SAM & SID trending measures have been adequately explored in terms of their capability to classify low-voltage motor coil arcing faults in this dissertation, the same is not true for SVM classification technique. The SVM is a relatively nascent concept that has garnered tremendous interest in the pattern recognition community in the last decade or so for its flexibility to be able to decipher highly non-linear patterns. While this dissertation briefly utilizes one aspect of the SVM to test the performance of SVM in classifying severity of motor coil arcing faults, the results do tend to be promising and indicative of tremendous research potential in this area.

Furthermore, the development of a real-time SVM-based motor coil arc fault severity classification module may go a long way in not only serving as an early warning systems for applications with huge motor coil windings but also drastically reduce the downtime associated unscheduled outages for motor coil winding maintenance.

All these areas are extensions of the research presented in this dissertation in various directions with the potential of tremendous contribution to the switchgear industry and industrial power system applications.

APPENDIX A

MEDIUM VOLTAGE SWITCHGEAR ARC FAULT DETECTION – ADDITIONAL SCENARIO RESULTS

BC8: Internal Arcing Fault – Non-linear device connected at Bus#5 with all capacitors connected

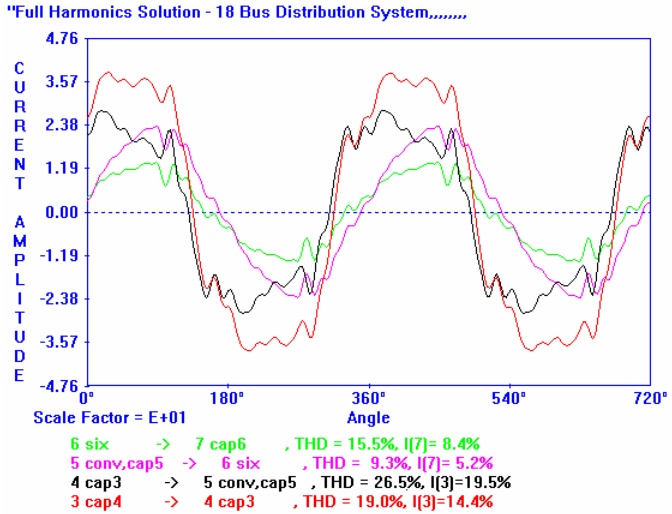

Current plots

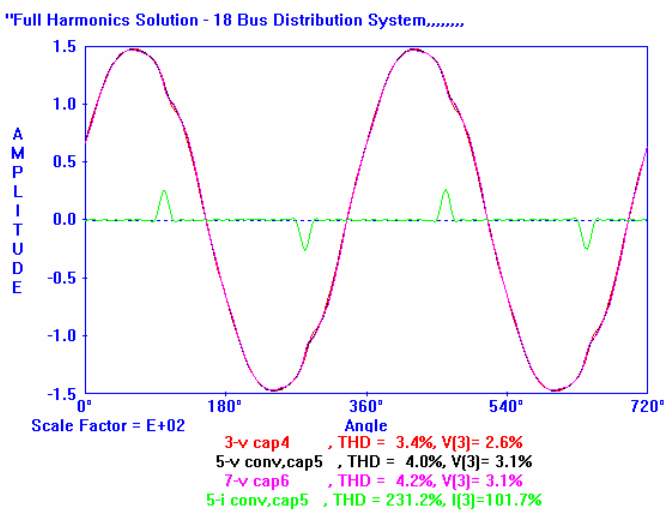

Voltage Plots

Harmonic Composition table for line current for internal fault with all capacitors connected

CASE BC8: Non-linear load simulation in 18-bus distribution system
with capacitor : Arc at Bus#5 **(Internal fault)**

Line	1st Harmonic		3st Harmonic		5st Harmonic		7st Harmonic		9st Harmonic		11st Harmonic		13st Harmonic		15st Harmonic		17st Harmonic		I1(%)	THDi(%)
	Mag [%]	Angle[Deg]	Mag [%]	Angle[Deg]	Mag [%]	Angle[Deg]	Mag [%]	Angle[Deg]	Mag [%]	Angle[Deg]	Mag [%]	Angle[Deg]	Mag [%]	Angle[Deg]	Mag [%]	Angle[Deg]	Mag [%]	Angle[Deg]		
3to4	36.28	41.60	5.22	139.10	3.34	-89.70	2.39	-28.20	0.31	105.90	0.44	37.90	1.40	166.40	0.49	-114.40	0.27	139.50	36.30	19.00
4to5	24.16	56.30	4.70	140.00	3.22	-84.10	1.83	-13.90	0.20	-124.30	0.82	47.40	1.68	174.20	0.38	-81.90	0.57	152.40	24.20	26.50
5to6	19.60	9.50	0.60	131.40	0.51	-152.90	1.01	-67.60	0.52	87.60	0.34	-115.00	0.45	101.70	0.51	-142.60	0.24	18.50	19.60	9.30
6to7	11.36	22.10	0.60	131.40	0.46	-141.50	0.95	-58.70	0.52	87.60	0.33	-109.50	0.44	106.20	0.51	-142.60	0.24	21.20	11.40	15.50
50to1	93.20	52.00	10.58	132.30	1.62	-165.20	1.81	-51.30	0.89	84.90	0.66	-116.60	0.76	2.10	0.14	99.30	0.14	-23.60	93.20	11.70
51to50	98.60	28.70	0.00	0.00	1.64	-135.20	1.85	-81.40	0.00	0.00	0.69	-86.60	0.81	-28.00	0.00	0.00	0.17	6.30	98.60	2.70
1to20	43.34	53.30	4.15	124.10	3.40	107.40	2.15	153.10	0.55	-82.00	0.19	133.50	0.94	-37.20	0.78	35.10	0.53	174.80	43.30	13.80
20to21	34.98	59.80	3.67	123.70	3.15	106.00	2.23	149.10	0.75	-86.80	0.38	75.50	0.25	-99.80	0.34	17.50	0.35	170.70	35.00	15.50
21to22	2.20	-5.90	0.00	0.00	0.02	38.20	0.01	115.60	0.00	0.00	0.01	142.30	0.02	-106.10	0.00	0.00	0.01	93.10	2.20	1.60
21to23	26.05	48.00	2.58	122.90	2.47	101.40	2.08	143.50	0.95	-91.30	0.85	59.50	1.68	166.90	0.86	-130.50	0.35	3.10	26.00	18.20

BC9: External Arcing Fault – Non-linear device connected at Bus#7 with all capacitors connected

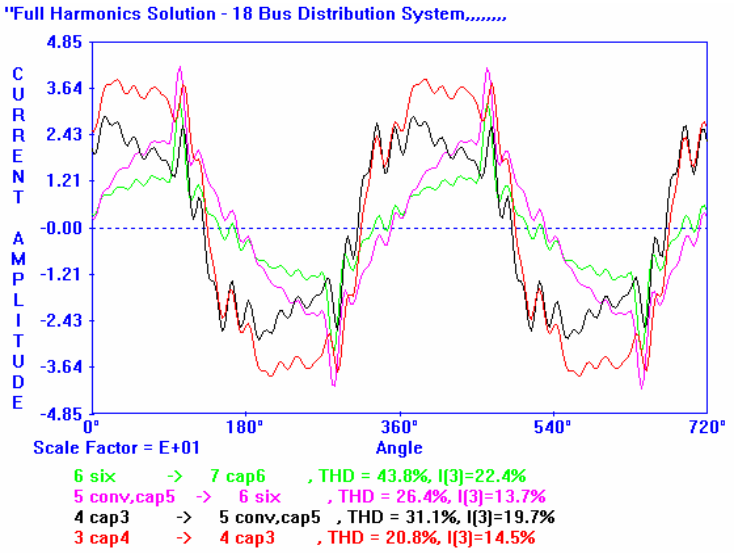

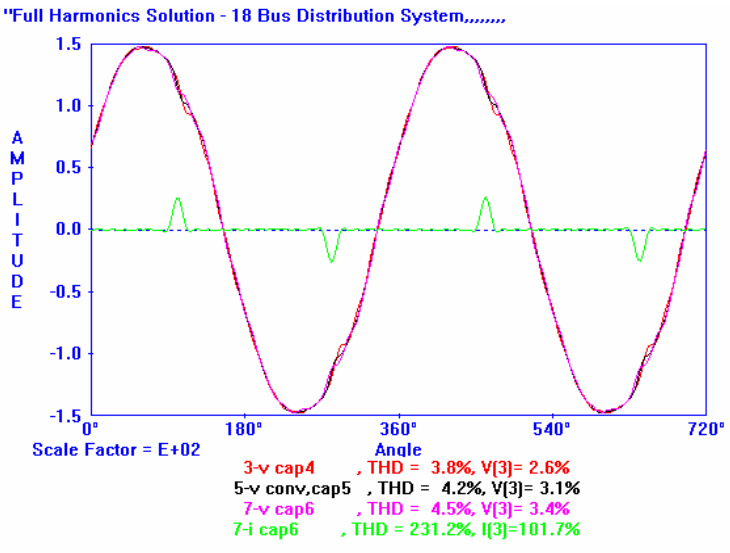

Current Plots Voltage Plots

Harmonic Composition table for line current for external fault with all capacitors connected

CASE BC9: Non-linear load simulation in 18-bus distribution system
with capacitor : Arc at Bus#7 **(External fault)**

Line	1st Harmonic		3st Harmonic		5st Harmonic		7st Harmonic		9st Harmonic		11st Harmonic		13st Harmonic		15st Harmonic		17st Harmonic		I1(%)	THDi(%)
	Mag [%]	Angle[Deg]	Mag [%]	Angle[Deg]	Mag [%]	Angle[Deg]	Mag [%]	Angle[Deg]	Mag [%]	Angle[Deg]	Mag [%]	Angle[Deg]	Mag [%]	Angle[Deg]	Mag [%]	Angle[Deg]	Mag [%]	Angle[Deg]		
3to4	36.29	41.60	5.28	136.60	3.50	-92.40	2.62	-32.00	0.36	103.50	0.55	31.30	1.99	158.10	0.81	-119.30	0.53	125.80	36.30	20.80
4to5	24.16	56.20	4.75	137.50	3.37	-86.70	2.00	-17.80	0.23	-126.70	1.04	40.80	2.38	165.90	0.63	-86.90	1.14	138.70	24.20	31.10
5to6	21.82	7.20	3.00	142.40	2.41	-69.40	1.32	93.00	1.77	-98.10	1.91	59.10	1.92	-160.70	1.33	10.00	1.58	163.00	21.80	26.40
6to7	13.39	16.40	3.00	142.40	2.50	-67.60	1.44	88.10	1.77	-98.10	1.92	58.40	1.97	-160.20	1.33	10.00	1.59	163.20	13.40	43.80
50to1	93.20	52.00	10.69	129.80	1.69	-167.80	1.98	-55.20	1.04	82.50	0.83	-123.10	1.07	-6.20	0.23	94.40	0.29	-37.30	93.20	12.00
51to50	98.60	28.70	0.00	0.00	1.71	-137.90	2.02	-85.20	0.00	0.00	0.88	-93.20	1.15	-36.30	0.00	0.00	0.33	-7.40	98.60	3.20
1to20	43.34	53.30	4.20	121.60	3.56	104.70	2.35	149.30	0.65	-84.40	0.24	126.90	1.34	-45.50	1.29	30.10	1.05	161.10	43.30	15.20
20to21	34.98	59.80	3.70	121.20	3.30	103.40	2.44	145.20	0.88	-89.20	0.49	69.00	0.36	-108.10	0.56	12.50	0.70	157.10	35.00	16.70
21to22	2.20	-5.90	0.00	0.00	0.02	35.50	0.01	111.80	0.00	0.00	0.01	135.70	0.03	-114.40	0.00	0.00	0.01	79.40	2.20	2.20
21to23	26.05	48.00	2.61	120.40	2.58	98.80	2.27	139.70	1.11	-93.60	1.08	52.90	2.38	158.60	1.42	-135.50	0.70	-10.60	26.00	21.00

BC10: Internal Arcing Fault – Non-linear device connected at Bus#5 with capacitor at Bus#5 removed

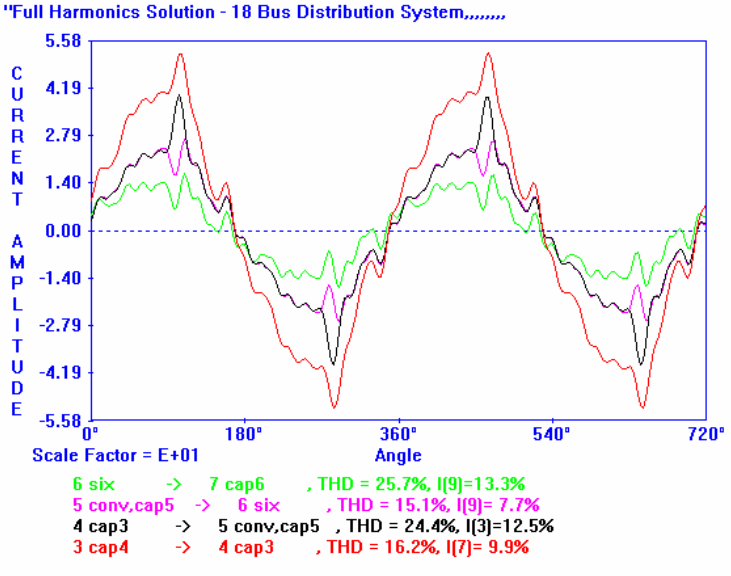

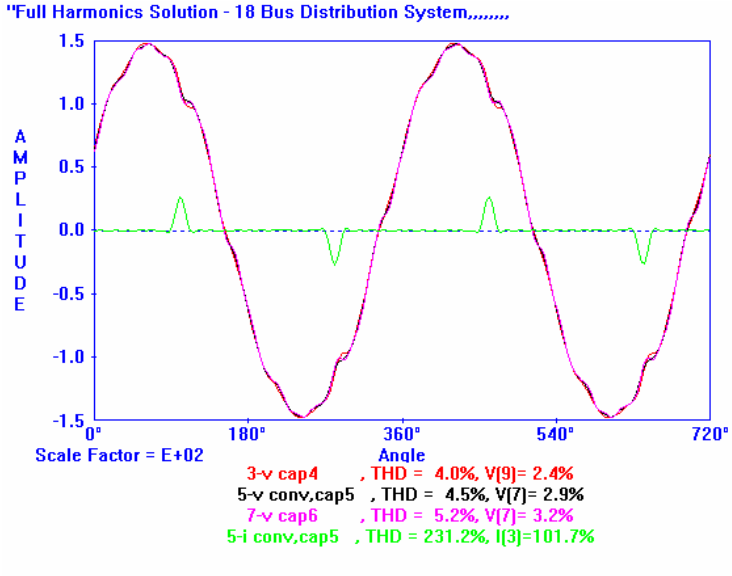

Current Plots Voltage Plots

Harmonic Composition table for line current for internal fault with all capacitors connected except bus #5

CASE BC10: Non-linear load simulation in 18-bus distribution system with capacitors in other buses except bus 5 : Arc at Bus#5 **(Internal fault)**

Line	1st Harmonic		3st Harmonic		5st Harmonic		7st Harmonic		9st Harmonic		11st Harmonic		13st Harmonic		15st Harmonic		17st Harmonic		I1(%)	THDi(%)
	Mag [%]	Angle[Deg]	Mag [%]	Angle[Deg]	Mag [%]	Angle[Deg]	Mag [%]	Angle[Deg]	Mag [%]	Angle[Deg]	Mag [%]	Angle[Deg]	Mag [%]	Angle[Deg]	Mag [%]	Angle[Deg]	Mag [%]	Angle[Deg]		
3to4	37.06	10.10	3.11	146.80	2.60	-67.70	3.65	57.50	0.93	113.80	0.72	53.00	1.38	-156.90	1.39	-79.50	0.37	159.00	37.10	16.20
4to5	22.50	6.70	2.80	147.70	2.50	-62.00	2.80	71.70	0.60	-116.30	1.35	62.50	1.66	-149.10	1.08	-47.10	0.79	171.80	22.50	24.40
5to6	20.23	8.70	0.36	139.10	0.40	-130.90	1.55	18.00	1.55	95.60	0.56	-99.90	0.44	138.40	1.46	-107.80	0.33	37.90	20.20	15.10
6to7	11.70	20.60	0.36	139.10	0.36	-119.40	1.45	26.90	1.55	95.60	0.54	-94.30	0.43	142.80	1.46	-107.80	0.33	40.70	11.70	25.70
50to1	87.39	38.80	6.31	140.00	1.26	-143.10	2.76	34.40	2.66	92.90	1.09	-101.40	0.75	38.80	0.40	134.10	0.20	-4.20	87.40	8.70
51to50	90.19	16.70	0.00	0.00	1.27	-113.10	2.82	4.30	0.00	0.00	1.14	-71.50	0.80	8.70	0.00	0.00	0.23	25.70	90.20	3.80
1to20	43.37	51.70	2.48	131.80	2.65	129.50	3.28	-121.20	1.65	-74.10	0.31	148.60	0.93	-0.50	2.20	69.90	0.72	-165.80	43.40	13.30
20to21	34.85	58.10	2.19	131.40	2.45	128.10	3.40	-125.20	2.25	-78.80	0.64	90.70	0.25	-63.10	0.96	52.30	0.48	-169.80	34.80	15.50
21to22	2.23	-5.90	0.00	0.00	0.02	60.20	0.01	-158.70	0.00	0.00	0.01	157.40	0.02	-69.40	0.00	0.00	0.01	112.50	2.20	1.50
21to23	26.14	46.30	1.54	130.60	1.92	123.50	3.17	-130.80	2.84	-83.30	1.41	74.60	1.66	-156.50	2.44	-95.70	0.48	22.60	26.10	22.70

BC11: External Arcing Fault – Non-linear device connected at Bus#7 with capacitor at Bus#5 removed

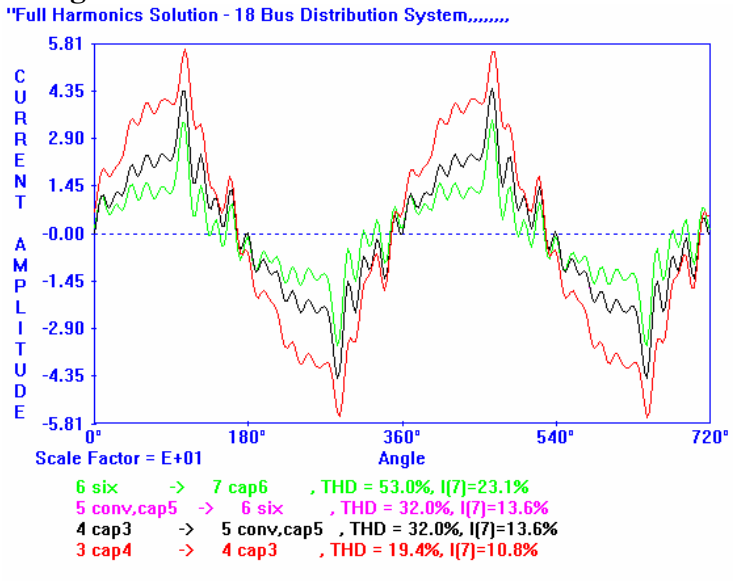

Current plots

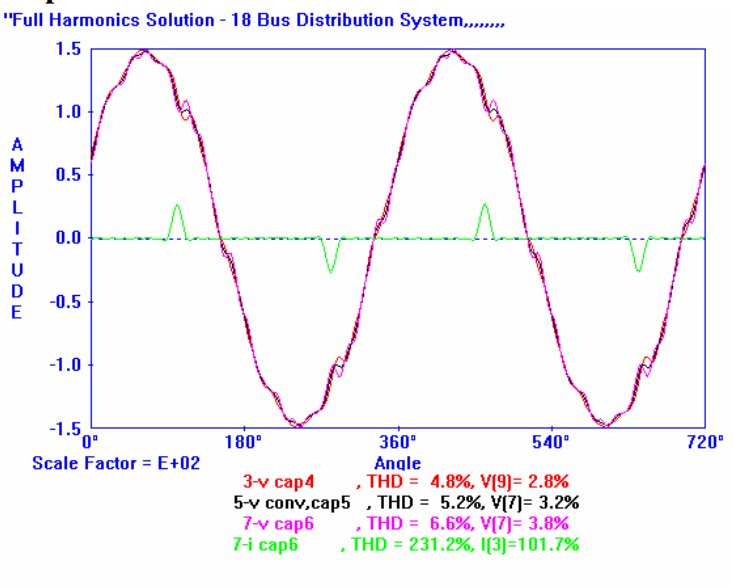

Voltage Plots

Harmonic Composition table for line current for external fault with all capacitors connected except bus #5

CASE BC11: Non-linear load simulation in 18-bus distribution system with capacitors in other buses except bus 5 : Arc at Bus#7 **(External fault)**

Line	1st Harmonic		3st Harmonic		5st Harmonic		7st Harmonic		9st Harmonic		11st Harmonic		13st Harmonic		15st Harmonic		17st Harmonic		I1(%)	THDi(%)
	Mag [%]	Angle[Deg]	Mag [%]	Angle[Deg]	Mag [%]	Angle[Deg]	Mag [%]	Angle[Deg]	Mag [%]	Angle[Deg]	Mag [%]	Angle[Deg]	Mag [%]	Angle[Deg]	Mag [%]	Angle[Deg]	Mag [%]	Angle[Deg]		
3to4	37.08	10.00	3.17	144.90	2.72	-70.40	4.00	53.60	1.08	112.60	0.92	46.40	1.96	-165.30	2.24	-83.80	0.73	145.10	37.10	19.40
4to5	22.53	6.60	2.85	145.80	2.62	-64.70	3.06	67.80	0.70	-117.60	1.72	55.90	2.35	-157.50	1.75	-51.30	1.57	158.00	22.50	32.00
5to6	22.53	6.60	2.85	145.80	2.62	-64.70	3.06	67.90	0.70	-117.60	1.72	55.90	2.35	-157.50	1.75	-51.30	1.58	158.00	22.50	32.00
6to7	13.82	15.20	2.85	145.80	2.67	-63.00	3.19	72.40	0.70	-117.60	1.76	54.60	2.38	-156.40	1.75	-51.30	1.60	158.30	13.80	53.00
50to1	87.40	38.80	6.41	138.10	1.32	-145.80	3.02	30.50	3.10	91.60	1.38	-108.10	1.06	30.40	0.65	129.90	0.40	-18.00	87.40	9.30
51to50	90.19	16.70	0.00	0.00	1.33	-115.80	3.09	0.40	0.00	0.00	1.45	-78.10	1.14	0.30	0.00	0.00	0.46	11.90	90.20	4.40
1to20	43.37	51.70	2.52	129.90	2.77	126.70	3.59	-125.10	1.92	-75.30	0.40	142.00	1.32	-8.90	3.57	65.70	1.45	-179.60	43.40	16.30
20to21	34.85	58.10	2.22	129.50	2.57	125.40	3.72	-129.10	2.62	-80.10	0.81	84.00	0.35	-71.50	1.55	48.10	0.96	176.40	34.80	17.80
21to22	2.23	-5.90	0.00	0.00	0.02	57.50	0.01	-162.60	0.00	0.00	0.02	150.80	0.03	-77.80	0.00	0.00	0.02	98.70	2.20	2.20
21to23	26.14	46.30	1.56	128.70	2.01	120.80	3.47	-134.70	3.31	-84.50	1.79	68.00	2.35	-164.90	3.95	-99.90	0.97	8.70	26.10	28.50

TC1: Internal Arcing Fault – Non-linear device connected at Bus#5 with line between Bus#4-#5 as GY-GY transformer

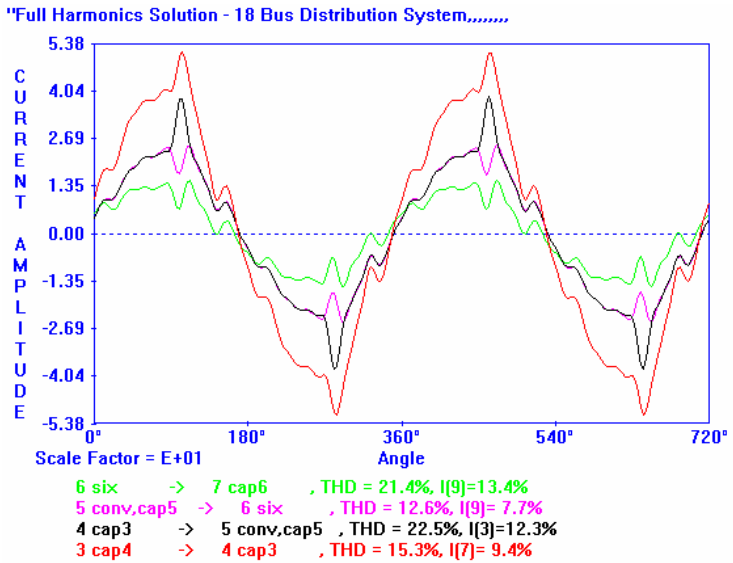

Current Plots

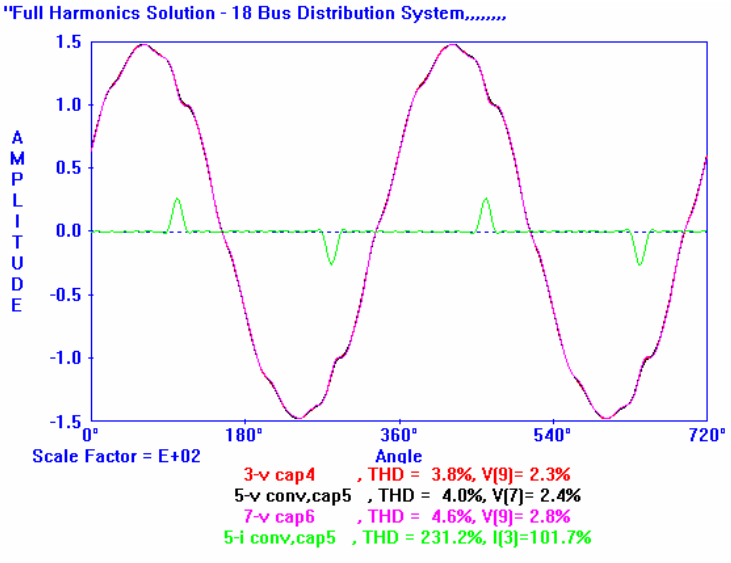

Voltage Plots

Harmonic Composition table for line current for internal fault with all capacitors connected except bus #5 and line 4-5 GY-GY Transformer

CASE TC1: Line 4 to 5 is Transformer GY-GY : with capacitors at other buses except bus 5 : Arc at Bus#5 **(Internal fault)**

Line	1st Harmonic		3st Harmonic		5st Harmonic		7st Harmonic		9st Harmonic		11st Harmonic		13st Harmonic		15st Harmonic		17st Harmonic		I1(%)	THDi(%)
	Mag [%]	Angle[Deg]	Mag [%]	Angle[Deg]	Mag [%]	Angle[Deg]	Mag [%]	Angle[Deg]	Mag [%]	Angle[Deg]	Mag [%]	Angle[Deg]	Mag [%]	Angle[Deg]	Mag [%]	Angle[Deg]	Mag [%]	Angle[Deg]		
3to4	36.97	10.30	3.06	147.60	2.52	-64.80	3.48	63.70	0.90	116.70	0.64	58.90	1.07	-145.30	1.19	-56.70	0.24	175.00	37.00	15.30
4to5	22.42	7.00	2.76	148.40	2.43	-59.10	2.67	78.00	0.58	-113.50	1.19	68.40	1.28	-137.50	0.93	-24.30	0.52	-172.20	22.40	22.50
5to6	20.15	9.10	0.32	139.70	0.30	-137.20	1.29	20.70	1.56	96.90	0.70	-107.00	0.33	75.90	1.08	-105.60	0.52	9.80	20.10	12.60
6to7	11.65	21.00	0.32	139.70	0.27	-125.70	1.21	29.60	1.56	96.90	0.68	-101.40	0.33	80.30	1.08	-105.60	0.51	12.50	11.70	21.40
50to1	87.37	38.90	6.20	140.80	1.22	-140.20	2.63	40.60	2.57	95.70	0.96	-95.60	0.58	50.40	0.35	156.90	0.13	11.80	87.40	8.50
51to50	90.19	16.80	0.00	0.00	1.23	-110.30	2.69	10.60	0.00	0.00	1.01	-65.60	0.62	20.30	0.00	0.00	0.15	41.70	90.20	3.50
1to20	43.37	51.70	2.43	132.60	2.56	132.30	3.13	-114.90	1.59	-71.20	0.28	154.50	0.72	11.10	1.90	92.70	0.48	-149.80	43.40	12.50
20to21	34.85	58.10	2.15	132.20	2.38	131.00	3.24	-119.00	2.17	-76.00	0.56	96.50	0.19	-51.40	0.83	75.10	0.32	-153.80	34.80	14.80
21to22	2.23	-5.90	0.00	0.00	0.02	63.10	0.01	-152.50	0.00	0.00	0.01	163.30	0.02	-57.80	0.00	0.00	0.01	128.50	2.20	1.30
21to23	26.14	46.30	1.51	131.30	1.86	126.40	3.02	-124.50	2.74	-80.40	1.24	80.50	1.28	-144.80	2.11	-72.90	0.32	38.60	26.10	21.00

TC2: Internal Arcing Fault – Non-linear device connected at Bus#5 with line between Bus#4-#5 as Delta-GY transformer

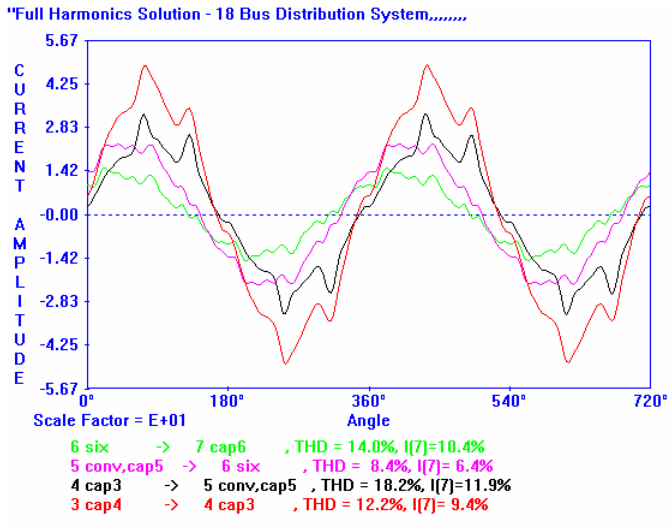

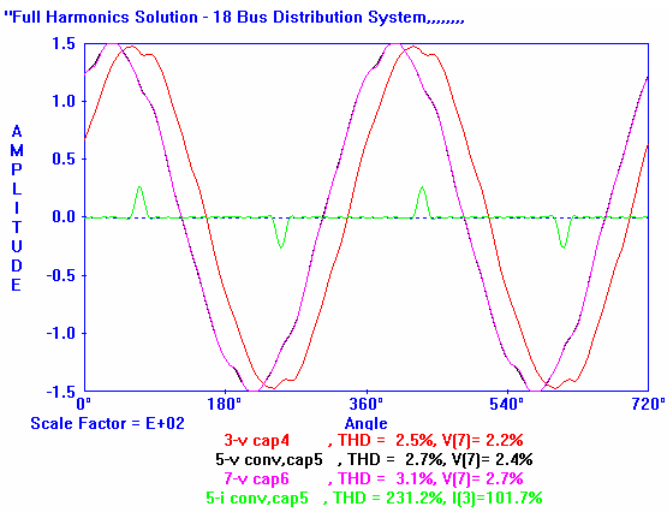

Current Plots

Voltage Plots

Harmonic Composition table for line current for internal fault with all capacitors connected except bus #5 and line 4-5 Delta-GY Transformer

CASE TC2: Line 4 to 5 is Transformer Delta-GY : with capacitors at other buses except bus 5 : Arc at Bus#5 **(Internal fault)**

Line	1st Harmonic		3st Harmonic		5st Harmonic		7st Harmonic		9st Harmonic		11st Harmonic		13st Harmonic		15st Harmonic		17st Harmonic		I1(%)	THDi(%)
	Mag [%]	Angle[Deg]	Mag [%]	Angle[Deg]	Mag [%]	Angle[Deg]	Mag [%]	Angle[Deg]	Mag [%]	Angle[Deg]	Mag [%]	Angle[Deg]	Mag [%]	Angle[Deg]	Mag [%]	Angle[Deg]	Mag [%]	Angle[Deg]		
3to4	36.97	10.3	0	0	2.52	115.2	3.481	-116.3	0	0	0.635	58.9	1.072	-145.3	0	0	0.242	-5	37	12.2
4to5	22.42	7	2.426	120.9	2.665	-102	1.19	68.4	1.284	-137.5	0.519	7.8	22.4	18.2	0	0	0.52	7.80	22.40	18.20
5to6	20.15	39.1	0.005	-123.4	0.304	12.8	1.289	-129.3	0.041	177.2	0.699	-137	0.335	105.9	0.11	117.5	0.52	159.8	20.1	8.4
6to7	11.65	51	0.005	-123.4	0.272	24.3	1.21	-120.4	0.041	177.2	0.68	-131.4	0.328	110.3	0.11	117.5	0.514	162.5	11.7	14
50to1	87.37	38.9	0	0	1.221	39.8	2.632	-139.4	0	0	0.955	-95.6	0.579	50.4	0	0	0.132	-168.2	87.4	3.6
51to50	90.19	16.8	0	0	1.234	69.7	2.688	-169.4	0	0	1.007	-65.6	0.623	20.3	0	0	0.15	-138.3	90.2	3.5
1to20	43.37	51.7	0	0	2.563	-47.7	3.127	65.1	0	0	0.276	154.5	0.721	11.1	0	0	0.479	30.2	43.4	9.6
20to21	34.85	58.1	0	0	2.376	-49	3.243	61	0	0	0.56	96.5	0.192	-51.4	0	0	0.318	26.2	34.8	11.7
21to22	2.232	-5.9	0	0	0.018	-116.9	0.009	27.5	0	0	0.011	163.3	0.017	-57.8	0	0	0.006	-51.5	2.2	1.3
21to23	26.14	46.3	0	0	1.861	-53.6	3.023	55.5	0	0	1.239	80.5	1.284	-144.8	0	0	0.319	-141.4	26.1	15.3

APPENDIX B

MATLAB CODES – MEDIUM VOLTAGE SWITCHGEAR ARC FAULT DETECTION: HARMONIC CONTENT EVALUATION

```
close all;
clear all; clc;

inputfile = 'Hall_effect_sensor.lvm';
data = load(inputfile);
Fs = 18000;
h = 24;
nPoint = 900;

% Calculate fast fourier transform
Ypri = fft(data(:,2),nPoint);
mYpri = abs(Ypri);                  % magnitude of each component
pYpri = (angle(Ypri))*180/pi;     % phase in degree
Ysec = fft(data(:,3),nPoint);
mYsec = abs(Ysec);
pYsec = (angle(Ysec))*180/pi;
f = (0:length(Ypri)-1)'*Fs/length(Ypri);
Nindex = find(f==60);
nYpri = mYpri/mYpri(Nindex)*100;       % normalized magnitude to fundamental frequency
nYsec = mYsec/mYsec(Nindex)*100;
rYpri = pYpri-pYpri(Nindex);           % reletive phase angle with respect to phase of fundamental
frequency
rYsec = pYsec-pYsec(Nindex);
rYpri = mod(rYpri,360);
rYsec = mod(rYsec,360);
FFTY = zeros(nPoint,1);
Fsave = [1:2:h];
Findex=[];
fprintf('%5s %10s %15s %15s    %15s %15s\n\n','Hth','Freq[Hz]','%Abs Pri','relDeg Pri','%Abs Sec','relDeg
Sec');
for a=1:length(Fsave)
   N = find(f==60*Fsave(a));
   Findex = [Findex N];
   rYsec2(N) = mod(rYsec(N),360/Fsave(a));
   fprintf('%5d %10d %15.3f %15.2f    \n',Fsave(a),f(N),nYpri(N),rYpri(N));
   FFTY(N) = nYsec(N)/100*mYsec(Nindex)*exp(j*(rYsec(N)+pYsec(Nindex))*pi/180);
   FFTY(N) = nYsec(N)/100*mYsec(Nindex) * exp(j*(rYsec(N))*pi/180);
   FFTY(N) = FFTY(N)*exp(j*pYsec(Nindex)*pi/180);
end;

disp([FFTY(1:h) Ysec(1:h)]);
Ynew = ifft(FFTY);
[f(Findex) nYpri(Findex) pYpri(Findex) nYsec(Findex) pYsec(Findex)]
% Plot time signal
figure;
plot(data(1:nPoint,1),data(1:nPoint,2),'b'); grid on
axis([data(1,1), data(nPoint,1), -0.05 0.05]);
xlabel('Time [sec]');   ylabel('Magnitude [V]');
title('Raw Audio Signal for Ultrasonic Sensor for unknown arcing');

% Plot frequency component
figure;
subplot(2,1,1); plot(f,nYpri); grid on
axis([0 700 0 500]);
title('Frequency Spectrum of Audio Signal for unknown arcing');
ylabel('Normalized Magnitude [%]');
```

```
xlabel('Frequency Hz');
subplot(2,1,2); stem(f,pYpri); grid on
axis([0 60*h -200 200]);
ylabel('Phase [Degree]');
xlabel('Frequency [Hz]');
```

APPENDIX C

MATLAB CODE: LOW-VOLTAGE MOTOR COIL ARC FAULT SEVERITY CLASSIFICATION – SAM, SID & LDA APPROACHES

Main Program

```
% Generate the reference signature from Case1
clear
clc
close all
%% changing directories to load the matlab data file containing arcing data
%% for various cases
cd  ('C:/Doctorate/Software Development/Matlab codes/SAM-SID module')
load experiment_data.mat
%% finding the total number of rows for case 1 which shall form the
%% reference signature
size_case1 = size(case1_beg,1) + size(case1_mid,1) + size(case1_end,1);
%% sampling frequency of 18000 samples/sec
Fs = 18000;
case1_notch = [];
%% adding the rows of data for mid and end cases after beg case
case1_data = [case1_beg;case1_mid;case1_end];
for i = 1:size_case1
    %% pulling out the entire data in the ith row of the combined matrix
    %% for case1
   data_mid = case1_data(i,:);
   [n_filtered,f] = apply_notch(data_mid,Fs);
   %% obtaining power spectral density estimate of filtered data
   [Pxx_notch,F_notch] = psd(n_filtered(1001:end),17000,Fs);
   case1_signature(i,:) = feature_extract(F_notch,Pxx_notch);
end
ref_signature = mean(case1_signature);
% utilizing the original cases first
test_data  =
[case1_beg;case1_mid;case1_end;case2_beg;case2_mid;case2_end;case3_beg;case3_mid;case3_end;case4
_beg;case4_mid;case4_end;case5_beg;case5_mid;case5_end];

%Start testing
for i = 1:size(test_data,1)
   data_mid = test_data(i,:);
   [n_filtered,f] = apply_notch(data_mid,Fs);
   [Pxx_notch,F_notch] = psd(n_filtered(1001:end),17000,18000);
   test_signature(i,:) = feature_extract(F_notch,Pxx_notch);
   SAM_index_original(i) = SAM_function(test_signature(i,:),ref_signature);
   SID_index_original(i) = SID_function(test_signature(i,:),ref_signature);
end
% utilizing intermediate case data
cd  ('C:/Doctorate/Software Development/Matlab codes')
load intermediate_cases_data.mat

test_data34a  = [case34a_beg;case34a_mid;case34a_end];
test_data34b =  [case34b_beg;case34b_mid;case34b_end];
test_data34c =  [case34c_beg;case34c_mid;case34c_end];
cd('C:/Doctorate/Software Development/Matlab codes/SAM-SID Module')
%Start testing
index_counter_34a = 0;
for i = 1:size(test_data34a,1)
   data_mid = test_data34a(i,:);
   [n_filtered,f] = apply_notch(data_mid,Fs);
```

```
  [Pxx_notch,F_notch] = psd(n_filtered(1001:end),17000,18000);
  test_signature(i,:) = feature_extract(F_notch,Pxx_notch);
  index_counter_34a= index_counter_34a +1;
  SAM_index_intermediate34a(index_counter_34a) = SAM_function(test_signature(i,:),ref_signature);
  SID_index_intermediate34a(index_counter_34a) = SID_function(test_signature(i,:),ref_signature);
end
index_counter_34b_start = index_counter_34a;
index_counter_34b_end = index_counter_34a;
for i = 1:size(test_data34b,1)
  data_mid34b = test_data34b(i,:);
  [n_filtered,f] = apply_notch(data_mid34b,Fs);
  [Pxx_notch,F_notch] = psd(n_filtered(1001:end),17000,18000);
  test_signature(i,:) = feature_extract(F_notch,Pxx_notch);
  index_counter_34b_end = index_counter_34b_end + 1;
  SAM_index_intermediate34b(index_counter_34b_end) =
SAM_function(test_signature(i,:),ref_signature);
  SID_index_intermediate34b(index_counter_34b_end) = SID_function(test_signature(i,:),ref_signature);
end
index_counter_34c_start= index_counter_34b_end;
index_counter_34c_end = index_counter_34b_end;
for i = 1:size(test_data34c,1)
  data_mid = test_data34c(i,:);
  [n_filtered,f] = apply_notch(data_mid,Fs);
  [Pxx_notch,F_notch] = psd(n_filtered(1001:end),17000,18000);
  test_signature(i,:) = feature_extract(F_notch,Pxx_notch);
  index_counter_34c_end = index_counter_34c_end+1;
  SAM_index_intermediate34c(index_counter_34c_end) =
SAM_function(test_signature(i,:),ref_signature);
  SID_index_intermediate34c(index_counter_34c_end) = SID_function(test_signature(i,:),ref_signature);
end


figure;plot(SAM_index_original,'b+'); hold on;grid
xlabel('Data no')
ylabel('SAM value')
title('Arcing Fault Severity Classification Results: SAM')
plot(SAM_index_intermediate34a,'r*'); hold on
plot((index_counter_34b_start:index_counter_34b_end),SAM_index_intermediate34b(index_counter_34b_
start:index_counter_34b_end),'gv'); hold on
plot((index_counter_34c_start:index_counter_34c_end),SAM_index_intermediate34c(index_counter_34c_
start:index_counter_34c_end),'mo'); hold on
legend('Original Cases -Case3(10.95%) Case4(21.9%)','Case34(a)-12.4%','Case34(b)-16.05%','Case34(c)-
19.7%',4)


figure;plot(SID_index_original,'b+'); hold on;grid
xlabel('Data no')
ylabel('SID value')
title('Arcing Fault Severity Classification Results: SID')
plot(SID_index_intermediate34a,'r*'); hold on
plot((index_counter_34b_start:index_counter_34b_end),SID_index_intermediate34b(index_counter_34b_s
tart:index_counter_34b_end),'gv'); hold on
plot((index_counter_34c_start:index_counter_34c_end),SID_index_intermediate34c(index_counter_34c_st
art:index_counter_34c_end),'mo'); hold on
legend('Original Cases -Case3(10.95%) Case4(21.9%)','Case34(a)-12.4%','Case34(b)-16.05%','Case34(c)-
19.7%',4)
```

```
% Classification by LDA (Linear Discriminant Analysis)
% Training set is selected
cd  ('C:/Doctorate/Software Development/Matlab codes')
load intermediate_cases_data.mat
test_data34  =
[case34a_beg;case34a_mid;case34a_end;case34b_beg;case34b_mid;case34b_end;case34c_beg;case34c_mi
d;case34c_end];

cd  ('C:/Doctorate/Software Development/Matlab codes/SAM-SID module')
load experiment_data.mat
test_data  =
[case1_beg;case1_mid;case1_end;case2_beg;case2_mid;case2_end;case3_beg;case3_mid;case3_end;test_d
ata34;case4_beg;case4_mid;case4_end;case5_beg;case5_mid;case5_end];


%Start testing
for i = 1:size(test_data,1)
   data_mid = test_data(i,:);
   [n_filtered,f] = apply_notch(data_mid,Fs);
   [Pxx_notch,F_notch] = psd(n_filtered(1001:end),17000,18000);
   test_signature(i,:) = feature_extract(F_notch,Pxx_notch);
end

training = test_signature([1 2 3 4 8 9 10 11 16 17 18 19 23 24 25 26 31 32 33 34 39 40 41 42 46 47 48 49
54 55 56 57],:);
group_original = [1 1 1 1 1 1 1 2 2 2 2 2 2 2 2 3 3 3 3 3 3 3 4 4 4 4 4 4 4 4 5 5 5 5 5 5 5 5 6 6 6 6 6 6 6 7 7 7
7 7 7 7 7 8 8 8 8 8 8 8 8 8];
group = [1 1 1 1 2 2 2 2 3 3 3 3 4 4 4 4 5 5 5 5 6 6 6 6 7 7 7 7 8 8 8 8];
[gmeans,mm,R,ngroups] = training_UTA(training, group, 'linear');
% Classify training data
for i = 1:size(training,1)
    [tmp_tr(i), class_tr(i)] = classify_test(training(i,:), gmeans, mm, ngroups, R);
end
figure;plot(class_tr,'ro');grid
hold
plot(group,'b+')
xlabel('Data no')
ylabel('Class no')
legend('Estimated','Actual','class
1:Case1','class2:Case2','class3:case3','class4:case34a','class5:case34b','class6:case34c','class7:case4','class8:
case5',4)
title('Training data classification')

sample=test_signature;
% Classify both training and testing data
for i = 1:size(sample,1)
    [tmp(i), class(i)] = classify_test(sample(i,:), gmeans, mm, ngroups, R);
end
figure;plot(class,'ro');grid
hold
plot(group_original,'b+')
xlabel('Data no')
ylabel('Class no')
```

```
legend('Estimated','Actual','class
1:Case1','class2:Case2','class3:case3','class4:case34a','class5:case34b','class6:case34c','class7:case4','class8:
case5',4)
title('Training+Testing data classification')
```

Feature Extraction Function

```
function [signature] = feature_extract(F_notch,s_notch)

% Computes the signature vector at 1st, 3rd, 5th, 7th harmonics and
% sidebands

% Find the sidebands around 60 Hz (40-50), (70-80)
temp_index_sideband_low_1 = find(F_notch>=40 & F_notch<=50);
temp_sideband_low_1 = max(s_notch(temp_index_sideband_low_1)');

temp_index_sideband_up_1 = find(F_notch>=70 & F_notch<=80);
temp_sideband_up_1 = max(s_notch(temp_index_sideband_up_1)');


% Find the sidebands around 3rd harmonic
temp_index_sideband_low_3 = find(F_notch>=160 & F_notch<=170);
temp_sideband_low_3       = max(s_notch(temp_index_sideband_low_3)');

temp_index_harmonic_3 = find(F_notch>=178 & F_notch<=182);
temp_harmonic_3 = max(s_notch(temp_index_harmonic_3)');

temp_index_sideband_up_3 = find(F_notch>=190 & F_notch<=200);
temp_sideband_up_3 = max(s_notch(temp_index_sideband_up_3)');


% Find the sidebands around 5th harmonic
temp_index_sideband_low_5 = find(F_notch>=280 & F_notch<=290);
temp_sideband_low_5 = max(s_notch(temp_index_sideband_low_5)');

temp_index_harmonic_5 = find(F_notch>=298 & F_notch<=302);
temp_harmonic_5 = max(s_notch(temp_index_harmonic_5)');

temp_index_sideband_up_5 = find(F_notch>=310 & F_notch<=320);
temp_sideband_up_5 = max(s_notch(temp_index_sideband_up_5)');


% Find the sidebands around 7th harmonic
temp_index_sideband_low_7 = find(F_notch>=400 & F_notch<=410);
temp_sideband_low_7 = max(s_notch(temp_index_sideband_low_7)');

temp_index_harmonic_7 = find(F_notch>=418 & F_notch<=422);
temp_harmonic_7 = max(s_notch(temp_index_harmonic_7)');

temp_index_sideband_up_7 = find(F_notch>=430 & F_notch<=440);
temp_sideband_up_7 = max(s_notch(temp_index_sideband_up_7)');

signature = 20*log10([temp_sideband_low_1 temp_sideband_up_1 temp_sideband_low_3
temp_harmonic_3 temp_sideband_up_3 temp_sideband_low_5 temp_harmonic_5 temp_sideband_up_5
temp_sideband_low_7 temp_harmonic_7 temp_sideband_up_7])+100;
```

SAM Function

```
function [SAM_value] = SAM_function(p,q)
temp1=sqrt(sum(p.^2));
temp2=sqrt(sum(q.^2));
SAM_value=acos(sum(p.*q)/(temp1*temp2));
```

SID Function

```
function [SID_value] = SID_function(p,q)
temp1=p/sum(p)+0.0000000001;
temp2=q/sum(q)+0.0000000001;
SID_value=sum(temp1.*log(temp1./temp2)+temp2.*log(temp2./temp1));
```

Notch Filter Function

```
function [n_filtered,f] = apply_notch(x,Fs)
% Application of a digital notch filter
%% determination of poles and zeros by angle equation
%% theta = (Fd/Fs) * 360
theta  = pi*60/(Fs/2); % 2pi*60/Fs
%% numerator of 2nd order IIR notch filter
%% 1-2*cosine(2*pi*Fo)z^-1+Z^-2
%Fo = Fd/Fs
B60 = [1,-2*cos(theta),1];
r60 = 0.85; % radius of pole at 60 hz %0.90
%%denominator of 2nd order IIR notch filter
%% 1-2*Rho*cosine(2*pi*Fo)z^-1+Rho^2*Z^-2
%% r60 defines locations of poles in unit circle
A60 = [1,-2*r60*cos(theta),r60^2];
%% defining the 1024 point IIR notch filter
[Hnotch,w] = freqz(B60,A60,1024)
f = w*(Fs/2)/pi;
%% filtered data
n_filtered = filter(B60,A60,x);
```

LDA Training Function

```
function [gmeans,mm,R,ngroups] = training_UTA(training, group, type)
[gindex,groups] = grp2idx(group);
nans = find(isnan(gindex));
if length(nans) > 0
   training(nans,:) = [];
   gindex(nans) = [];
end
ngroups = length(groups);
gsize = hist(gindex,1:ngroups);

[n,d] = size(training);

% Add training data to sample for error rate estimation
mm = n;
```

```
gmeans = repmat(NaN, ngroups, d);
for k = 1:ngroups
   gmeans(k,:) = mean(training(find(gindex == k),:),1);
end

D = repmat(NaN, mm, ngroups);
if n <= ngroups
   error('TRAINING must have more observations than the number of groups.');
end
% Pooled estimate of covariance
[Q,R] = qr(training - gmeans(gindex,:), 0);
R = R / sqrt(n - ngroups); % SigmaHat = R'*R
s = svd(R);
if any(s <= eps^(3/4)*max(s))
   error('The pooled covariance matrix of TRAINING must be positive definite.');
end
```

Test Data Classification Function

```
function [tmp, class] = classify_test(sample, gmeans, mm, ngroups, R)
% MVN relative log posterior density, by group, for each sample
for k = 1:ngroups
   A = (sample - repmat(gmeans(k,:), 1, 1)) / R;
   D(k) =  - .5*sum(A .* A, 2);
end
% find nearest group to each observation in sample data
[tmp class] = max(D);
```

APPENDIX D

MATLAB CODE: LOW-VOLTAGE MOTOR COIL ARC FAULT SEVERITY CLASSIFICATION – GAUSSIAN KERNEL-BASED SUPPORT VECTOR MACHINES (SVM)

```
echo off
% RBF-KERNEL based algorithm for using nonlinear SVM classifier
% with a RBF kernel.
echo on;

clc
% RBF-KERNEL based algorithm for using nonlinear SVM classifier
% with a RBF kernel.
%##########################################################################
%
%   This is a script-file for constructing and
%     testing a non-linear  SVM-based classifier
%     (with a RBF kernel) using OSU SVM CLASSIFIER TOOLBOX.
%   Note that the form of the RBF kernel is
%              exp(-Gamma*|X(:,i)-X(:,j)|^2)
%
%##########################################################################

pause % Strike any key to continue (Note: use Ctrl-C to abort)

clc
%##########################################################################
%
%   Load the training data and examine the dimensionality of the data
%
%##########################################################################
pause % Strike any key to continue

% load the training data
clear all
load DemoData_Train_test

pause % Strike any key to continue

% take a look at the data and verify  the dimensions
% of the input data
who

size(Labels)
size(Samples)

pause % Strike any key to continue

clc
%##########################################################################
%
%   Construct a nonlinear SVM classifier (with RBF kernel)
%     using the training data
%   Note that the form of the RBF kernel is
%     exp(-Gamma*|X(:,i)-X(:,j)|^2)
%
%##########################################################################
pause % Strike any key to continue

% set the value of Gamma if you don't want use its default value,
```

```
% which is 1.
Gamma = 2;

% By using this format, the default values of u, Epsilon, CacheSize
% are used. That is, u=0.5, Epsilon=0.001, and CacheSize=45MB
[AlphaY, SVs, Bias, Parameters, nSV, nLabel]=u_RbfSVC(Samples, Labels, Gamma);


% End of the SVM classifier construction
%
% The resultant SVM classifier is jointly determined by
%  "AlphaY", "SVs", "Bias", "Parameters", and "Ns".
%

pause % Strike any key to continue

% Save the constructed nonlinear SVM classifier
save SVMClassifier_arc AlphaY SVs Bias Parameters nSV nLabel;

pause % Strike any key to continue


clc
%#########################################################################
%
%   Test the constructed nonlinear SVM Classifier
%
%#########################################################################
pause % Strike any key to continue

% Load the constructed nonlinear SVM classifier
clear all
load SVMClassifier_arc

pause % Strike any key to continue

% have a look at the variables determining the SVM classifier
who

pause % Strike any key to continue

% load test data
load DemoData_actual_test

pause % Strike any key to continue

% Test the constructed SVM classifier using the test data
% begin testing ...
[ClassRate, DecisionValue, Ns, ConfMatrix, PreLabels]= SVMTest(Samples, Labels, AlphaY, SVs,
Bias,Parameters, nSV, nLabel);
% end of the testing

pause % Strike any key to continue

% The resultant confusion matrix of this 5-class classification problem is:
ConfMatrix
```

```
pause % Strike any key to continue
 load SVMClassifier_arc

[Labels, DecisionValue]= SVMClass(Samples, AlphaY, SVs, Bias, Parameters, nSV, nLabel)
load DemoData_actualclass_test
% Compare the resultant labels with the true labels of the data
plot(1:length(TrueLabels),TrueLabels,'b-',1:length(TrueLabels),Labels,'r.');
ylabel('Motor Coil Arc Fault Severity Class');
xlabel('Pattern Index');
legend('Estimated','Actual',0); Grid on
title('Testing Data Classification: Gaussian Kernel-based SVM')



echo off
```

APPENDIX E

MATLAB CODES - HARMONIC CONTENT EVALUATION – MATHEWS & STOKES/OPPENLANDER MODEL VS TEST-BENCH MOTOR COIL ARC FAULT CURRENT

Main Program

```
clear
close
clc
% defining values of basic parameters
%peak value of voltage, arc voltage and omega
Vmax = 277*sqrt(2);
Varc = 140;
w= 2*pi*60; % Frequency (rad/sec)
count =1;
x0=[0]'; % Initial Condition
% defining the period of simulation
flag =0;
tini=0;
tfin=0.1;
% perform the process till period has not ended
while tini <= tfin
   t = tini
   %if system voltage less than recovery voltage (375V) no arc current
   if ((Vmax *sin(w*t))<375 & (Vmax *sin(w*t))>=0)
      iarc(count) =0;
      time_arc(count) = t;
      Vsup(count) = Vmax *sin(w*time_arc(count));
      Varc_array(count) = 0;
      count = count +1;
      tini = tini + 0.000055556;
      %if system voltage greater than or equal to recovery voltage
      % utilize the differential equation defined by arcing circuit to
      % compute arc current
   elseif (Vmax *sin(w*t))>= 375
      tini = t;
      tf = t;
      flag = 1;
      % integrate the differential equation till arc current falls below
      % zero - all energy dissipiated
      % calculate time
      while flag == 1
         tf = tf + 0.000055556;
         t= tf;
         dt=0.00005556; % Integration Time Step
         tspan=[tini:dt:t]'; % Simulation Time
         m=length(tspan); % Number of Samples
         p(:,1)=[0]'; % Initial Condition Vector

         for i= 1:m-1
            f1p = dt*eq_motion(p(:,i),tspan(i));
```

```
            f2p = dt*eq_motion(p(:,i)+0.5*f1p,tspan(i));
            f3p = dt*eq_motion(p(:,i)+0.5*f2p,tspan(i));
            f4p = dt*eq_motion(p(:,i)+f3p,tspan(i));
            p(:,i+1) = p(:,i)+1/6*(f1p+2*f2p+2*f3p+f4p);
        end
        length_array = size(p);
        if (p(length_array(2)))<=0
            flag = 0;
        end
    end
    % perform the integration again for the entire period determined
    % above
    tspan = [tini:0.000055556:t]';
    m=length(tspan); % Number of Samples
    p(:,1)=[0]'; % Initial Condition Vector
    for i= 1:m-1
        f1p = dt*eq_motion(p(:,i),tspan(i));
        f2p = dt*eq_motion(p(:,i)+0.5*f1p,tspan(i));
        f3p = dt*eq_motion(p(:,i)+0.5*f2p,tspan(i));
        f4p = dt*eq_motion(p(:,i)+f3p,tspan(i));
        p(:,i+1) = p(:,i)+1/6*(f1p+2*f2p+2*f3p+f4p);
    end
    % append the results of the arc current, time stamp, arc voltage &
    % supply voltage to master arrays
    length_array = size(p);
    for j = 1:length_array(2)
            iarc(count) = p(j);
            time_arc(count) = tspan(j);
            Vsup(count) = Vmax *sin(w*time_arc(count));
             Varc_array(count) = 140;
            count=count+1;
        end
      tini= tf+ 0.000055556;
% negative half cycle voltage does not fall below -375V
% arc current is zero
% update master arrays
elseif (Vmax *sin(w*t))<=0 & (Vmax *sin(w*t))>-375
    0
    iarc(count) =0;
    time_arc(count) = t;
    Vsup(count) = Vmax *sin(w*time_arc(count));
    Varc_array(count) = 0;
    count = count +1;
    tini = tini +0.000055556;
% negative half cycle voltage falls below -375V
% integrate differential equation iteratively to obtain time for
```

```
% magnetic energy to dissipiate
elseif (Vmax *sin(w*t))<=-375
   1
   tini = t;
   tf = t;
   flag = 1;
   while flag == 1
      tf = tf + 0.000055556;
      t=tf;
      dt=0.000055556; % Integration Time Step
      tspan=[tini:dt:t]'; % Simulation Time
      m=length(tspan); % Number of Samples
      p(:,1)=[0]'; % Initial Condition Vector

      for i= 1:m-1
         f1p = dt*eq_motion1(p(:,i),tspan(i));
         f2p = dt*eq_motion1(p(:,i)+0.5*f1p,tspan(i));
         f3p = dt*eq_motion1(p(:,i)+0.5*f2p,tspan(i));
         f4p = dt*eq_motion1(p(:,i)+f3p,tspan(i));
         p(:,i+1) = p(:,i)+1/6*(f1p+2*f2p+2*f3p+f4p);
      end
      length_array = size(p);
      if (p(length_array(2)))>=0
         flag = 0;
      end
   end
   % perform integration over pre-determined time period to obtain arc
   % current signature
   dt=0.000055556; % Integration Time Step
   tspan=[tini:dt:t]'; % Simulation Time
   m=length(tspan); % Number of Samples
   p(:,1)=[0]'; % Initial Condition Vector
   for i= 1:m-1
      f1p = dt*eq_motion1(p(:,i),tspan(i));
      f2p = dt*eq_motion1(p(:,i)+0.5*f1p,tspan(i));
      f3p = dt*eq_motion1(p(:,i)+0.5*f2p,tspan(i));
      f4p = dt*eq_motion1(p(:,i)+f3p,tspan(i));
      p(:,i+1) = p(:,i)+1/6*(f1p+2*f2p+2*f3p+f4p);
   end
   % update master arrays
   length_array = size(p);
   for j = 1:length_array(2)
      iarc(count) = p(j);
      time_arc(count) = tspan(j);
      Vsup(count) = Vmax *sin(w*time_arc(count));
      Varc_array(count) = -140;
```

```
        count=count+1;
      end
      tini= tf+ 0.000055556;
   end
end
% plot ar current, arc voltage and supply voltage with time

subplot(3,1,1),plot(time_arc,iarc); grid on
xlabel('Time (secs)')
ylabel('Iarc (amps)')
title('Plots for Supply Voltage, Arc Voltage & Current - Matthews Model - 25mH
shorted')

% title('histograms for different number of samples')
subplot(3,1,2),plot(time_arc,Vsup); grid on
xlabel('Time (secs)')
ylabel('Vsupply (volts)')
subplot(3,1,3),plot(time_arc,Varc_array); grid on
xlabel('Time (secs)')
ylabel('Varc (volts)')
% save relevant variables from workspace into matlab data file for FFT
% analysis
save 'C:\Documents and Settings\Mandhir Sahni\Desktop\arcing fault current-
Gammon\arc_25mH_test' iarc Varc_array Vsup time_arc;
```

Differential Equation Functions

```
function xdot=eq_motion1(x,t);
% Parameter Declaration
Vmax = 277*sqrt(2);
% Vmax = 120*sqrt(2);
R = 0.1783;
L = 43.31e-3;
Varc = -140;
% Varc = -60;
w= 2*pi*60; % Frequency (rad/sec)
%flag = 0;
% % Differential Equation
% xdot= -(R/L)*x + (Vmax/L)*sin(w*t) - (Varc/L);

xdot= (Vmax/L)*sin(w*t) - (Varc/L);

%xdot= t;
```

```
function xdot=eq_motion(x,t);
% Parameter Declaration
Vmax = 277*sqrt(2);
% Vmax = 120*sqrt(2);
R = 0.1783;
L = 43.31e-3;
Varc = 140;
% Varc = 60;
w= 2*pi*60; % Frequency (rad/sec)
%flag = 0;
% % Differential Equation
% xdot= -(R/L)*x + (Vmax/L)*sin(w*t) - (Varc/L);

xdot= (Vmax/L)*sin(w*t) - (Varc/L);

%xdot= t;
```

Harmonic Content Evaluation Function

```
close all;
clear all; clc;
% load ('C:\Documents and Settings\Mandhir Sahni\Desktop\arcing fault current-
Gammon\arc_25mH_test.mat')
inputfile ='C:\Doctorate\coil arc testing\Final Tests-Report 5-20-06\comprehensive
analysis\beg\rawsignal_case5_beg.lvm'
data = load(inputfile)
iarc = data(:,2);
count = 0;
nPoint = 400;
for p = 1:2:13,
   sum_term = 0;
   for k = 1:nPoint,
      exp_term = (-2*pi*i)*(p/nPoint)*k;
      current_term = iarc(k)*exp(exp_term);
      sum_term = sum_term + current_term;
   end
   if p ==1
       harm_mag_fun = abs(sum_term/sqrt(nPoint));
    else
   count = count+1;
   harm_mag(count) = abs(sum_term/sqrt(nPoint));
   harm_per(count) = (harm_mag(count)/harm_mag_fun)*100;
   harm_order(count) = p;
end
end
```

```
bar(harm_order,harm_per); grid on
xlabel('harmonic order')
ylabel('harmonic percentage of fundamental')
title('Harmonic Content in arcing current from test-bench Design Alternative #1 - 25mH
Shorted')

figure
load ('C:\Documents and Settings\Mandhir Sahni\Desktop\arcing fault current-
Gammon\arc_25mH_test.mat')
% inputfile ='C:\Doctorate\coil arc testing\Final Tests-Report 5-20-06\comprehensive
analysis\beg\rawsignal_case5_beg.lvm'
% data = load(inputfile)
% iarc = data(:,2);
count = 0;
nPoint = 440;
for p = 1:2:13,
   sum_term = 0;
   for k = 1:nPoint,
      exp_term = (-2*pi*i)*(p/nPoint)*k;
      current_term = iarc(k)*exp(exp_term);
      sum_term = sum_term + current_term;
   end
   if p ==1
       harm_mag_fun = abs(sum_term/sqrt(nPoint));
    else
   count = count+1;
   harm_mag(count) = abs(sum_term/sqrt(nPoint));
   harm_per(count) = (harm_mag(count)/harm_mag_fun)*100;
   harm_order(count) = p;
end
end
bar(harm_order,harm_per); grid on
xlabel('harmonic order')
ylabel('harmonic percentage of fundamental')
title('Harmonic Content in arcing current from Matthews Model (277/480V) - 25mH
Shorted')
```

REFERENCES

1. Tammy Gammon, John Mathews, “Instantaneous Arcing-Fault Models developed for Building system Analysis”, IEEE Transactions on Industry Applications, Vol. 37, No.1, January/February 2001.
2. Lee, W.J.; Sahni, M.; Methaprayoon, K.; Kwan, C.; Ren, Z.; Sheeley, J., “A Novel Approach for Arcing Fault Detection for Medium/Low-Voltage Switchgear”, IEEE Industrial & Commercial Power System Technical Conference , April 2006
3. Tammy Gammon, John Mathews, “The Historical Evolution of Arcing-Fault models for Low Voltage systems”, IEEE Industrial & Commercial Power System Technical Conference , 2-6 May 1999.
4. J Slepian and A P Strom, “Arcs in low-voltage AC networks”, AIEE Transactions, Vol. 50, September 1931.
5. O R Schurig, “Fault voltage drop and impedance at short circuit currents in low-voltage circuits”, AIEE Transactions, vol 60, 1941
6. http://www.arcfault.org/ArcFaultDetecti.htm
7. http://www.iasa.com.au/folders/Publications/pdf_library/gazettemv.pdf
8. http://www.mikeholt.com/mojonewsarchive/NEC-HTML/HTML/What-is-Arc-Flash~20040512.php
9. http://www.arcfault.org/ResidentialArcF.htm

10. Fontchastagner, J.; Chadebec, O.; Schellekens, H.; Meunier, G.; Mazauric, V, "Coupling of an electrical arc model with FEM for vacuum interrupter designs", IEEE Transactions on Magnetics, May 2005.
11. Terzija, V.V.; Koglin, H.-J, "Long arc in still air: testing, modeling, simulation and model parameter estimation", Ninth International Conference on Harmonics and Quality of Power, 2000, Volume 1, 1-4 Oct. 2000 Page(s):36 - 44 vol.1.
12. Doublet, L.; Jemaa, N.B.; Hauner, F.; Jeannot, D, "Electrical arc phenomena and its interaction on contact material at 42 volts DC for automotive applications", Proceedings of the 50th IEEE Holm Conference on Electrical Contacts, 2004.
13. B. Smith, "An approach to graphs of linear forms (Unpublished work style)," unpublished.
14. McBride, J.W.; Weaver, P.M, "Review of arcing phenomena in low voltage current limiting circuit breakers", IEE Proceedings- Science, Measurement and Technology, Volume 148, Issue 1, Jan. 2001.
15. Terzija, V.V.; Koglin, H.-J, "On the modeling of long arc in still air and arc resistance calculation" , IEEE Transactions on Power Delivery, Volume 19, Issue 3, July 2004
16. Gammon T, Mathews J, "Instantaneous arcing-fault models developed for building system analysis", IEEE Transactions on Industry Applications, Vol. 37, Issue 1, Jan-Feb 2001.
17. Gammon T, Mathews J, "Arcing-fault models for low-voltage power systems", Industrial and Commercial Power Systems Technical Conference, May 2000.

18. Gammon, T.; Matthews, J., “Conventional and recommended arc power and energy calculations and arc damage assessment” , IEEE Transactions on Industry Applications, Volume 39, Issue 3, May-June 2003.
19. IEEE Guide for Testing Medium-Voltage Metal-Enclosed Switchgear for Internal Arcing Faults, 2002.
20. Roger C Dugan, Surya Santoso, Mark F. McGranaghan, H. Wayne Beaty, “Electrical Power Systems Quality”.
21. J. Lewis Blackburn, “Protective Relaying, Principles and Applications”, Second Edition.
22. Arcing-fault models for low-voltage power systems Gammon, T.; Matthews, J.;Industrial and Commercial Power Systems Technical Conference, 2000. Conference Record. Papers Presented at the 2000 Annual Meeting. 2000 IEEE,7-11 May 2000 Page(s):119 - 126 Digital Object Identifier 10.1109/ICPS.2000.854363
23. H. Szu, X.-Y. Yang, B. Telfer, and Y. Sheng, "Neural Network and Wavelet Transform for Scale-Invariant Data Classification," Phys. Rev. E, Vol. 48, pp. 1497--1501, 1993.
24. Analysis and detection of arcing faults in low-voltage electrical power systems,Ece, D.G.; Wells, F.M.;,Electrotechnical Conference, 1994. Proceedings., 7th Mediterranean,12-14 April 1994 Page(s):929 - 935 vol.3 ;Digital Object Identifier 10.1109/MELCON.1994.380949
25. Charytoniuk, W.; Lee, W.J.; Chen, M.S.; Cultrera, J.; Maffetone, T.; Industrial and Commercial Power Systems Technical Conference, 2000.

Conference Record. Papers Presented at the 2000 Annual Meeting. 2000 IEEE,7-11 May 2000 Page(s):15 - 20 ;Digital Object Identifier 10.1109/ICPS.2000.854352

26. R. E. Lee and M. T. Bishop, "Performance testing of the ratio ground relay on a four-wire distribution feeder," *IEEE Trans. Power App. Syst.*, vol. PAS-102, pp. 2943–2949, Sep. 1983.
27. F. Sultan, G. W. Swift, and D. J. Fedirchuk, "Detecting arcing downed-wires using fault current flicker and half-cycle asymmetry," *IEEE Trans. Power Delivery*, vol. 9, pp. 461–469, Jan. 1994.
28. C. Benner, P. Carswell, and B. D. Russell, "Improved algorithm for detecting arcing faults using random fault behavior," *Elect. Power Syst. Res.*, vol. 17, no. 1, pp. 49–56, 1989.
29. F. Sultan, G. W. Swift, and D. J. Fedirchuk, "Detection of high impedance arcing faults using a multi-layer perceptron," *IEEE Trans. Power Delivery*, vol. 7, pp. 1871–1877, Oct. 1992.
30. T. S. Sidhu, G. Singh, and M. S. Sachdev, "Arcing fault detection using artificial neural networks," *Neurocomput.*, vol. 23, no. 1–3, pp. 225–241, Dec. 1998.
31. A new technique for detection and location of arcing faults in power system apparatus,Sidhu, T.S.; Singh, G.; Sachdev, M.S.;Electrical and Computer Engineering, 1998. IEEE Canadian Conference on,Volume 1, 24-28 May 1998 Page(s):185 - 188 vol.1 ;Digital Object Identifier 10.1109/CCECE.1998.682713
32. Lab VIEW based implementation of remedial action for DC arcing faults in a spacecraft,Momoh, J.A.; Kumar, D.M.V.; Ishola-Salawu, A.S.; Sowah, R.;

Button, R.;,Power Engineering Society General Meeting, 2003, IEEE,Volume 1, 13-17 July 2003 Page(s): Digital Object Identifier 10.1109/PES.2003.1267226

33. On-line detection and location of low-level arcing in dry-type transformers,Sidhu, T.S.; Sagoo, G.S.; Sachdev, M.S.; Power Delivery, IEEE Transactions on,Volume 17, Issue 1, Jan. 2002 Page(s):135 - 141 ;Digital Object Identifier 10.1109/61.974200
34. A new arcing fault modeling and detection technique for navy IPS power system,Momoh, J.A.; Ishola-Salawu, A.S.; Power Engineering Society General Meeting, 2006. IEEE 18-22 June 2006 Page(s):7 pp. ;Digital Object Identifier 10.1109/PES.2006.1709620
35. http://en.wikipedia.org/wiki/Support_vector_machine
36. A novel approach for spectral unmixing, classification, and concentration estimation of chemical and biological agents Kwan, C.; Ayhan, B.; Chen, G.; Jing Wang; Baohong Ji; Chein-I Chang;,Geoscience and Remote Sensing, IEEE Transactions on Volume 44, Issue 2, Feb. 2006 Page(s):409 - 419 Digital Object Identifier 10.1109/TGRS.2005.860985
37. http://people.revoledu.com/kardi/tutorial/LDA/index.html
38. http://people.revoledu.com/kardi/tutorial/LDA/LDA.html

39. "A Practical Guide to Support Vector Classification", Chih-Wei Hsu, Chih-Chung Chang & Chih-Jen Lin, Department of Computer Science & Information Engineering, National Taiwan University.
40. "Support Vector Machines", Piyush Kumar
41. "The safety benefits of arc resistant metalclad medium voltage switchgear", Kalkstein, E.W.; Doughty, R.L.; Paullin, A.E.; Jackson, J.; Ryner, J.; Petroleum and Chemical Industry Conference, 1994. Record of Conference Papers., Institute of Electrical and Electronics Engineers Incorporated Industry Applications Society 41st Annual;12-14 Sept. 1994 Page(s):309 – 317
42. "A new, intelligent digital arc detection system for air- and gas-insulated switchgear**",**Jakob, K.; Schels, W.; Electricity Distribution. Part 1. Contributions. 14th International Conference and Exhibition on (IEE Conf. Publ. No. 438) Volume 1, 2-5 June 1997 Page(s):32/1 - 32/5 vol.1
43. "Internal arc-proof switchgear: arc modelling and active protection", Marchi, M.; Perdoncin, F.; Electricity Distribution. Part 1. Contributions. 14th International Conference and Exhibition on (IEE Conf. Publ. No. 438) Volume 1, 2-5 June 1997 Page(s):6/1 - 6/5 vol.1
44. "Internal faults in distribution switchgear-where are we now and where are we going?",Klaus, D.W.; Balnaves, D.; Trends in Distribution Switchgear: 400V-145kV for Utilities and Private Networks, 1998. Fifth International Conference on (Conf. Publ. No. 459); 10-12 Nov. 1998 Page(s):68 – 72
45. "On-line condition monitoring system of medium-voltage switchgear", Zongqian Shi; Yongpeng Meng; Wu Yang; Dan Ding; Shenli Jia; Mingzhe Rong;

Yonghong Cheng; Transmission and Distribution Conference and Exhibition 2002: Asia Pacific. IEEE/PES;Volume 3, 6-10 Oct. 2002 Page(s):2290 - 2294 vol.3 ; Digital Object Identifier 10.1109/TDC.2002.1177821

46. " A Tutorial on Support Vector Machines for Pattern Recognition" , Christopher J C Burges, Bell Laboratories, Lucent Technologies, Data Mining & Knowledge Discovery, 2, 121-167 (1998)

BIOGRAPHICAL INFORMATION

Mandhir Singh Sahni was born in the erstwhile district of Rewa, in the central state of Madhya Pradesh in India, November 4, 1979. Mandhir Sahni received his primary and high school education from the reputed Wynberg Allen School, Mussoorie, Uttar Pradesh, India from 1987-1996. He received his degree in Bachelor of Engineering , Electrical & Electronics Engineering, from B.M.S College of Engineering, Bangalore, India from 1997-2001. He followed that up with his Masters of Science degree in Electrical Engineering with an immaculate 4.0 GPA with a master's thesis titled "Design & Implementation of Control Algorithms for Real-time Static Load Control using LabVIEW & Programmable Logic Controllers", in 2004-05 under his current supervising professor Dr. Wei-Jen Lee. During the tenure of his graduate studies, Mandhir received numerous scholastic accolades such as being awarded University Scholar for the academic sessions 2004-05 and 2005-06, inducted into Who's Who for Students at American Universities 2004-05, received Rudolf Herman's Doctoral Fellowship for outstanding Doctoral students, awarded All-American Scholar Award and being inducted into academic honor societies such as Tau Beta Pi, Eta Kappa Nu and Phi Beta Delta. He was also the recipient of the prestigious Energy Systems Research Scholarship numerous times for his consistent and state-of-the-art research contributions to the research center.

His research interests include power quality, power system protective relaying, application of statistical and pattern recognition methods to low/medium voltage arc fault detection and classification and energy markets. Mandhir has 2 accepted and 2 pending journal papers spanning his research interests and about 7 conference papers. Mandhir has also been working full-time as a Senior Energy Analyst at PwrSolutions Inc for the last 1 and a half years developing state-of-the-art LMP forecasting methodologies for various energy markets in the US such as ERCOT, PJM, NYISO, ISO-NE and CAISO. Mandhir has also been the author of 2 white papers documenting the LMP forecasting methodology and the need to transition to predictive operations in the RTO-centric LMP energy markets in the US.

That apart, Mandhir, in his capacity as Senior Energy Analyst, has authored over 30 reports assessing various aspects of the energy markets in the US including a comprehensive ERCOT Nodal Assessment and its relative impact on the DFW metro-plex assessing complex market issues such as allocation inter-zonal and intra-zonal congestion and the allocation/auction of CRR's/ARR's in the proposed nodal market in ERCOT in 2009. Mandhir has also carried out numerous transmission assessment, generation interconnection, system feasibility studies for entities within the US and international entities such as Jordan, Saudi Arabia and Indonesia as United States Trade Development (USTDA) projects.